ABSTRACT

MCGUIRE, ASHLYN HENSON. When a Hemoglobin Acts as a Catalytic Enzyme: Mechanistic Studies of Dehaloperoxidase. (Under the direction of Dr. Reza A. Ghiladi).

The marine hemoglobin dehaloperoxidase (DHP) from the terebellid polychaete *Amphitrite ornata* is the first multifunctional hemoprotein with both an O_2-transport function and biologically-relevant peroxidase and peroxygenase activities. Previously, DHP was demonstrated to catalyze the oxidation of a wide variety of metabolites found in the environment *A. ornata* resides in, including halophenols, haloindoles, and pyrroles, as well as compounds of anthropogenic origin such as nitrophenols. Here, we will demonstrate the oxidation of another class of small-molecule pollutants, haloguaiacols, as well as nonnative substituted 4-R-guaiacols (R = NO_2, MeO, Me), using dehaloperoxidase. Substrate oxidation and product identification were performed by utilizing biochemical assays monitored by both spectroscopic and spectrometric techniques. As representative substrates, 4-haloguaiacols (4-F-, 4-Cl-, and 4-Br-) undergo oxidative dehalogenation in the presence of DHP and hydrogen peroxide, yielding 2-methoxybenzoquinone (2-MeOBQ) as one of the primary products. ^{18}O-labeling studies confirmed that oxygen incorporation was derived exclusively from water, consistent with substrate oxidation via DHP's peroxidase activity. Stopped-flow UV-visible spectroscopic studies demonstrated that 2-MeOBQ was capable of reducing DHP from its peroxidase resting ferric oxidation state to the O_2-transport active oxyferrous state, the latter of which was also determined to be capable of catalyzing guaiacol oxidation. Taken together, the results demonstrated here establish substituted guaiacols as a new class of DHP substrate that adds to an already diverse list, and further expands on the unique multifunctional nature of DHP and its ability to oxidize a wide range of toxic substrates, contributing to the survival of *A. ornata.*

As DHP is a hemoenzyme, the reactivity of the previous substrates originates from the oxidation of Fe(III) protoporphyrin IX (PPIX) by H_2O_2 to Fe(IV). By replacing the heme with a structurally similar cofactor, changes in the enzymes reactivities were probed. The native heme cofactor is easily removed through Teale's acid/butanone extraction; the apoenzyme could then uptake the new porphyrins (Mn-, Co-, Cu-PPIX and meso- and deutero-PIX). The reconstituted enzymes demonstrated both increased and decreased reactivity when compared. The metal-variants could not retain the native enzymes reactivity, but Fe-meso- and Fe-deutero-PIX demonstrated increased activities. Trihalophenol oxidation (peroxidase activity) turnover was increased 6-fold with the nonnative enzyme, while maintaining its catalytic efficiency. The oxidation of 1-methoxynaphthalene to Russig's Blue (peroxygenase activity) demonstrated an increase in both the turnover number and the catalytic efficiency by 11-fold and 8-fold, respectively, for Meso-DHP. Mechanistic studies on the meso-PIX, deutero-PIX, and Mn-PPIX were also examined by stopped-flow UV-vis. New reactivities of DHP were also explored with both native DHP and the mutants. These processes included C-H activation chemistry: styrene epoxidations, sp^3-hydroxlations, and carbene transfer chemistry.

When a Hemoglobin Acts as a Catalytic Enzyme: Mechanistic Studies of Dehaloperoxidase

by
Ashlyn Henson McGuire

A dissertation submitted to the Graduate Faculty of
North Carolina State University
in partial fulfillment of the
requirements for the degree of
Doctor of Philosophy

Chemistry

Raleigh, North Carolina
2020

APPROVED BY:

Reza A. Ghiladi Committee Chair	Stefan Franzen
Elon Ison	David Shultz

BIOGRAPHY

Ashlyn McGuire was born on October 19, 1992 to Lori and Randy Henson in Boone, North Carolina. She graduated high school from Watauga High. She attended Appalachian State University beginning in 2011 to study chemistry. During this time, she met her now husband, Wilson McGuire. After graduating with bachelor of science degree in Chemistry with Honors in 2015, she began graduate school in Chemistry at North Carolina State University and joined Dr. Reza Ghiladi's research group. While attending North Carolina State University she was involved in several collaborations including a one-month travel fellowship in Spring 2017 to work with Dr. Pat Hutchings at the Australian Museum in Sydney to collect and analyze the hemoglobin of marine polychaetes. In Summer of 2017 and Spring of 2019, she travelled to Nagoya, Japan to work with Dr. Watanabe and Dr. Shoji of Nagoya University to study nonnative cofactor incorporation into dehaloperoxidase to expand the reactivity. She now lives in Durham, NC with her husband and pets, Arthur and Nala.

ACKNOWLEDGMENTS

I would like to express my gratitude to my family and friends who supported me during this stage of my life. Most especially, my husband, whose continued support and motivation was essential during the last five years. To my classmates and labmates (GG's) who I've have been so lucky to meet and work alongside. I would also like to recognize my advisor, Dr. Reza Ghiladi for his guidance and continued support, both academic and personal, who afforded me the tools and opportunities to grow into a better scientist.

TABLE OF CONTENTS

LIST OF TABLES

LIST OF FIGURES

CHAPTER 1

Introduction

1.1. PEROXIDASES

Peroxidases are enzymes capable of the oxidation of substrates with hydrogen peroxide acting as the electron acceptor. Heme peroxidases can be described by three protein classes: Class I, II, and III.[1] Class I peroxidases are characterized by a conserved proximal tryptophan residue; examples include yeast cytochrome *c* peroxidase, ascorbate peroxidase, and catalase peroxidase isolated from bacteria.[2–4] Class II peroxidases, such as lignin and manganese peroxidase, originate from fungal organisms.[5] Class III are defined as secretory plant peroxidases such as horseradish peroxidase (HRP).[6]

The peroxidase mechanism is initiated from the reduction of hydrogen peroxide to water and the ferric enzyme is oxidized to Compound I in which a π-cation radical is located on the porphyrin ring (Figure 1.1). Radical transfer to a neighboring amino acid has been documented in some peroxidase systems; this enzymatic intermediate is known as Compound ES. A substrate (e.g. phenol, aromatic amine) can then reduce Compound I (or Compound ES) to Compound II in a one-electron step. A second equivalent of the substrate will reduce the enzyme back to its peroxidase resting state; both single electron steps yield product radicals.[1]

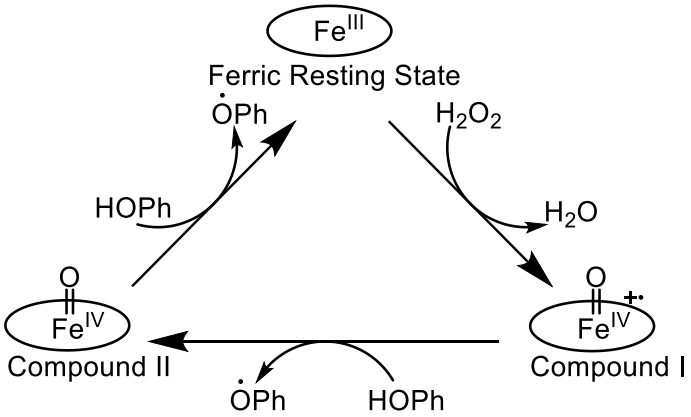

Figure 1.1. General peroxidase mechanism

1.2. PEROXYGENASES

Similar to the previously discussed peroxidase chemistry, the peroxygenase class of enzymes also utilizes hydrogen peroxide as the oxidant to catalyze substrate oxidation. Unlike peroxidase chemistry, peroxygenases are able to transfer an O-atom to the active site of the enzyme. A general peroxygenase mechanism is shown in Figure 1.2.[7] Hydrogen peroxide will react with the ferric form of the enzyme to produce Compound 0 (structure II) which quickly loses the hydroxy group to produce water, leaving a high-valent iron-oxo species with a π-cation radical delocalized on the porphyrin ring (Compound I, structure III). The ferric enzyme is regenerated when the ferryl O-atom is incorporated into the substrate (step 8).

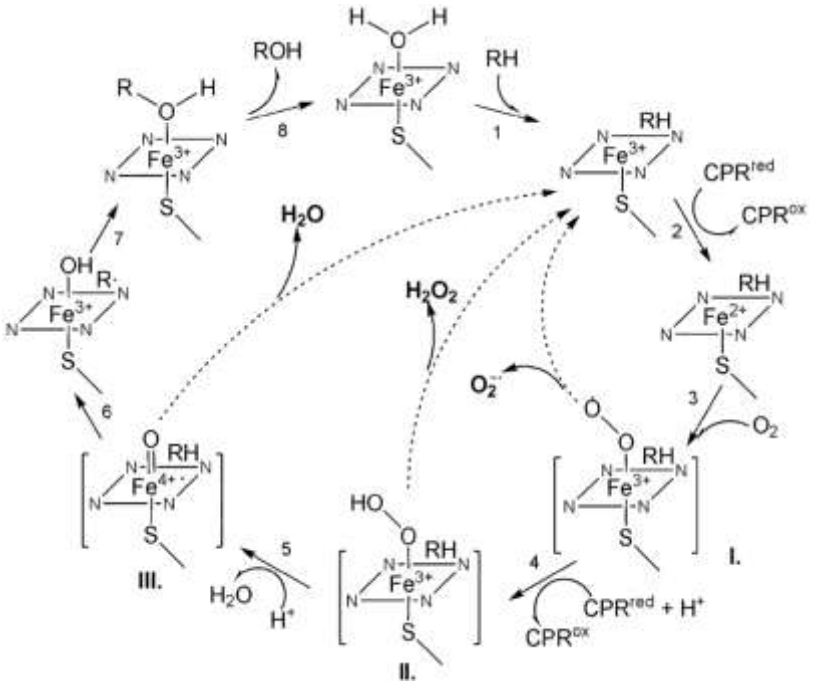

Figure 1.2. P450 catalytic cycle adapted from Wei, L *et. al.*[7] I, superoxo intermediate; II, hydroperoxy intermediate (Compound 0); III, iron-oxene intermediate (Compound I).

1.3. DEHALOPEROXIDASE

The previously discussed enzyme functions all exist in one unique marine annelid globin. The terebellid polychaete, *Amphitrite ornata*, resides in a benthic environment that possesses a diverse

assortment of toxic haloaromatic compounds produced through both anthropogenic and natural sources. Brominated aromatic compounds are a common defense mechanism of other sediment-dwelling marine polychaetes and hemichordates that co-inhabit in the coastal mudflats with *A. ornata*.[8,9] These marine annelids include *Saccoglossus kowalevskii* and *Saccoglossus bromophenolosus* (both hemichordata), which produce bromoindoles and bromopyrroles, and *Notomastus lobatus* (polychaeta), which produces mono-, di-, and tribromophenols and mono- and dibromovinylphenols.[10]

These compounds cause a significant strain to other infaunal organisms that co-inhabit these coastal mudflats. *A. ornata* possesses a unique globin, dehaloperoxidase, that is capable of protecting the annelid from the toxic chemicals in its environment via its native oxidative chemistry. The first recorded DHP enzymatic activity was the oxidative dehalogenation of 2,4,6-trichlorophenol to 2,6-dichloroquinone (Figure 1.3A).[10] The oxygen incorporated into the quinone product was determined to originate from water rather than hydrogen peroxide consistent with a peroxidase mechanism for DHP. Dehaloperoxidase was later shown to also possess peroxygenase activity towards certain substrates such as indoles, pyrroles and nitrophenols.[11–13] For these substrates, oxygen-atom incorporation was monitored; for example, 5-bromoindole was oxidized in the presence of DHP and hydrogen peroxide to 5-bromo-3-oxindole, in which the oxygen incorporated was exclusively derived from hydrogen peroxide (Figure 1.3B).

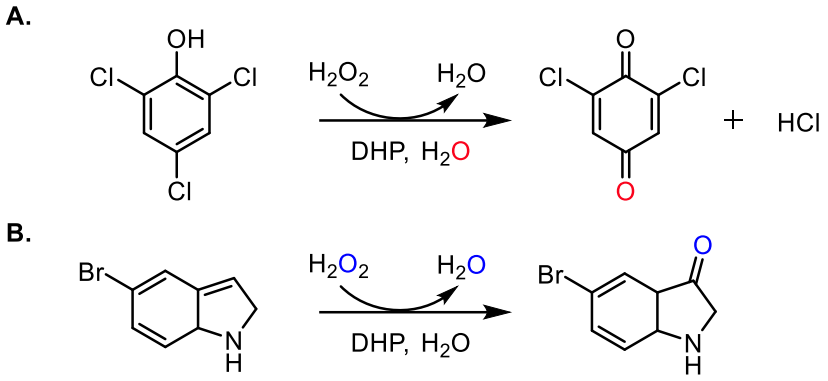

Figure 1.3. DHP catalyzed peroxidase and peroxygenase reactions. A) DHP and H_2O_2 catalyzed oxidative dehalogenation of trichlorophenol to dichloroquinone. B) DHP and H_2O_2 catalyzed oxidation of 5-bromoindole to 5-bromo-3-oxindole.

1.4. NONNATIVE HEME COFACTORS

Metalloproteins provide a useful scaffold to conduct specific reactions with a high degree of chemoselectivity and catalyst turnover, while being economically and environmentally favorable when compared to traditional catalytic methods. The scope of the previously discussed peroxidase and peroxygenase chemistry can be expanded by modifying the heme cofactor to other nonnative metals through a simple heme extraction through protein acidification as first described by Teale (Figure 1.4).[14]

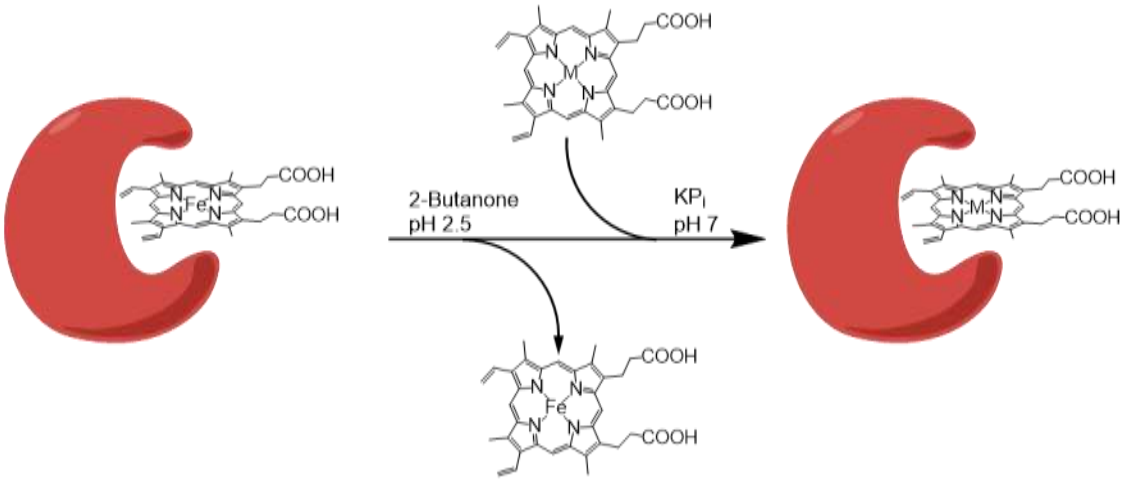

Figure 1.4. Reconstitution of metalloprotein with nonnative cofactor

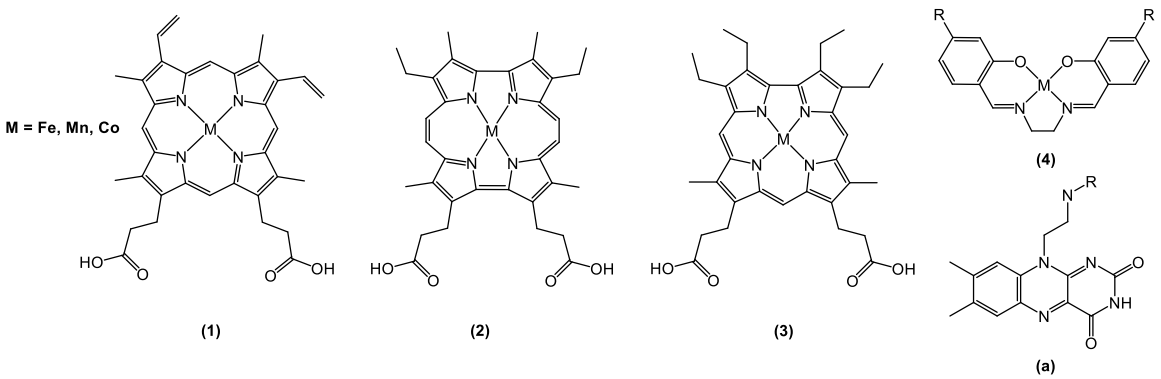

Figure 1.5. A selection of metal complexes successfully substituted into metalloproteins: (1) protoporphyrin IX (PPIX); (2) porphycene; (3) corrole; (4) salen; (a) flavin-isoalloxazine ring, attached via a propionate arm of (1).

By utilizing nonnative cofactors (Figure 1.5), new or enhanced protein reactivity and functionality can be explored. Dehaloperoxidase is classified as a globin and can often be compared to myoglobin which has been extensively studied in regard to substituting nonnative cofactors. Hisaeda and coworkers incorporated Fe(III) porphycene (**2**) which resulted in the increased oxidation rate of guaiacol, styrene and thioanisole compared to the native globin.[15] An Fe-corrole cofactor (**3**) was also inserted in myoglobin and increased the native peroxidase activity with guaiacol.[16] The same lab also incorporated an isoalloxazine flavin moiety (**a**) into the native porphyrin to increase P-450-like dioxygen activation.[17] Nonnative metal cofactors have also been examined using first row transition metals (M = Cr, Mn, Co). Choudhry demonstrated that Mn protoporphyrin IX substituted myoglobin was capable of oxidizing 1,4-cyclohexadiene, an ability native myoglobin does not possess.[18] Cobalt-porphycene substitution in myoglobin was also examined as Co^{II} is capable of reversibly binding O_2 and is also EPR active, factors that provide a model of Fe^{II}-globins where spectroscopy may fail. Hisaeda also demonstrated that O_2-binding was enhanced from the previously discussed Fe-porphycene.[15,19] Cofactors have also been used that do not possess traditional porphyrin-derived structures, such as metal-salens (**4**, achiral, water-insoluble catalysts). Utilizing the nonnative salen compounds in protein scaffolds provides a new

technique to enhance substrate reactivity and direct product enantioselectivity. The chemoselectivity of thioanisole sulfoxidation in myoglobin was explored by Lu and coworkers who were able to covalently attach the Mn-salen in the myoglobin active site. This approach demonstrated that the polar environment of the protein was necessary for the catalyst's chemoselectivity.[20–22]

Dehaloperoxidase has enhanced peroxidase activity when compared to myoglobin, enabling its comparison with horseradish peroxidase (HRP) and cytochrome *c* peroxidase. These conical peroxidase enzymes have been extensively studied to determine how nonnative heme cofactors can affect the protein's native functions. Yonetani and coworkers determined that Mn-protoporphyrin substituted HRP retained reactivity with hydrogen peroxide to form stable enzymatically active peroxidase intermediates, differing from the less stable Mn-cytochrome *c*.[23] Hoffman and Wang analyzed Co-PPIX-substituted HRP and determined that native peroxidase is attenuated as it does not react with H_2O_2 to form Compound I. It does, however, bind oxygen to form an analogue of the oxygenated form of cytochrome P-450 (oxyperoxidase) since accepting an electron from a reducing agent would be more favorable than the one-electron reduction of O_2.[24] In the study mentioned above, Hayashi and coworkers incorporated Fe-corrole in apo-HRP which resulted in in the opposite effect it had on the peroxidase activity of myoglobin.[16]

References

(1) Dunford, H. B. *Peroxidases and Catalases*, 2nd ed.; John Wiley and Sons, Inc.: Hoboken, 2010.

(2) Fülöp, V.; Ridout, C. J.; Greenwood, C.; Hajdu, J. Crystal Structure of the Di-Haem Cytochrome c Peroxidase from Pseudomonas Aeruginosa. *Structure* **1995**, *3* (11), 1225–1233.

(3) Sharp, K. H.; Mewies, M.; Moody, P. C. E.; Raven, E. L. Crystal Structure of the Ascorbate Peroxidase–ascorbate Complex. *Nat. Struct. Biol.* **2003**, *10* (4), 303–307.

(4) Yamada, Y.; Fujiwara, T.; Sato, T.; Igarashi, N.; Tanaka, N. The 2.0 A Crystal Structure of Catalase-Peroxidase from Haloarcula Marismortui. *Nat. Struct. Biol.* **2002**, *9* (9), 691–695.

(5) Hiner, A. N. P.; Ruiz, J. H.; López, J. N. R.; Cánovas, F. G. G.; Brisset, N. C.; Smith, A. T.; Arnao, M. B.; Acosta, M.; Rodri, J. N.; López, A.; et al. Reactions of the Class II Peroxidases, Lignin Peroxidase and Arthromyces Ramosus Peroxidase, with Hydrogen Peroxide: Catalase-Like Activity, Compound III Formation, and Enzyme Inactivation. *J. Biol. Chem.* **2002**, *277* (30), 26879–26885.

(6) Veitch, N. C. Horseradish Peroxidase: A Modern View of a Classic Enzyme. *Phytochemistry* **2004**, *65* (3), 249–259.

(7) Wei, L.; Locuson, C. W.; Tracy, T. S. Polymorphic Variants of CYP2C9 : Mechanisms Involved in Reduced Catalytic Activity. *Mol. Pharmacol.* **2007**, *72* (5), 1280–1288.

(8) D'Antonio, J.; D'Antonio, E. L.; Thompson, M. K.; Bowden, E. F.; Franzen, S.; Smirnova, T.; Ghiladi, R. A. Spectroscopic and Mechanistic Investigations of Dehaloperoxidase B from Amphitrite Ornata. *Biochemistry* **2010**, *49* (31), 6600–6616.

(9) Roach, M. P.; Chen, Y. P.; Woodin, S. A.; Lincoln, D. E.; Lovell, C. R.; Dawson, J. H. Notomastus Lobatus Chloroperoxidase and Amphitrite Ornata Dehaloperoxidase Both Contain Histidine as Their Proximal Heme Iron Ligand. *Biochemistry* **1997**, *36* (8), 2197–2202.

(10) Chen, Y. P.; Woodin, S. A.; Lincoln, D. E.; Lovell, C. R. An Unusual Dehalogenating Peroxidase from the Marine Terebellid Polychaete Amphitrite Ornata. *J. Biol. Chem.* **1996**, *271* (9), 4609–4612.

(11) Barrios, D. A.; D'Antonio, J.; McCombs, N. L.; Zhao, J.; Franzen, S.; Schmidt, A. C.; Sombers, L. A.; Ghiladi, R. A. Peroxygenase and Oxidase Activities of Dehaloperoxidase-Hemoglobin from Amphitrite Ornata. *J. Am. Chem. Soc.* **2014**, *136* (22), 7914–7925.

(12) McCombs, N.; Smirnova, T.; Ghiladi, R. Oxidation of Pyrrole by Dehaloperoxidase-Hemoglobin: Chemoenzymatic Synthesis of Pyrrolin-2-Ones. *Catal. Sci. Technol.* **2017**.

(13) McCombs, N. L.; D'Antonio, J.; Barrios, D. A.; Carey, L. M.; Ghiladi, R. A. Nonmicrobial Nitrophenol Degradation via Peroxygenase Activity of Dehaloperoxidase-Hemoglobin from Amphitrite Ornata. *Biochemistry* **2016**, *55* (17), 2465–2478.

(14) Teale, F. Cleavage of the Haem-Protein Link by Acid Methylethylketone. *Biochim. Biophys. Acta* **1959**, *35* (20), 543.

(15) Hayashi, T.; Murata, D.; Makino, M.; Sugimoto, H.; Matsuo, T. Crystal Structure and Peroxidase Activity of Myoglobin Reconstituted with Iron Porphycene. *Inorg. Chem.* **2006**, *45* (26), 1011–1015.

(16) Matsuo, T.; Hayashi, A.; Abe, M.; Matsuda, T.; Hisaeda, Y.; Hayashi, T. Meso-Unsubstituted Iron Corrole in Hemoproteins: Remarkable Differences in Effects on

Peroxidase Activities between Myoglobin and Horseradish Peroxidase. *J. Am. Chem. Soc.* **2009**, *131*, 15124–15125.
(17) Matsuo, T.; Hayashi, T.; Hisaeda, Y. Reductive Activation of Dioxygen by a Myoglobin Reconstituted with a Flavohemin. *J. Am. Chem. Soc.* **2002**, *124*, 11234–11235.
(18) Bond, W. C.; Stone, K. L.; Hua, J.; Choudhry, H. Manganese-Substituted Myoglobin: Characterization and Reactivity of an Oxidizing Intermediate towards a Weak C-H Bond. *Inorganics* **2015**, *3*, 219–229.
(19) Matsuo, T.; Tsuruta, T.; Maehara, K.; Sato, H.; Hisaeda, Y. Preparation and O2 Binding Study of Myoglobin Having a Cobalt Porphycene. *Inorg. Chem.* **2005**, *44* (25), 1456–1461.
(20) Carey, J. R.; Ma, S. K.; Pfister, T. D.; Garner, D. K.; Kim, H. K.; Abramite, J. A.; Wang, Z.; Guo, Z.; Lu, Y. A Site-Selective Dual Anchoring Strategy for Artificial Metalloprotein Design. *J. Am. Chem. Soc.* **2004**, *126*, 10812–10813.
(21) Zhang, J.; Garner, D. K.; Liang, L.; Chen, Q.; Lu, Y. Protein Scaffold of a Designed Metalloenzyme Enhances the Chemoselectivity in Sulfoxidation of Thioanisole. *Chem. Commun.* **2008**, 1665–1667.
(22) Lu, Y.; Sieracki, N.; Marshall, N. Design of Functional Metalloproteins. *Nature* **2009**, *460*, 855–862.
(23) Yonetani, T.; Asahura, T. Studies on Cytochrome c Peroxidase. *Biochem. Phys.* **1969**, *244* (17), 4580–4588.
(24) Wang, M.-Y.; Hoffman, B.; Hollenberg, P. Cobalt-Substituted Horseradish Peroxidase. *J. Biol. Chem.* **1977**, *252* (18), 6268–6275.

Chapter 2

Substituted Guaiacols as New Substrates for Dehaloperoxidase B from *Amphitrite ornata*: Mechanistic and Structural Studies

Ashlyn H. McGuire, Leiah M. Carey, Safaa Dali, and Reza A. Ghiladi

Department of Chemistry, North Carolina State University, Raleigh, North Carolina, 27695

Author Contributions: Ashlyn H. McGuire is responsible for all work excluding crystallographic work (Leiah M. Carey) and 6-Br-G HPLC and substrate binding studies (Safaa Dali).

ABSTRACT: The dehaloperoxidase-hemoglobin (DHP) from the terebellid polychaete *Amphitrite ornata* is a multifunctional hemoprotein that catalyzes the oxidation of a wide variety of substrates, including halo-/nitro-phenols, haloindoles, and pyrroles, via peroxidase and/or peroxygenase mechanisms. To probe whether substrate substituent effects can modulate enzyme activity in DHP, we investigated its reactivity against a panel of *o*-guaiacol substrates given their presence (from native/halogenated and non-native/anthropogenic sources) in the benthic environment that *A. ornata* inhabits. Using biochemical assays supported by spectroscopic, spectrometric, and structural studies, DHP was found to catalyze the H_2O_2-dependent oxidative dehalogenation of 4-haloguaiacols (F, Cl, Br) to 2-methoxybenzoquinone (2-MeOBQ). ^{18}O-labeling studies confirmed that O-atom incorporation was derived exclusively from water, consistent with substrate oxidation via a peroxidase-based mechanism. The 2-MeOBQ product further reduced DHP to its oxyferrous state, providing a link between the substrate oxidation and O_2-carrier functions of DHP. Nonnative substrates resulted in polymerization of the initial substrate with varying degrees of oxidation, with 2-MeOBQ identified as a minor product. When viewed alongside the reactivity of previously studied phenolic substrates, the results here show that simple substituents effects can serve as functional switches between peroxidase and

peroxygenase activities in this multifunctional catalytic globin. More broadly, when including recent findings on DHP activity with nitrophenols and azoles, the results here further demonstrate the breadth of heterocyclic compounds of anthropogenic origin that can potentially disrupt marine hemoglobins or function as environmental stressors, findings that may be important when assessing the environmental impact of these pollutants (and their metabolites) on aquatic systems.

Keywords: globin; guaiacol; heme; peroxidase; peroxygenase; structure-function

INTRODUCTION

Guaiacol (methoxyphenol), a major component of wood lignin, is released into the environment from both anthropogenic and natural sources,[1-3] some examples of which include: i) biomass burnings, where during the combustion of wood lignin the semi-volatile guaiacol-derived pollutants can be aerosolized, enter the troposphere, and can further react with atmospheric nitrogen-containing species to yield nitroguaiacols,[4] which are generally considered to be more toxic than the parent compound, ii) the paper-pulp industry, where during the bleaching of wood pulp the bleaching agents (molecular chlorine, hypochlorite, etc.) react with lignin, resulting in chlorinated phenolic derivatives (i.e. chloroguaiacols, chlorocatechols), and iii) as derivatives of polybrominated diphenyl ethers that originate both artificially (from chemical transformations of polybrominated flame-retardant chemicals) and naturally (as biosynthetic compounds produced by marine bacteria).[5] These compounds are then released into the environment through wastewater effluent[2, 6] or via precipitation,[7, 8] leading to contamination of both water and soil. With recent reports demonstrating that guaiacol pollutants are acutely toxic to a level that meets the European toxicity classification of 'harmful',[9] there is an increasing need to assess the impact of these compounds, including their metabolites, on the environment.

Although enzyme-catalyzed guaiacol oxidation has been extensively examined,[10-16] most studies have focused on enzymes from microbial or plant origins. As such, the mechanisms by which infaunal organisms cope with guaiacol pollutants as environmental stressors, produced either natively as halometabolites by other organisms or from anthropogenic sources, remains relatively understudied by comparison. Our platform for exploring the interactions of such environmental pollutants with infaunal organisms is *Amphitrite ornata*, a sediment-dwelling marine polychaete.[17] Inhabiting coastal mudflats that are rich in biogenically produced halometabolites excreted from other organisms,[18] *A. ornata* faces stressors that include brominated

indoles, pyrroles, phenols, and – of particular relevance to the present study – guaiacols. To overcome the challenges posed from this diverse array of toxic haloaromatic compounds, *Amphitrite ornata* employs its hemoglobin to function both as a detoxification enzyme and as an O_2-transport protein.[19-21] Named dehaloperoxidase (DHP), this coelomic hemoglobin[22] possesses an unusually broad substrate profile encompassing halophenols,[20, 23] haloindoles,[24] and (halo)pyrroles,[25] and as such is the first known multifunctional catalytic globin to possess biologically-relevant peroxidase[26-33] and peroxygenase[24, 25, 34] activities, as well as an oxidase[24] activity that leads to the formation of indigo derivatives. DHP also exhibits activity against compounds of anthropogenic origin, including the H_2O_2-dependent oxidation of mono- and di-nitrophenols,[34] as is also capable of binding azole species,[35] including imidazole, benzotriazole, benzimidazole, and indazole.

DHP has two isoenzymes encoded by separate genes,[36] A and B, which differ by only five amino acid substitutions (note ‑ isoenzyme A is listed first): I/L9, R/K32, Y/N34, N/S81, and S/G91. Although these two isoenzymes are structurally identical,[37] DHP B consistently exhibits a greater reactivity than isoenzyme A, and as such recent studies have focused on this variant.[29] Mechanistic studies have shown that both isoenzymes appear to function via a Poulos−Kraut type mechanism[38]: ferric DHP reacts with H_2O_2 to form DHP Compound I,[39] an iron(IV)-oxo porphyrin π-cation radical species. In WT DHP, Compound I rapidly converts in DHP to an iron(IV)-oxo heme center with a tyrosyl radical that has been termed Compound ES[32, 33, 40] by analogy with cytochrome *c* peroxidase, whereas in mutants such as DHP B (Y28F/Y38F),[31] the Compound I species can be investigated directly. These peroxide-activated forms of DHP initially return to the ferric resting state upon substrate oxidation, although further reduction to oxyferrous DHP has been noted under some conditions.[24, 25, 34, 40, 41]

Given the diverse functions (O_2-carrier, peroxidase, peroxygenase, oxidase) exhibited by DHP across this broad panel of substrates, we have previously suggested that the substrate itself can act to modulate enzyme activity in DHP,[29, 30] with binding/orientation (relative to the ferryl iron), pKa, and redox potential all being key determinants as to which mechanism leads to substrate oxidation. More interestingly, however, it also appears that substituent effects may play a pseudo-allosteric role (Figure 1): the peroxidase substrate phenol is converted to a peroxygenase substrate upon addition of a 4-nitro substituent,[34] whereas 4-Br-phenol is an inhibitor[42] of peroxidase and peroxygenase activities in DHP. These substituent effects suggest that it may be possible to modulate DHP activity by switching the substrate oxidation mechanism, not through traditional mutagenesis or heme cofactor modification, but through selection of the substrate itself.

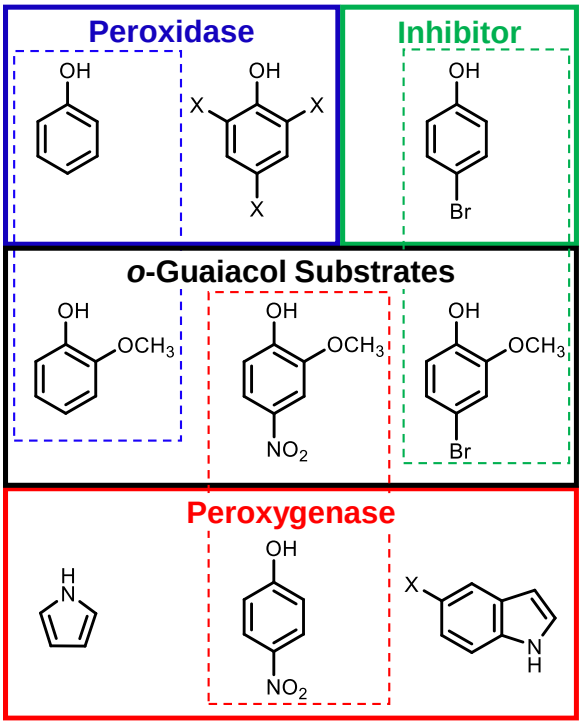

Figure 2.1. DHP peroxidase (blue), peroxygenase (red), and oxidase (green) substrates and *o*-guaiacol structures (black); X = F, Cl, Br, I.

To investigate how guaiacol pollutants may undergo biotransformations by infaunal organisms, and to probe the role of substituent effects as modulators/regulators of the multiple activities in DHP, we evaluated a panel of 4-X-guaiacol (X = -F, -Cl, -Br, -NO_2, -OMe, -Me) substrates using a combination of spectroscopic methods, biochemical assays, and isotope labelling studies. The basis for selecting guaiacols (Figure 1) within the context of substituent/electronic effects is: i) the addition of the methoxy substituent to phenol (blue box), 4-nitrophenol (red box), and 4-Br-phenol (green box) will enable us to probe its effect on the peroxidase,[19] peroxygenase,[24, 25, 34] and inhibition[42] pathways of DHP relevant to the putative guaiacol substrates, ii) haloguaiacols are native to the benthic environment of *A. ornata*,[18, 43] and likely represent physiologically-relevant substrates, while anthropogenic analogs, such as 4-nitroguaiacol[4] and 4-chloroguaiacol[2], are relevant as environmental stressors, and iii) guaiacol oxidation is well understood with respect to monofunctional heme proteins,[10, 13, 14, 44] but is unknown with respect to multifunctional catalytic globins. As will be shown, the results establish that guaiacols are indeed substrates for DHP, and demonstrate that simple substituents effects can be used as a functional switch between peroxidase and peroxygenase activities in modulating the activity of this multifunctional catalytic globin. More broadly, when viewed along with our recent findings employing nitrophenols[34] and azoles,[35] the results further demonstrate the breadth of heterocyclic compounds of anthropogenic origin that can potentially disrupt marine hemoglobins or function as environmental stressors, findings that may be important when assessing the environmental impact of these pollutants (and their metabolites) on aquatic systems.

EXPERIMENTAL PROCEDURES

Materials. Ferric samples of WT DHP B were expressed and purified as previously reported.[37, 40] Oxyferrous DHP B was prepared by the aerobic addition of excess ascorbic acid to ferric DHP

B, followed by removal of the reducing agent via a PD-10 desalting column.[41] Enzyme concentration was determined spectrophotometrically using ε_{soret}=116,400 M^{-1} cm^{-1}.[40] Horse skeletal muscle (HSM) myoglobin and horseradish peroxidase (HRP) were purchased from Sigma-Aldrich and enzyme concentrations were determined using ε_{soret} = 188,000 $M^{-1}cm^{-1}$ [45] and 102,000 $M^{-1}cm^{-1}$,[46] respectively. Solutions of H_2O_2 were prepared fresh daily in 100 mM KP_i (pH 7) and kept on ice until needed. Isotopically labeled $H_2{}^{18}O_2$ (90% ^{18}O-enriched) and $H_2{}^{18}O$ (98% ^{18}O-enriched) were purchased from Icon Isotopes (Summit, NJ). Stock solutions of guaiacols (10 mM) were prepared in MeOH and stored in the dark at -80 °C until needed. Acetonitrile (MeCN) was HPLC grade, and all other reagent-grade chemicals were purchased from VWR, Sigma-Aldrich or Fisher Scientific and used without further purification.

Guaiacol Binding Studies. The guaiacol substrate dissociation constants (K_d) were determined in triplicate for DHP in 100 mM KP_i (pH 7) containing 6.25% MeOH at 25 °C using a Cary 50 UV-vis spectrophotometer per previously published protocols.[24, 47] The UV-visible spectrometer was referenced with 50 μM WT DHP B in 100 Mm KP_i (pH 7) in 6.25% MeOH. Spectra were acquired in the presence of guaiacol substrate concentrations (3.75-50 equiv) while maintaining constant DHP B (50 μM) and methanol concentrations. Analyses of the Q-band region (450-600 nm) was performed using the ligand binding function in Grafit (Erithacus Software Ltd.).

HPLC Activity Studies. Reactions were performed in triplicate at pH 7 (unless otherwise indicated) in 100 mM KP_i containing 5% MeOH at 25 °C. Assay components (250 μL final volume) included 10 μM enzyme, 500 μM substrate (in MeOH), and the reaction was initiated by the addition of 500 μM H_2O_2. Experiments were also performed in the presence of 500 μM 4-bromophenol, 500 μM D-mannitol, 100 mM DMPO or 10% v/v DMSO, which were added prior to the addition of H_2O_2. The reactions were quenched after 5 min with excess catalase. A 100 μL

aliquot was diluted 10-fold with 900 µL 100 mM KP_i (pH 7). The samples were analyzed using a Waters 2796 Module coupled with a Waters 2996 photodiode array detector and equipped with a Thermo Fisher Scientific ODS Hypersil (150 mm × 4.6 mm) 5 µM particle size C_{18} column. Separation was performed using a linear gradient of binary solvents (solvent A, H_2O + 0.1% TFA; solvent B, acetonitrile + 0.1% TFA). The elution consisted of the following conditions: (1.5 mL/min A:B) 95:5 to 5:95 linearly over 12 min, 5:95 isocratic for 2 min, 5:95 to 95:5 over 1 min, then isocratic for 3 min. Data analysis was performed using the Waters Empower software package.

Product Determination by LC-MS. Analysis was carried out on a Thermo Fisher Scientific Exactive Plus Orbitrap mass spectrometer using a heated electrospray ionization (HESI) probe. The samples were introduced via LC injection into the mass spectrometer at a flow rate of 250 µL/min (solvent A, H_2O + 0.1% formic acid; solvent B, acetonitrile + 0.1% formic acid) after elution from a Thermo Hypersil Gold (50 x 2.1 mm, particle size 1.9 µm) C_{18} column. The mass spectrometer was operated in positive and negative modes. Spectra were collected while scanning from 100-1500 *m*/*z*. Data analysis was performed using Thermo Xcalibur software. The assay included 10 µM DHP B, 500 µM substrate and 500 µM H_2O_2 in buffer (5 mM KP_i, pH 7) with a final volume of 250 µL, and was allowed to react for 5 min before quenching with catalase. A 10 µL aliquot of the undiluted reaction was injected for LC-MS analysis. For the ^{18}O-labeling studies, unlabeled H_2O_2 was replaced with $H_2{}^{18}O_2$, and/or the KP_i buffer was replaced with $H_2{}^{18}O$ to ensure >90% labeled $H_2{}^{18}O$.

Stopped-Flow UV-Visible Spectroscopy Studies. Optical spectra were recorded using a Bio-Logic SFM-400 triple-mixing stopped-flow instrument coupled to a rapid scanning diode array UV-visible spectrophotometer. Protein and hydrogen peroxide solutions were prepared in 100 mM

KP_i (pH 7), and the guaiacol substrates were dissolved in buffer containing 4% methanol. Data were collected (900 scans total) over a three-time domain (1.5, 15, 150 ms) using the Bio-Kine 32 software package (Bio-Logic). All data were evaluated using the Specfit Global Analysis System software package (Spectrum Software Associates) and fit with SVD analysis as either one-step, two species or two-step, three species irreversible mechanisms, where applicable. For data that did not properly fit these models, experimentally obtained spectra at selected time points detailed in the figure legends are shown. Kinetic data were baseline corrected using the Specfit autozero function when appropriate.

Double-mixing experiments were performed using an aging line prior to the second mixing step to observe Compound I/ES/II reactivity with the guaiacol substrates (5-50 equiv): i) Compound I was pre-formed by the reaction of ferric DHP B (Y28F/Y38F) with 10 equiv of H_2O_2 in an aging line for 85 ms[31] prior to mixing with the substrate; ii) Compound ES was pre-formed by reaction of ferric WT DHP B with 10 equiv of H_2O_2 in an aging line for 500 ms[40]; and iii) Compound II was formed from oxyferrous DHP B pre-incubated with 1 equiv of TCP and reacted with 10 equiv of H_2O_2 in an aging line for 3 s.[41]

Protein Crystallization and X-ray Diffraction Studies. Non-His tagged DHP B was overexpressed and purified per literature.[29, 30, 37] DHP B crystals were obtained through the hanging-drop vapor diffusion method. The crystals were grown from mother liquor solutions of 32% PEG 3350 and 0.2 M ammonium sulfate at pH 6.4, and were equilibrated against identical reservoir solutions. Protein to mother liquor ratios varied between 1:1, 1.33:1, 1.66:1, and 2:1. At 4 °C crystals grew from each condition after 3 days. The crystals were soaked for 12 hours in substrate enhanced reservoir solutions identical to the mother liquor. Substrate final concentrations were all 100 mM (5% DMSO v/v). The crystals were cryo-protected by briefly dipping them in

reservoir solution containing 20% glycerol and then cryocooled in liquid N_2. Data were collected at 100 K on the SER-CAT 22-BM beamline at the APS synchrotron facility, utilizing a wavelength of 1.00 Å. All data were scaled and integrated using HKL2000,[48] molecular replacement was performed with Phaser-MR[49] from the PHENIX[50] and CCP4[51] suite of programs using 3IXF[37] as the search model. Model building and manual placement of waters utilized COOT[52] and refinement was carried out using refmac[53] and phenix.refine.[54]

RESULTS

DHP-Catalyzed Guaiacol Reactivity with H_2O_2. The hydrogen peroxide-dependent reaction of ferric DHP B with guaiacol substrates at pH 7 was monitored via HPLC, and the corresponding substrate conversion percentages are reported in Table 1. Reactions were initiated upon addition of 500 μM H_2O_2 to a solution containing 10 μM enzyme and 500 μM guaiacol, incubated at 25 °C for 5 min, and then quenched with catalase. With the exception of *o*-guaiacol (32.4%), all substrates exhibited very high conversion, with the 4-X-guaiacol series (X = F, Cl, Br) essentially being fully oxidized (>99.7%), and 5- and 6-Br-guaiacol only slightly diminished. Non-native guaiacol substrates (4-NO_2-, 4-Me-, and 4-MeO-guaiacol) were also found to be very reactive (92.8-98.6%). No turnover of substrate was observed in the absence of H_2O_2 (non-oxidant control) or enzyme (non-enzymatic control).

Using 4-Br-guaiacol as a representative substrate owing to its similarity to previously studied halophenols,[55] the following observations were noted: i) a minimal pH effect was observed (pH 5 < pH 7 ≈ pH 8); ii) substrate conversions were also found to be identical when the assays were initiated from the oxyferrous ('hemoglobin-like') or ferric ('peroxidase-like') oxidation states, in line with previous observations for DHP for the oxidation of TCP via a peroxidase mechanism,[41] and the oxidation of haloindoles,[24] nitrophenols,[34] and pyrroles[25] via a peroxygenase cycle; iii)

both DHP B and the canonical peroxidase HRP yielded complete conversion of the substrate to product(s), although the product distributions were found to be different (*vide infra*); iv) horse skeletal muscle myoglobin exhibited a 3.4-fold attenuation in reactivity. These results support that DHP reactivity with guaiacols is on a par with classical peroxidase enzymes, yet is greater than other members of the globin family.

Mechanistic studies were also employed to elucidate key details of the reaction of 4-Br-guaiacol with DHP. Under anaerobic conditions, substrate conversion (99.7%) was identical to the aerobic reaction, showing no dependence on molecular oxygen. The addition of the hydroxyl radical scavengers D-mannitol (99.7%) and dimethyl sulfoxide (DMSO; 99.6%) also exhibited no effect on the oxidation of 4-Br-guaiacol, suggesting that freely diffusible hydroxyl radicals are not involved in the reaction. Similarly, the radical scavenger 5,5-dimethyl-1-pyrroline N-oxide (DMPO) did not show reduced 4-Br-guaiacol reactivity (99.4%). However, DMPO did significantly inhibit substrate conversion of 5-Br-guaiacol (27.6 ± 1.1% vs. 90.0 ± 1.0%) and 4-NO_2-guaiacol (28.5 ± 1.3% vs. 92.8 ± 0.2%), indicating a difference between these substrates pertaining to the diffusibility of substrate radicals (*vide infra*). When the peroxidase and peroxygenase inhibitor 4-bromophenol (K_d = 1.15 mM[42, 56]) was added, substrate conversion was minimally decreased by 1.2-fold, suggesting that 4-bromophenol has only a slight inhibitory effect on 4-Br-guaiacol oxidation.

Table 2.1. DHP-catalyzed oxidation of substituted guaiacols.[a]

Substrate	Conversion (%)
Substrate Variation	
Ferric WT DHP B, pH 7	
+ *o*-guaiacol	32.4 (±0.2)
+ 4-F-guaiacol	>99.9
+ 4-Cl-guaiacol	99.7 (±0.1)
+ 4-Br-guaiacol	99.7 (±0.2)
+ 5-Br-guaiacol	90.0 (±1.0)
+ 6-Br-guaiacol	88.8 (±0.2)
+ 4-NO_2-guaiacol	92.8 (±0.2)
+ 4-MeO-guaiacol	94.6 (±1.2)
+ 4-Me-guaiacol	98.6 (±0.3)
pH Studies (4-Br-guaiacol)	
pH 5	90.5 (±0.2)
pH 8	99.6 (±0.1)
Enzyme Variation	
Oxyferrous WT DHP B	
+ 4-Br-guaiacol	99.7 (±0.1)
+ 5-Br-guaiacol	84.8 (±2.0)
HRP	
+ 4-Br-guaiacol, pH 6	>99.9
Myoglobin (HSM)	
+ 4-Br-guaiacol	29.3 (±2.8)
+ 5-Br-guaiacol	32.9 (±2.0)
Mechanistic Probes (Ferric WT DHP B)	
4-Br-guaiacol	
+ 500 µM mannitol	99.7 (±0.2)
+ 10% DMSO	99.6 (±0.1)
+ 100 mM DMPO	99.4 (±0.2)
+ 500 µM 4-BP	84.8 (±0.1)
anaerobic	99.7 (±0.2)
- H_2O_2	*n.d.*
- enzyme	*n.d.*
5-Br-guaiacol	
+ 100 mM DMPO	27.6 (±1.1)
4-NO_2-guaiacol	
+ 100 mM DMPO	28.5 (±1.3)

[a] Reaction conditions: [enzyme] = 10 µM, [guaiacol] = [H_2O_2] = 500 µM, 5% MeOH/100 mM KP_i (v/v), pH 7 unless otherwise noted; *n.d.* = no reactivity detected; DMPO: 5,5-dimethyl-1-pyrroline N-oxide; 4-BP: 4-bromophenol.

Identification of Reaction Products by HPLC and LC-MS. The HPLC chromatograms for the reaction of ferric WT DHP B with guaiacol substrates are shown in Figure 2 and Figure S1, and a list of the products by their retention times and masses is provided in Tables S1 and S2. Although identification of the exact chemical structures was not pursued, the products generally consisted of dimers, trimers, and tetramers with varying degrees of oxidation, in line with previous reports for heme enzyme catalyzed oxidation of guaiacol.[10, 57-59] For the 4-X-guaiacols (X = F, Cl, Br), dehalogenation products were also identified, an expected result given the DHP-catalyzed oxidative dehalogenation of 2,4,6-trihalophenols to their corresponding 2,6-dihaloquinones has been well established.[19, 55]

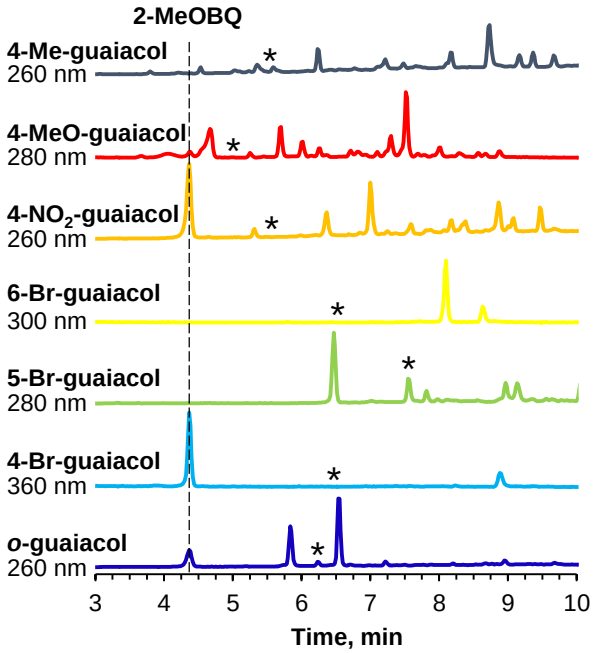

Figure 2.2 HPLC chromatograms at the indicated detection wavelength depicting the reaction of DHP B with guaiacol substrates. Reaction conditions: [DHP B] = 10 µM, [guaiacol] = [H_2O_2] = 500 µM; 5% MeOH/100 mM KP_i (v/v) at pH 7. The reaction was quenched after 5 minutes with the addition of excess catalase (t_R = 9 min). The 2-MeOBQ product is highlighted at t_R = 4.5 min. * = retention time of initial substrate.

Interestingly, a common product with a characteristic retention time of t_R = 4.5 min was observed in the oxidation of six substrates: *o*-guaiacol, 4-X-guaiacol (X = F, Cl, Br), 4-MeO-

guaiacol and 4-NO_2-guaiacol. This product exhibited an identical retention time, UV−visible spectrum (Figure S2), and mass (m/z 139.04, $[M + H]^+$) as an authentic commercial sample of 2-methoxy-1,4-benzoquinone (2-MeOBQ; see Figure S3 for the corresponding calibration curve). The amount of 2-MeOBQ produced varied 10-fold across these six substrates: 4-F-guaiacol (398 ± 14 μM), 4-Cl-guaiacol (397 ± 23 μM), 4-Br-guaiacol (374 ± 3 μM), 4-MeO-guaiacol (231 ± 1 μM), 4-NO_2-guaiacol (42 ± 3 μM), and *o*-guaiacol (35 ± 1 μM), representing 80%, 79%, 75%, 46%, 8.3% and 7.0% of the starting material being converted to 2-MeOBQ, respectively. Formation of 2-MeOBQ implies dehalogenation (-HX, X = F^-, Cl^-, Br^-), loss of methanol (-MeOH) or loss of nitrite (HNO_2) from the aforementioned substrates, although no attempts to identify the leaving groups were made. No such 2-MeOBQ product was seen in the reactions with 4-Me-guaiacol, 5-Br-guaiacol, or 6-Br-guaiacol. In the presence of the radical scavenger DMPO, the 2-MeOBQ product was unaffected for the 4-Br-guaiacol reaction, however no 2-MeOBQ was observed when DMPO was included in the reaction with 4-NO_2-guaiacol, and fewer product peaks were noted in the reaction with 5-Br-guaiacol (data not shown).

Isotopically-labeled Oxygen Studies. To determine the origin of the O-atom incorporated into the 2-MeOBQ product, studies employing labeled $H_2{}^{18}O$ and $H_2{}^{18}O_2$ (98% and 90% ^{18}O-atom enriched, respectively) were performed with 4-Br-guaiacol as the substrate, and subsequently analyzed by LC-MS. The corresponding background-subtracted total ion chromatograms (TICs) are shown in Figure 3. In the presence of unlabeled H_2O and $H_2{}^{18}O_2$, no significant increase in mass was observed (*m/z*: 139.04; Figure 3A), when compared to the unlabeled H_2O/H_2O_2 conditions (*m/z*: 139.04; data not shown), suggesting that the source of O-atom incorporation was not H_2O_2. The reaction employing $H_2{}^{18}O$ and unlabeled H_2O_2 resulted in an increase of 2 and 4 Da in 2-MeOBQ (*m/z*: 139.04, 4.9%; 141.04, 38.1%, 143.04, 57.0%; Figure 3B), suggesting

scrambling from solvent was occurring for both O atoms in 2-MeOBQ. Importantly, the $H_2{}^{18}O/H_2{}^{18}O_2$ double-label reaction produced similar results (*m/z*: 139.04, 6.1%; 141.04, 40.3%, 143.04, 53.6%; Figure 3C) as the $H_2{}^{18}O/H_2{}^{16}O_2$ reaction, providing unequivocal evidence that the O-atom was derived from exclusively from H_2O with no O-atom incorporation from H_2O_2, consistent with a peroxidase mechanism for guaiacol oxidation by DHP.

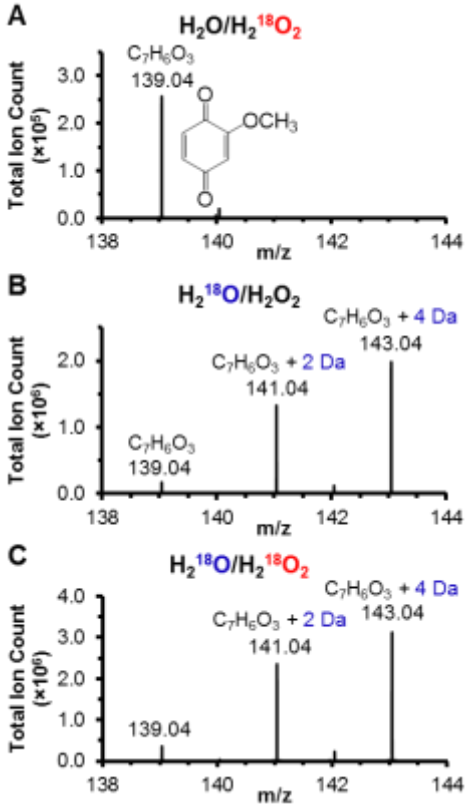

Figure 2.3. ESI-MS total ion chromatogram for the DHP B and 4-Br-guaiacol reaction product. A) $H_2{}^{16}O/H_2{}^{18}O_2$, B) $H_2{}^{18}O/H_2{}^{16}O_2$, and C) $H_2{}^{18}O/H_2{}^{18}O_2$. Reaction conditions: [DHP] = 10 µM, [4-Br-guaiacol] = [H_2O_2] = 500 µM, 5% MeOH/100 mM KPi (v/v) at pH 7 and 25 °C.

Guaiacol Binding Studies. The electronic absorption spectra of ferric DHP B in the presence of guaiacol substrates were recorded in 100 mM KP_i (pH 7) containing 6.25% MeOH (v/v). No significant systematic changes in the Soret band were observed upon ligand binding (data not shown), thus precluding its use for substrate binding studies. The Q-band region, however, showed

well-behaved optical difference spectra (Figures S4 and S5) upon titration of the guaiacol substrates (3.75-100 eq), enabling the determination of the corresponding apparent dissociation constants (K_d values). In general, the substituted guaiacols exhibited weaker binding affinities to ferric DHP B than other substrates/ligands, including haloindoles,[24] nitrophenols,[34] and azoles[35] (Table 2). For the 4-X-guaiacol panel of substrates, a trend in K_d was observed of increasing binding affinity as the size of the halogen atom increased: H < F < Cl < Br. An identical trend has been previously noted for the 5-X-indole series (F < Cl < Br < I) as observed in both substrate binding and resonance Raman studies,[24] and correlates well with the increased affinity of the halogen for occupying the Xe1 binding site (a hydrophobic cavity surrounded by amino acids L100, F21, F24, F35, and V59) as determined from crystallographic studies of 4-halophenols binding to DHP.[60] When compared to the binding of the known[42] DHP B inhibitor 4-Br-phenol (1.15 mM[56]), the 4-Br-guaiacol binding affinity is significantly stronger, which rationalizes the minimal impact this inhibitor had on 4-Br-guaiacol conversion (*vide supra*).

Table 2.2. K_d Values for Substrate Binding to Ferric WT DHP B at pH 7.

Substrate	K_d (μM) at pH 7	Reference
Guaiacol		
o-guaiacol	14712 ± 714	[a]
4-F-G	2438 ± 207	[a]
4-Cl-G	493 ± 53	[a]
4-Br-G	374 ± 42	[a]
4-MeO-G	*n.d.*	[a]
4-Me-G	1433 ± 97	[a]
4-NO_2-G	1341 ± 26	[a]
5-Br-G	1745 ± 340	[a]
6-Br-G	1332 ± 342	[a]
Phenol		
4-BP	1150	56
4-NP	262 ± 23	34
2,4-dNP	105 ± 21	34
Indole		
5-Cl-indole	317 ± 23	24
5-Br-indole	150 ± 10	24
5-I-indole	62 ± 10	24
Azole		
imidazole	52 ± 2	35
benzotriazole	82 ± 2	35
benzimidazole	110 ± 8	35

[a] this work; *n.d.*, no detectable change in absorbance after addition of 100 equiv 4-MeO-G.

X-ray Crystallographic Studies of WT DHP B Complexed with Guaiacols. Crystal structures were determined to atomic resolution for DHP in complex with five different guaiacol substrates. X-ray data collection and refinement statistics are provided in Table S3, and selected distances are provided in Table 3. For each structure, WT DHP B crystallized with two molecules (A and B) per asymmetric unit, in agreement with all previously reported dehaloperoxidase crystal structures.[19] Each guaiacol substrate (4-Br-G, 5-Br-G, 6-Br-G, 4-NO_2-G and 6-MeO-G) was found to bind in the distal pocket (Figure 4) with partial occupancy, sharing the distal pocket with a water molecule ligated to the heme Fe. As such, these DHP–guaiacol complexes are the first examples observed of ligand binding in DHP without the displacement of the distal water molecule. With the exception of 5-Br-G, all guaiacols exhibited a single binding site that was virtually identical for 4-

Br-G (Figure 4A), 4-NO_2-G (Figure 4E) and 4-MeO-G (Figure 4D): the substrates were oriented for favorable π-stacking interactions with F21, their methoxy substituents were found in the Xe1 binding site (a hydrophobic cavity surrounded by amino acids L100, F21, F24, F35, and V59 that was shown to bind Xe),[60] the 4-X substituents (Br, NO_2 or MeO groups) were directed away from the heme in a hydrophobic region deeper in the distal cavity (reorienting F60 to accommodate the bulkier NO_2 and MeO substituents), and the phenolic OH for each was directed toward the heme Fe and within H-bonding distance to both H55 (N^{ε}) and the heme-bound distal water. Two conformations were observed for 5-Br-G, assigned as 5-Br-G_A and 5-Br-G_B: the binding orientation of 5-Br-G_A (Figure 4B) is similar to the 4-X-G (X = Br, NO_2 or MeO) binding sites, however the Br atom resides closer to the cavity entrance. In addition, the 4-X-G molecules are better positioned for stronger π-stacking interactions with F21 than 5-Br-G_A, which is reflected in i) the 4.6-fold and 1.3 fold stronger binding affinities of 4-Br-G and 4-NO_2-G, respectively, when compared to 5-Br-G, and ii) higher occupancies of the 4-X-G substrates compared to 5-Br-G (4-Br-G, 90% > 4-MeO-G, 75% > 4-NO_2-G, 70% > 5-Br-G, 35%$_A$/30%$_B$). In contrast, a rotation of the guaiacol molecule in the distal pocket was observed for 5-Br-G_B and 6-Br-G (Figures 4B and 4C), with the Br atoms located in the Xe1 binding site, the OH and methoxy groups oriented toward the top of the distal pocket, reduced π-stacking interactions with F21, and the unsubstituted region of the ring directed toward the heme cofactor. H55 is out of optimal H-bonding distance with regard to 5-Br-G_B (Table 3), yet is well-positioned to interact with the MeO oxygen of 6-Br-G.

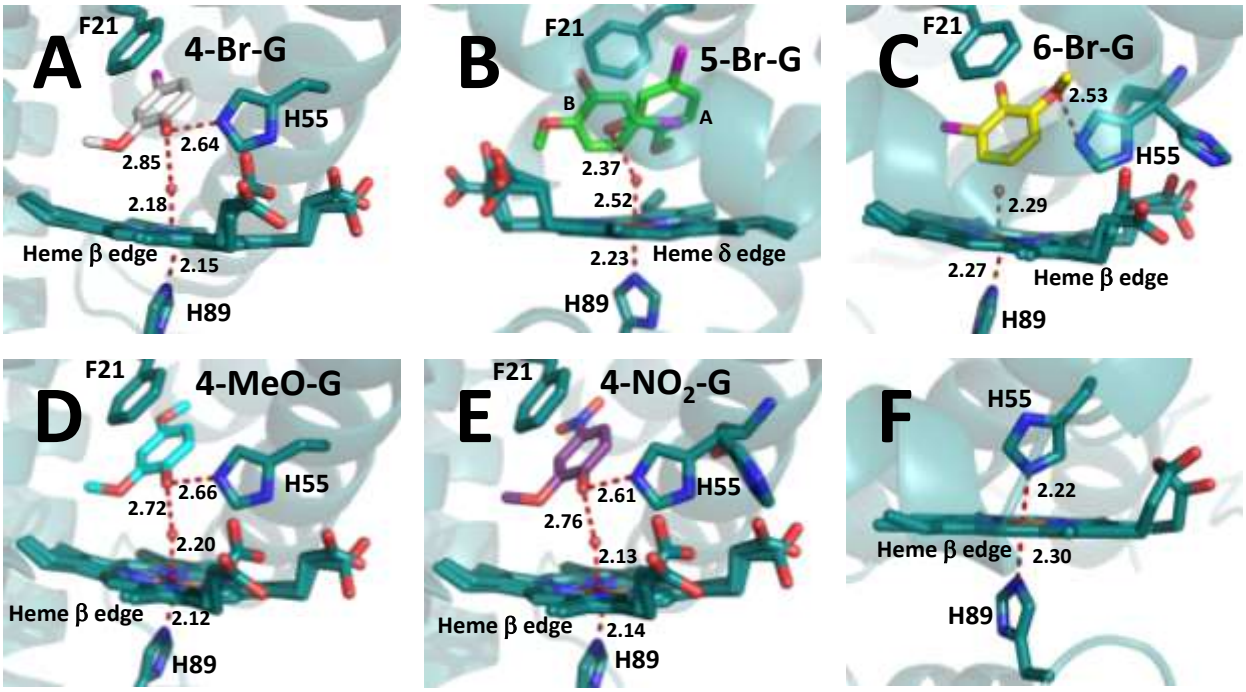

Figure 2.4. X-ray crystal structures of DHP B complexed with A) 4-Br-guaiacol (gray; 6CKE), B) 5-Br-guaiacol (green; 6CRE), C) 6-Br-guaiacol (yellow; 6CO5), D) 4-methoxy-guaiacol (cyan; 6CH6), and E) 4-nitro-guaiacol (purple; 6CH5). The Br atom for each substrate in panels A-C is colored magenta for clarity. F) The bis-histidine hexacoordinated form of DHP.

As a side note, each guaiacol structure exhibited one of the two protomers in a bis-histidine ligated (hexacoordinated) heme orientation (Figure 4F). We have previously[35] observed such a hemichrome species in DHP B when complexed with benzotriazole using crystals grown from PEG 4000 (as opposed to PEG 3350 here). Other DHP complexes (unpublished results) have exhibited the bis-histidine ligation in a single protomer when PEG 3350 was used, and as such we surmise that this coordination is attributable to the use this precipitant during crystallization, and is not exclusive to the guaiacol complexes. The functional consequences (if any) of the bis-histidine ligation were not further explored here.

Table 2.3. Selected distances (Å) for DHP B-guaiacol complexes (protomer A).[a]

	4-Br-G [b]	**5-Br-G**	**6-Br-G** [b]	**4-NO_2-G**	**4-MeO-G**
PDB accession code	6CKE	6CRE	6CO5	6CH5	6CH6
Substrate occupancy	90%	A: 35% / B: 30%	40%	70% [c]	75%
Distal H_2O occupancy	100%	58%	34%	100%	90%
H55 $N^{\varepsilon}\cdots OH$ (guaiacol)	2.64^{int}	$2.47_A{}^{int}/6.52_B{}^{ext}$	4.78^{ext}	$2.61^{int}/8.35^{ext}$	$2.66^{int}/9.54^{ext}$
H55 $N^{\delta}\cdots OH$ (guaiacol)	4.62^{int}	$4.42_A{}^{int}/5.51_B{}^{ext}$	6.38^{ext}	$4.55^{int}/7.34^{ext}$	$4.65^{int}/7.55^{ext}$
F21 $C^{\zeta}\cdots C^1$ (guaiacol)	3.76	4.17_A (C^2)/4.36_B (C^3)	4.05 (C^4)	3.71	3.73
F21 $C^{\gamma}\cdots C^4$ (guaiacol)	3.97	3.67_A (C^5)/3.76_B (C^6)	3.71 (C^1)	3.78	3.93
Fe···OH (guaiacol)	4.85	$4.78_A/7.28_B$	6.75	4.75	4.74
$Fe\cdots O^{C2}$ (guaiacol)	4.62	$4.71_A/6.08_B$	6.96	4.71	4.68
Fe···X (guaiacol)	Br^{C4}: 8.43	Br^{C5}: $8.21_A/5.43_B$	Br^{C6}: 5.61	N^{C4}: 8.04	O^{C4}: 7.85
$^{guaiacol}OH\cdots$distal H_2O	2.85	2.37_A	----	2.76	2.72
Fe···distal water	2.18	2.52	2.29	2.13	2.20
Fe···H55 N^{δ}	6.68	$6.38^{int}/8.98^{ext}$	6.54	$6.44^{int}/8.80^{ext}$	$6.64^{int}/9.73^{ext}$
Fe···H55 N^{ε}	6.01	$5.84^{int}/10.17^{ext}$	5.68	$5.88^{int}/10.18^{ext}$	$5.91^{int}/11.59^{ext}$
Fe···H89 N^{ε}	2.15	2.23	2.27	2.14	2.12
Fe to pyrrole-N plane	0.062	0.063	0.062	0.059	0.059

[a] the two 5-Br-G conformations are denoted as subscripted A or B as shown in Figure 4B, and the two H55 conformations are designated as interior (^{int}) or exterior (^{ext}). [b] for 4-Br-G and 6-Br-G, H55 was found to be exclusively in the interior and exterior conformations, respectively. [c] 4-NO_2–G also exhibited an additional slightly shifted conformation, but of minor occupancy, and therefore not described.

Stopped-flow UV-visible Spectroscopic Studies with 4-Br-guaiacol. Single and double-mixing stopped-flow UV-visible spectroscopic methods were used to investigate the reaction of 4-Br-guaiacol (as a representative 4-X-guaiacol substrate) with DHP B. Studies were performed with H_2O_2-activated DHP B (i.e., pre-formed as Compound I [DHP B(Y28F/Y38F)],[31] Compound ES,[32, 40] or Compound II[41]), or by pre-incubating DHP B with 4-Br-guaiacol followed by addition of H_2O_2. For the majority of the studies described below, the data did not properly fit one-step/two species or two-step/three species irreversible mechanisms, and as such experimentally obtained spectra at selected time points detailed in the figure legends are shown.

Compound I Reactivity – Generated in an initial mixing step of ferric DHP B (Y28F/Y38F) with 10 equiv H_2O_2 in an aging line for 85 ms,[31] Compound I was reacted with 10 equiv 4-Br-guaiacol at pH 7. The activated enzyme, Compound I [406 (Soret), 528, and 645 nm], was not observed (Figure 5A). Rather, ferric-like DHP B (Y28F/Y38F) [406 (Soret), 513, 640 (sh) nm, black] was the first spectrum recorded, and suggested that Compound I was reduced by the substrate within the mixing time (1.5 ms) of the stopped-flow apparatus. The rapid reaction of Compound I with 4-Br-guaiacol is virtually identical to its reactivity seen with 5-Br-indole,[24] 4-nitrophenol[34] and pyrrole[25] in that these substrates were also able to reduce Compound I to the ferric enzyme within the stopped-flow mixing time. The ferric enzyme then converted to a new DHP B species [427 (Soret), 556, and 578 (sh) nm, blue; t = 246 s] that appeared to be a mixture of both ferrous and oxyferrous DHP.[41]

Compound ES Reactivity – Ferric WT DHP B was rapidly mixed with 10 equiv of H_2O_2 at pH 7, incubated for 500 ms to allow for the maximum accumulation of Compound ES (ferryl heme + tyrosyl radical),[40] and subsequently mixed with 10-50 equiv 4-Br-guaiacol. As a representative reaction, the preformed Compound ES [418 (Soret), 546, 582 nm, black; t = 0 s] was converted in the presence of 10 equiv 4-Br-guaiacol to ferric DHP B [407 (Soret), 505, 640 (sh) nm, red; t = 8.8 s] that underwent further reduction to the resting oxyferrous state after 500 s (Figure 5B, Table 4). The progression of initial Compound ES reduction to the ferric enzyme, followed by a slower reduction to oxyferrous DHP, mirrors previous observations of Compound ES reactivity with haloindoles[24] and halophenols,[40] suggesting the similar product-driven reductions that occurred in those studies may also be present here with the guaiacol substrates.

Compound II Reactivity – Formed after 3 s in an ageing line from an initial mixing step of 10 equiv H_2O_2 with oxyferrous WT DHP B that was pre-incubated with 1 equiv 2,4,6-

trichlorophenol,[41] Compound II was reacted with 10 equiv 4-Br-guaiacol. The preformed Compound II [420 (Soret), 546, 584 nm, black; t = 0 s] initially converted to ferric DHP B [407 (Soret), 505, 640 (sh) nm, red; t = 17.4 s], was further reduced to oxyferrous DHP B [416 (Soret), 542, 578 (sh) nm, blue; t = 246 s], and remained stable as this species for the duration of the 500 s observation time (Figure 5C). The reduction of Compound II to ferric DHP by 4-Br-guaiacol here parallels the same observations made when employing TCP,[41] haloindole,[24] and pyrrole[25] substrates, as does the further reduction (presumably product-driven) to oxyferrous DHP, albeit virtually complete formation (in lieu of a mixture of ferric/oxyferrous DHP) was observed here (*vide infra*).

Oxyferrous Reactivity – It has been previously shown that oxyferrous DHP can be activated by H_2O_2 in the presence of halophenol,[41, 61, 62] haloindole,[24] and pyrrole[25] substrates, whereas in their absence, only a slight bleaching of the Soret band and/or long time scale conversion to Compound RH is observed. To investigate if guaiacols are able to facilitate this substrate-dependent activation of DHP, stopped-flow methods were employed to rapidly mix H_2O_2 (10 equiv) with a solution of oxyferrous DHP B that was preincubated with 10 equiv of 4-Br-guaiacol. The following spectral changes were noted: oxyferrous DHP B [416 (Soret), 542, 578 nm, black; t = 0 s] was oxidized to ferric DHP B [407 (Soret), 501, 640 (sh) nm, red; t = 7.3 s], followed by a gradual reduction back to the oxyferrous state [413 (Soret), 541, 578 nm, blue; t = 500 s] (Figure S6). Interestingly, no transiently-observed ferryl species were formed, which differs from the reaction performed in the presence of halophenol,[41] haloindole[24] and pyrrole[25] substrates where the Compound II intermediate was observed.

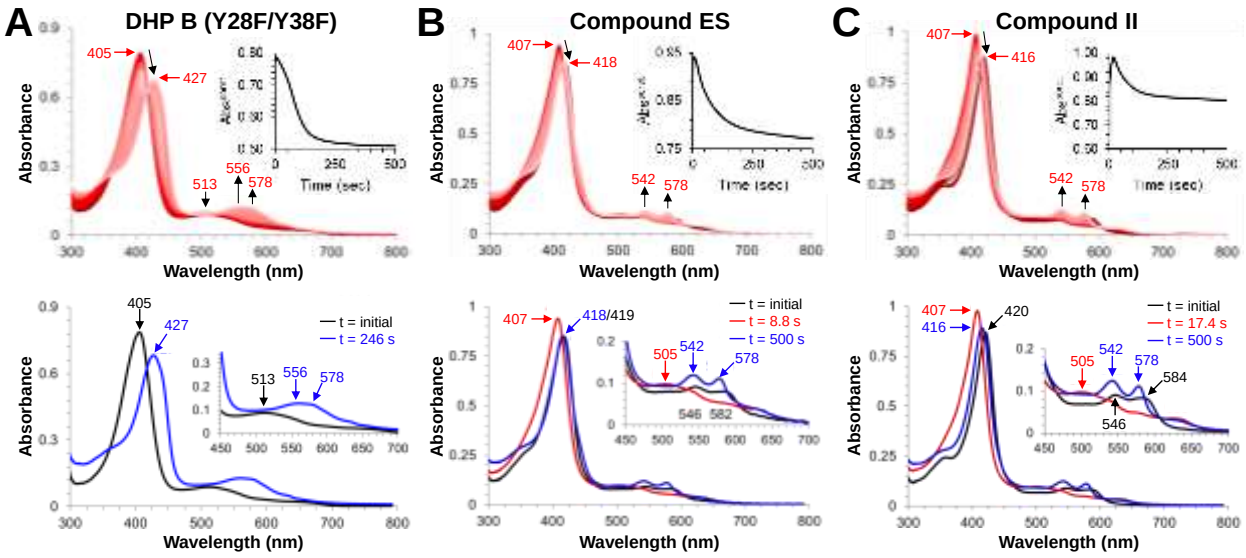

Figure 2.5. Kinetic data for the reaction of H_2O_2-activated DHP B with 4-Br-guaiacol. **A) DHP B (Y28F/Y38F):** top panel, stopped-flow UV−visible spectra of the double-mixing reaction of preformed Compound I (10 μM) with a 10-fold excess of 4-Br-guaiacol at pH 7.0 (900 scans over 500 s); inset: the single wavelength (408 nm) dependence on time obtained from the raw data; *bottom panel*, experimentally obtained spectra for Compound I reacted with 4-Br-guaiacol (black, t = 0 s), and its reduction to a ferrous-like species of DHP B was observed in the presence of 4-Br-guaiacol (blue, t = 246 s). **B) Ferric DHP B/Compound ES:** *top panel*, stopped-flow UV−visible spectra of the double-mixing reaction between ferric DHP B (10 μM) premixed with 10 equiv of H_2O_2 (500 ms) and then reacted with 10 equiv 4-Br-guaiacol at pH 7.0 (900 scans over 500 s); inset: the single wavelength (408 nm) dependence on time obtained from the raw data; *bottom panel*, experimentally obtained spectra of Compound ES (black, t = 0 s) reacted with 4-Br-guaiacol, resulting in ferric DHP B (red, t = 8.8 s) and further reduction to oxyferrous DHP B (blue, t = 500 s). **C) Ferric DHP B/Compound II:** *top panel*, stopped-flow UV−visible spectra of the single-mixing reaction between Compound II and 4-Br-guaiacol. Compound II was formed from an initial reaction between oxyferrous DHP B (10 μM) preincubated with 1 equiv of trichlorophenol and 10 equiv of H_2O_2 and reacted for 3 s prior to the second mix with 4-Br-guaiacol at pH 7.0 (900 scans over 500 s); inset: the single wavelength (408 nm) dependence on time obtained from the raw data; *bottom panel*, experimentally obtained spectra of Compound II (black, t = 0 s) reacted with 4-Br-guaiacol, resulting in ferric DHP B (red, t = 17.4 s) and further reduction to oxyferrous DHP B (blue, t = 246 s).

Double-mixing stopped-flow UV-visible spectroscopic methods were also used to investigate the reactivity of the remaining guaiacol substrates (10-50 equiv) with pre-formed Compound ES in a manner identical to that described above for 4-Br-guaiacol. Figures S7 and S8 display representative reactions of preformed Compound ES [418 (Soret), 546, 582 (sh) nm, black; t = 0

s] with 10 equiv of each of the guaiacol substrates, and Table 4 summarizes the optical data. Although the time required to do so varied over 40-fold (4.37 – 186 s), all substrates were found to reduce Compound ES to ferric DHP B. However, while four (*o*-guaiacol, 4-Br-G, 4-MeO-G, 4-NO_2-G) of the seven guaiacol reactions were found to further reduce the resultant ferric enzyme to the oxyferrous state, two were unable to do so: 4-Me-guaiacol (Figure S8A) and 5-Br-guaiacol (Figure S8B). Rather, the enzyme converted to a mixture of ferric DHP and the peroxidase-attenuated state Compound RH.[31, 32, 40] *Importantly*, the formation of oxyferrous DHP in these stopped-flow studies strongly correlated with the observation of 2-MeOBQ as identified in the HPLC studies above, suggesting that 2-MeOBQ could serve as a reducing agent of ferric DHP (*vide infra*). In the case of 6-Br-guaiacol (Figure S8C), the formation of a product that exhibited a strong absorption band ~450 nm that overlapped with the Soret and Q bands prevented any conclusive spectral assignments.

The main observations from these stopped-flow studies were i) H_2O_2-activated enzyme was reduced to ferric DHP by 4-Br-guaiacol, with the rate of reduction following the order: Compound I > Compound ES > Compound II, ii) the oxyferrous enzyme reacted with H_2O_2 in the presence of 4-Br-guaiacol, however without the formation of an observable Compound II species, iii) all of the reactions with 4-Br-guaiacol yielded oxyferrous DHP as a final observable species, and iv) 2-MeOBQ was identified as the putative reductant.

Table 2.4. Summary of Stopped-Flow UV-vis Spectroscopic Data for the Reaction of Compound ES with Guaiacol Substrates at pH 7.

Substrate	Compound ES → Ferric, time (s)	Observed ferric species λ_{max} (nm)	Ferric → Oxyferrous, time (s)	Final observed species λ_{max} (nm)
***o*-guaiacol**	26	409, 504, 640	> 500	411, 540, 578 (oxy/ferric mixture)
4-Br-G	9	407, 505, 640	> 500	418, 542, 578 (oxy)
5-Br-G	5	411, 505, 640	n/a	411, 505, 640 (Compound RH-like)
6-Br-G	n/o	n/o	n/o	420, 455 (product)
4-NO_2-G	186	410, 539 (sh)	> 500	412, 539, 576 (oxy/ferric mixture)
4-MeO-G	42	409, 503, 640	250	418, 543, 578 (oxy)
4-Me-G	30	409, 503, 640	n/a	409, 503, 640 (Compound RH-like)

n/a: not applicable (i.e., oxyferrous DHP was not formed)
n/o: not observable owing to product formation at 455 nm

Reduction of Ferric DHP B by 2-MeOBQ. Stopped-flow UV/visible spectroscopic methods were employed to explore if the 2-MeOBQ product was capable of the aerobic reduction of ferric DHP to yield the oxyferrous enzyme observed in the above studies. A solution of 8 μM ferric DHP B was rapidly mixed with authentic 2-MeOBQ (62.5 μM, Figure 6; 0.625, 6.25, and 625 μM, Figure S9) at pH 7, and monitored for 50 s. For 2-MeOBQ concentrations of 6.25-625 μM, the data were best fit to a two-step, three species irreversible mechanism: the first step (k_1) yielded an initial oxyferrous-like species whose spectral features were similar, but not identical, to oxyferrous DHP B [UV-visible spectrum: 419-20 (Soret), 542-4, 578 nm] that was subsequently fully formed in the second step (k_2). Interestingly, the reaction exhibited saturable kinetics with respect to k_1 and 2-MeOBQ, whereas k_2 was [2-MeOBQ]-independent (Figure S10). Even at a sub-stoichiometric concentration of 0.625 μM 2-MeOBQ (Figure S9A), a partial formation of oxyferrous DHP was observed. Overall, the reduction observed here with 2-MeOBQ was appreciably faster than that observed previously with 2,6-dichloro-1,4-dibenzoquinone (DCQ: k_{obs}

= 0.085 s^{-1}),[40] which is the product of the DHP-catalyzed oxidative dehalogenation of 2,4,6-trichlorophenol. These results support a "product-driven" reduction wherein the 2-MeOBQ product of guaiacol-oxidation via a DHP peroxidase activity reduces the peroxidase-active ferric DHP B to its hemoglobin-active oxyferrous state.

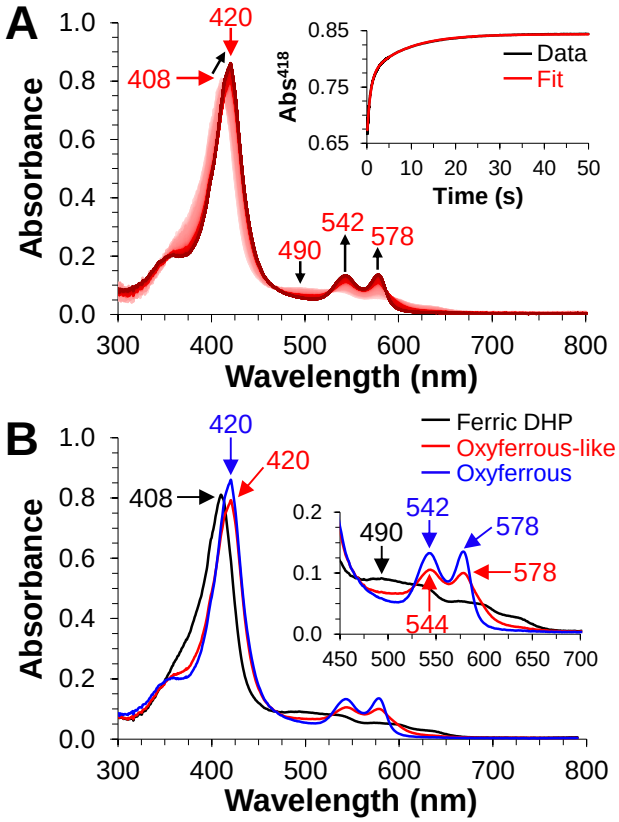

Figure 2.6. Kinetic data for the reaction of 2-MeOBQ with ferric DHP B. A) Stopped-flow UV−visible spectra of the single-mixing reaction between ferric DHP B (10 μM) reacted with 62.5 μM 2-MeOBQ at pH 7.0 (900 scans over 50 s); inset: the single wavelength (418 nm) dependence on time obtained from the raw data (black) and the corresponding fit (red). B) Calculated spectra of the three reaction components derived from the SVD analysis: ferric DHP B (black), an apparent mixture of ferric and oxyferrous DHP B (red), and oxyferrous DHP B (blue).

DISCUSSION

The activity studies reported here demonstrate that DHP B was able to catalyze the conversion of all guaiacols studied under physiological conditions. With the exception of *o*-guaiacol that only had a 30% conversion to products, both monosubstituted native-halogenated guaiacols (-F, -Cl, -

Br) and nonnative guaiacols (-Me, -OMe, -NO_2) were converted in high yields (>90%) to monomeric and oligomeric product(s). Isotopic labeling studies unequivocally demonstrated that the oxygen atom incorporated into the products for the 4-Br-guaiacol reaction originated exclusively from H_2O, while radical scavengers were shown to inhibit substrate conversion. Together, these results provide support that guaiacol oxidation follows a radical-based peroxidase mechanism. Moreover, the oxidation of the guaiacol substrates could be initiated from either the traditional peroxidase ferric oxidation state, or from the oxyferrous form of the enzyme that is relevant to the O_2-transport function of DHP as the coelomic hemoglobin of *A. ornata*.

These results are consistent with the well-established peroxidase activity of DHP B with trihalophenol substrates,[11] as well as with previous studies of guaiacol oxidation by other peroxidase enzymes, specifically myoglobin and other heme peroxidases where it has been used as a classic substrate in kinetic assays owing to the formation of the highly colored (λ_{max} = 470 nm) 3,3'-dimethoxy-4,4'-biphenoquinone reaction product.[58, 63] Some notable examples of guaiacol oxidation in these systems include i) monitoring the peroxidase activity of myoglobin mutants via guaiacol oxidation,[64-66] and ii) the oxidation of guaiacol by horseradish peroxidase,[57, 59] lignin peroxidase,[10] and manganese peroxidase.[67] In those systems, the products were identified as guaiacol dimers (i.e., 3,3'-dimethoxy-4,4'-biphenoquinone and its reduced analog 3,3'-dimethoxy-4,4'-diphenol), trimers, and tetramers, with the guaiacol moieties linked through the carbon ortho to the phenol group.[57] The monomer, 2-MeOBQ, however was not observed in those studies, but it has been previously identified in the case of laccase-catalyzed phenol dehydrogenation,[68] and in studies of guaiacol oxidation employing small molecule catalysts (i.e., silver oxide, ferric chloride and chromium trioxide).[69, 70] The results presented herein demonstrate that DHP B is capable of oxidizing 4-R-guaiacols (with the exception of R = Me) to 2-MeOBQ,

either as the major product (R = F, Cl, Br), or as a minor product (R = H, MeO, NO_2).

The formation of 2-MeOBQ further establishes the 'product-driven' reduction observed in DHP that appears to be a hallmark of this catalytic hemoglobin: at +206 ± 6 mV,[40] the Fe^{III}/Fe^{II} redox couple for DHP B is higher than most other hemoglobins (e.g., human Hb, + 158 mV;[71] horse heart Hb, + 152 mV;[72] horse heart Mb, + 46 mV;[73] sperm whale Mb, −43 mV[74]), and significantly more so than other peroxidases (e.g., myeloperoxidase, −5 mV;[75] cytochrome *c* peroxidase, −182 mV;[76] HRP, −266 mV[77]). Demonstrated first with 2,6-dichloroquinone (DCQ),[40] the oxidation product of its peroxidase activity with 2,4,6-trichlorophenol, and later with 5-Br-3-oxindole,[24] the oxidation product of its peroxygenase activity with 5-Br-indole, DHP has been shown (almost counterintuitively) to be susceptible to reduction by the oxidation products of its catalytic activities. Here, we provide strong evidence that the 'product-driven' reduction is attributable to 2-MeOBQ, which may serve as a 'rescue' of the enzyme to return to its oxyferrous state, thereby enabling this multifunctional hemoglobin to maintain its O_2-transport function after cycling peroxidase activity.

Importantly, activation of oxyferrous DHP in the presence of guaiacol substrate and H_2O_2 was also demonstrated, suggesting that the entire catalytic cycle can be initiated from, and ultimately return to, the hemoglobin-active O_2-carrier state. How such a substrate-dependent activation of oxyferrous DHP occurs has been the subject of several studies, and two possible mechanisms have been suggested: i) trace amounts of the ferric enzyme react with H_2O_2 and substrate, thereby generating diffusible substrate radicals that oxidize oxyferrous DHP to the catalytically-active ferric form,[61, 62] or ii) substrate binding to DHP destabilizes the oxyferrous state in the presence of hydrogen peroxide, leading to a reaction between ferrous DHP and H_2O_2 that activates the enzyme via a Compound II intermediate that is subsequently quickly reduced to the ferric enzyme.[41] Here,

we employed the spin trap 5,5-dimethyl-1-pyrroline-N-oxide (DMPO) to scavenge diffusible radicals, and noted that the 4-Br-guaiacol reaction was unaffected by DMPO, giving the same substrate conversion and 2-MeOBQ product formation observed in its absence. Accordingly, these data suggest that the reaction of 4-Br-guaiacol does not generate a diffusible radical species, and although they are not directly supportive of an oxyferrous destabilization mechanism, appear to rule out the one involving diffusible substrate radicals. However, as both 5-Br-G and 4-NO_2-G exhibited reduced substrate conversion in the presence of the spin trap, we cannot rule out a substrate radical-based oxyferrous activation mechanism for these substrates.

The lack of an effect by DMPO on 4-Br-guaiacol reactivity suggests that either two successive one-electron oxidation steps[78] occur without the substrate radical diffusing out of the active site, or that a single two-electron oxidation occurs. The question thus arises as to why oxidation via electron transfer is preferred with guaiacol substrates, as opposed to O-atom transfer, given that DHP is capable of both. To address this, we turn to the X-ray crystallographic studies to provide insight: 4-Br-G, 5-Br-G_A, 4-NO_2-G and 4-MeO-G bind near the α-edge of the heme cofactor (Figure 7, panels A and B), similar to other peroxidase substrates, i.e., TBP[79] and one of the two TCP[27] sites (Figure 7, panels C and D). In the context of the comparisons shown in Figure 1, the X-ray crystal structures demonstrate the following: i) when compared to the peroxygenase substrate 4-nitrophenol (4-NP) binding site (Figure 7C/D, blue),[34] which is positioned close to the heme center in an orientation that allows for direct O-atom transfer from the activated ferryl intermediate, the 4-Br-G, 5-Br-G_A, 4-NO_2-G and 4-MeO-G binding sites are at a greater distance from the heme Fe that is not conducive to O-atom transfer; ii) when compared to the 4-Br-phenol inhibitor site (Figure 7C/D, orange) that binds directly above the heme-Fe in a manner that likely inhibits H_2O_2 activation, 4-Br-G resides further from the heme face, allowing for H_2O_2 binding

and subsequent catalytic activity; and iii) although the structure of the DHP–*o*-guaiacol complex was not obtained, we can surmise that it likely either binds in a nearly identical fashion as 4-Br-G, or that the methoxy substituent re-orients to occupy the Xe1 site, either of which would preclude O-atom transfer on the basis of distance arguments. Finally, the crystal structures also demonstrate that the hypothetical site of oxygen atom insertion (i.e., the phenol ring carbon closest to the activated heme) is sterically hindered by the methoxy group itself, thus precluding oxygen atom transfer and supporting oxidation via electron transfer (i.e., a peroxidase mechanism). Interestingly, the guaiacol substrates that share a common binding motif, i.e. 4-Br-G, 4-NO_2-G, 4-MeO-G (and presumably including 4-F-G and 4-Cl-G whose structures were not determined but are likely similar to that of the brominated analog), all form 2-MeOBQ as their primary oxidation product. Taken together, the methoxy substituent appears to play a role in positioning the guaiacol substrate for oxidation via electron (but not O-atom) transfer, with the substitution pattern on the phenol ring (4-X vs. 5/6-X) also dictating product outcome.

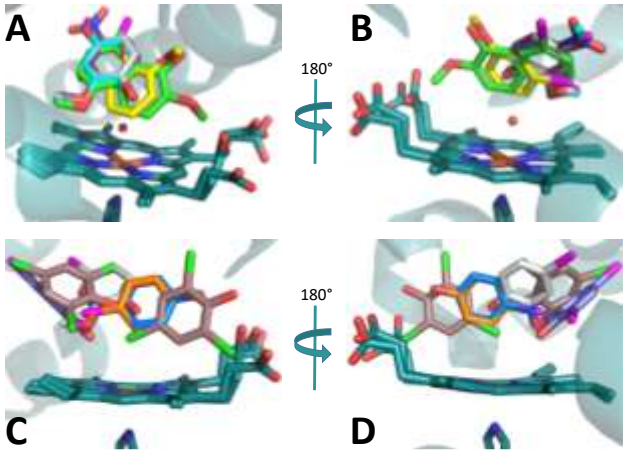

Figure 2.7. Superposition of selected DHP substrates. Guaiacol binding sites superposition provided in panels **A** and **B** for 4-Br-G (silver, 4CKE), 5-Br-G (green, 5CRE), 6-Br-G (yellow, 6CO5), 4-NO_2-G (purple, 6CH5) and 4-MeO-G (cyan, 6CH6). Panels **C** and **D** provide the superposition of 4-Br-G (silver) with peroxidase substrates TBP (purple, 4FH6[79]) and TCP (brown, 4KMW and 4KMV[27]), peroxygenase substrate 4NP (blue, 5CHQ[34]) and inhibitor 4BP (orange, 3LB2[56]).

On the basis of the results obtained above, and through previously established mechanisms for peroxidases (including dehaloperoxidase,[19, 21, 40] and more traditional ones such as HRP[80]), we propose the following catalytic cycle for the *in vitro* hydrogen peroxide-dependent oxidation of guaiacols by DHP (Scheme 1): ferric DHP B reacts with 1 equiv H_2O_2 forming a two-electron oxidized ferryl species (step i-a), either as Compound I [31] or Compound ES[40], which is subsequently reduced in the presence of guaiacol substrate to the ferric enzyme, yielding 2-MeOBQ. This can occur in one of two ways: the first possibility is through two consecutive one-electron oxidations[78] of 4-X-guaiacol (steps ii and iii), wherein 2-MeOBQ can form via a diffusible phenoxy 4-X-G• radical that is subsequently oxidized by activated DHP, or through the disproportionation[81] of two 4-X-G• radicals. The formation of diffusible radicals is consistent with radical-radical coupling reactions that account for the observed higher molecular weight products (i.e., dimers, trimers, etc., Table S1 and Table S2) as these are unable to form within the steric constraints of the DHP active site. The second possibility is via a direct two-electron oxidation (step i-b), i.e., in the case of 4-Br-guaiacol, where 2-MeOBQ formation occurs without a diffusible substrate radical, a result that is consistent both with the lack of observed higher molecular weight species that are derived from radical-radical recombination, and with the lack of an effect on product yield when employing the radical quencher DMPO. Regardless of which pathway results in its formation, the 2-MeOBQ product reduces ferric DHP aerobically to the oxyferrous form of the enzyme (step iv), which itself can be activated for peroxidase function in the presence of H_2O_2 and guaiacol substrate, presumably through a Compound II species (step v). These latter two steps highlight the versatility of DHP as a catalytic hemoglobin in that the resting form of the enzyme can be the O_2-transport oxyferrous state, which is typically inactive for monofunctional peroxidases.[82]

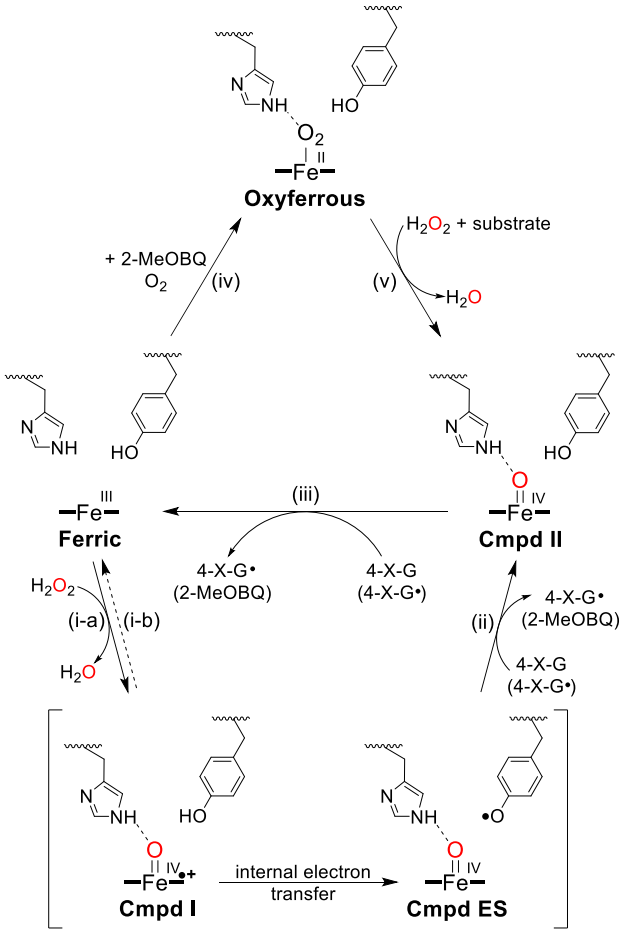

Scheme 1. Proposed catalytic cycle for the oxidation of 4-X-guaiacols by DHP B.

CONCLUSION

In summary, dehaloperoxidase has been shown to catalyze peroxidase activity with guaiacol substrates. Enzyme-catalyzed oxidations of *o*-guaiacol have been previously reported, but substituted guaiacols have remained relatively unstudied until now. In the reported system, guaiacol derivatives were found to be better substrates than the parent compound. HPLC studies indicated that the whole panel of guaiacol substrates had an extremely high substrate conversion when compared to other known DHP B substrates. The most interesting result was the 4-

haloguaiacol series resulting in 2-MeOBQ as the major product (>75 % of product distribution). Stopped-flow UV-vis studies supported that 2-MeOBQ acted similarly to the previously studied 2,6-dihaloquinone (product of TXP) in which both compounds would act as a reducing agent towards the ferric state of DHP B to return the enzyme to its oxyferrous globin resting state. These observations support that the multifunctional nature of DHP B may have evolved due to the environmental pressures of naturally produced toxic aromatic compounds. This unique substrate directed reduction and oxidation of the globin's heme center provides a mode in which DHP B can act as a globin (O_2 transport) and as an agent for organism survival against small molecule toxins. DHP's reactivity with guaiacol substrates add to a diverse and expanding list that includes trihalophenols, haloindoles, nitrophenols, and pyrroles, and further expands on DHP's unique multifunctional nature and ability to react with a wide range of substrates.

References

(1) Samet, Y.; Wali, I.; Abdelhédi, R. *Environ. Sci. Pollut. Res.* **2011**, *18* (9), 1497.
(2) Samet, Y.; Ayadi, M.; Abdelhedi, R. *Water Environ. Res.* **2009**, *81* (12), 2389–2397.
(3) Pokhrel, D.; Viraraghavan, T. *Science of the Total Environment*. 2004, pp 37–58.
(4) Lauraguais, A.; Coeur-Tourneur, C.; Cassez, A.; Deboudt, K.; Fourmentin, M.; Choël, M. *Atmos. Environ.* **2014**, *86*, 155–163.
(5) Kroflič, A.; Grilc, M.; Grgić, I. *Sci. Rep.* **2015**, *5*, 8859.
(6) Larachi, F.; Leroux, M.; Hamoudi, S.; Bernis, A.; Sayari, A. *J. Chem. Eng. Data* **2000**, *45* (2), 404–408.
(7) *Canadian Environmental Protection Act , 1999*; Minister of Justice, 1999.
(8) Agarwal, V.; El Gamal, A. A.; Yamanaka, K.; Poth, D.; Kersten, R. D.; Schorn, M.; Allen, E. E.; Moore, B. S. *Nat. Chem. Biol.* **2014**, *10* (8), 640–647.
(9) Chen, Y. P.; Woodin, S. A.; Lincoln, D. E.; Lovell, C. R. *J. Biol. Chem.* **1996**, *271* (9), 4609–4612.
(10) Osborne, R. L.; Coggins, M. K.; Raner, G. M.; Walla, M.; Dawson, J. H. *Biochemistry* **2009**, *48* (20), 4231–4238.
(11) D'Antonio, J.; D'Antonio, E. L.; Thompson, M. K.; Bowden, E. F.; Franzen, S.; Smirnova, T.; Ghiladi, R. A. *Biochemistry* **2010**, *49* (31), 6600–6616.
(12) Chen, Y. P.; Lincoln, D. E.; Woodin, S. A.; Lovell, C. R. *J. Biol. Chem.* **1991**, *266* (35), 23909–23915.
(13) Roach, M. P.; Chen, Y. P.; Woodin, S. A.; Lincoln, D. E.; Lovell, C. R.; Dawson, J. H. *Biochemistry* **1997**, *36* (8), 2197–2202.
(14) Barrios, D. A.; D'Antonio, J.; McCombs, N. L.; Zhao, J.; Franzen, S.; Schmidt, A. C.; Sombers, L. A.; Ghiladi, R. A. *J. Am. Chem. Soc.* **2014**, *136* (22), 7914–7925.
(15) McCombs, N.; Smirnova, T.; Ghiladi, R. *Catal. Sci. Technol.* **2017**.
(16) McCombs, N. L.; D'Antonio, J.; Barrios, D. A.; Carey, L. M.; Ghiladi, R. A. *Biochemistry* **2016**, *55* (17), 2465–2478.
(17) Dumarieh, R.; D'Antonio, J.; Deliz-Liang, A.; Smirnova, T.; Svistunenko, D. A.; Ghiladi, R. A. *J. Biol. Chem.* **2013**, *288* (46), 33470–33482.
(18) Feducia, J.; Dumarieh, R.; Gilvey, L. B. G.; Smirnova, T.; Franzen, S.; Ghiladi, R. A. *Biochemistry* **2009**, *48* (5), 995–1005.
(19) Castro-Forero, A.; Jimenez, D.; Lopez-Garriga, J.; Torres-Lugo, M. *J Appl Polym Sci Symp* **2009**, *107* (2), 881–890.
(20) Goral, V.; Ryabov, A. *Biochem. Mol. Biol. Int.* **1998**, *45* (1), 61–71.
(21) De Serrano, V.; D'Antonio, J.; Franzen, S.; Ghiladi, R. A. *Acta Crystallogr. Sect. D Biol. Crystallogr.* **2010**, *66* (5), 529–538.
(22) Otwinowski, Z.; Minor, W. *Processing of X-ray diffraction data collected in oscillation mode, In Methods in Enzymology*; Carter, C. W., J., Sweet, R. M., Eds.; Academic Press: New York, 1997.
(23) McCoy, A. J.; Grosse-Kunstleve, R. W.; Adams, P. D.; Winn, M. D.; Storoni, L. C.; Read, R. J. *J. Appl. Crystallogr.* **2007**, *40* (4), 658–674.
(24) Adams, P. D.; Afonine, P. V; Bunkóczi, G.; Chen, V. B.; Davis, I. W.; Echols, N.; Headd, J. J.; Hung, L.-W.; Kapral, G. J.; Grosse-Kunstleve, R. W.; McCoy, A. J.; Moriarty, N. W.; Oeffner, R.; Read, R. J.; Richardson, D. C.; Richardson, J. S.; Terwilliger, T. C.; Zwart, P. H. *Acta Crystallogr. D. Biol. Crystallogr.* **2010**, *66* (Pt 2), 213–221.
(25) Emsley, P.; Lohkamp, B.; Scott, W. G.; Cowtan, K. *Acta Crystallogr. Sect. D Biol.*

Crystallogr. **2010**, *66* (4), 486–501.
(26) Afonine, P. V.; Grosse-Kunstleve, R. W.; Echols, N.; Headd, J. J.; Moriarty, N. W.; Mustyakimov, M.; Terwilliger, T. C.; Urzhumtsev, A.; Zwart, P. H.; Adams, P. D. *Acta Crystallogr. Sect. D Biol. Crystallogr.* **2012**, *68* (4), 352–367.
(27) Thompson, M. K.; Davis, M. F.; Serrano, V. De; Nicoletti, F. P.; Howes, B. D.; Smulevich, G.; Franzen, S. *Biophys. J.* **2010**, *99* (5), 1586–1595.
(28) McCombs, N. L.; Moreno-chicano, T.; Carey, L. M.; Franzen, S.; Hough, M. A.; Ghiladi, R. A. *Biochemistry* **2017**, *56*, 2294–2303.
(29) D'Antonio, J.; Ghiladi, R. A. *Biochemistry* **2011**, *50* (27), 5999–6011.
(30) Osborne, R. L.; Taylor, L. O.; Han, K. P.; Ely, B.; Dawson, J. H. *Biochem. Biophys. Res. Commun.* **2004**, *324* (4), 1194–1198.
(31) Taurog, A.; Dorris, M. L.; Guziec, F. S. *Anal. Biochem.* **1992**, *205* (2), 271–277.
(32) Doerge, D. R.; Divi, R. L.; Churchwell, M. I. *Anal. Biochem.* **1997**, *250* (250), 10–17.
(33) Hayashi, T.; Hitomi, Y.; Ando, T.; Mizutani, T.; Hisaeda, Y.; Kitagawa, S.; Ogoshi, H. *J. Am. Chem. Soc.* **1999**, *121* (34), 7747–7750.
(34) Sato, H.; Hayashi, T.; Ando, T.; Hisaeda, Y.; Ueno, T.; Watanabe, Y. *J. Am. Chem. Soc.* **2004**, *126* (2), 436–437.
(35) Matsuo, T.; Fukumoto, K.; Watanabe, T.; Hayashi, T. *Chem. - An Asian J.* **2011**, *6* (9), 2491–2499.
(36) Tonami, H.; Uyama, H.; Nagahata, R.; Kobayashi, S. *Chem. Lett.* **2004**, *33* (7), 796–797.
(37) Simmons, K. E.; Minard, R. D.; Bollag, J.-M. *Soil Sci. Soc. Am. J.* **1988**, *52*, 1356.
(38) Tien, M. *J. Biol. Chem.* **1995**, *270* (38), 22254–22258.
(39) Banci, L.; Ciofi-Baffoni, S.; Tien, M. *Biochemistry* **1999**, *38* (10), 3205–3210.
(40) Hwang, S.; Lee, C. H.; Ahn, I. S. *J. Ind. Eng. Chem.* **2008**, *14* (4), 487–492.
(41) Lindgren, B. *Acta Chem. Scandiavica* **1960**, *14*, 2089–2096.
(42) Schmalzl, K. J.; Forsyth, C. M.; Evans, P. D. *Wood Sci. Technol.* **1995**, *29* (4), 307–319.
(43) De Serrano, V.; Franzen, S. *Biopolymers* **2012**, *98* (1), 27–35.
(44) Wang, C.; Lovelace, L. L.; Sun, S.; Dawson, J. H.; Lebioda, L. *Biochemistry* **2013**, *52* (36), 6203–6210.
(45) Zhao, J.; De Serrano, V.; Zhao, J.; Le, P.; Franzen, S. *Biochemistry* **2013**, *52* (14), 2427–2439.

Supporting Information for

Chapter 2: Substituted Guaiacols as New Substrates for Dehaloperoxidase B from *Amphitrite ornata*: Mechanistic and Structural Studies

Ashlyn H. McGuire, Leiah M. Carey, Safaa Dali, and Reza A. Ghiladi*

Department of Chemistry, North Carolina State University, Raleigh, North Carolina, 27695

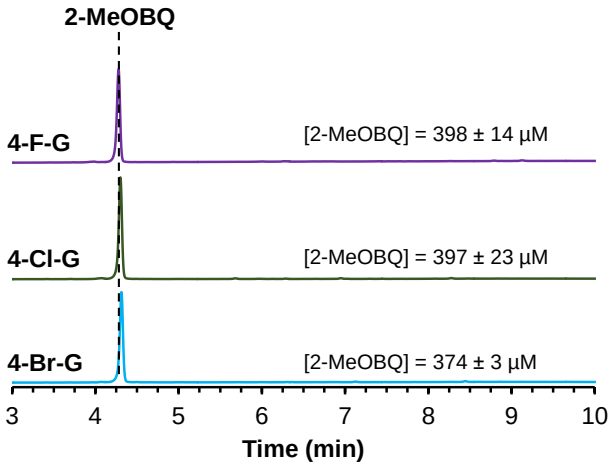

Figure S2.1. HPLC chromatograms (260 nm) of the reaction of 500 µM 4-X-guaiacol with 10 µM DHP B in the presence of 500 µM H_2O_2 at 25 °C in 5 % MeOH/100 mM KP_i (v/v) at pH 7. The reaction was quenched after 5 minutes with the addition of excess catalase. The 2-MeOBQ product is highlighted at t_R = 4.3 min.

Table S2.1. Guaiacol reaction products detected using LC-MS (positive ion mode).

Substrate	Product t_R (min)	*m/z*	Molecular Formula	Description	Footnotes
***o*-guaiacol**	3.9	139.04	$C_7H_6O_3$	Monomer, +1 O - 2 H; 2-MeOBQ	*a*
	6.4	245.08	$C_{14}H_{12}O_4$	Dimer, - 2 H	
	8.0	367.12	$C_{21}H_{18}O_6$	Trimer, - 2 H	
	11.5	489.15	$C_{28}H_{24}O_8$	Tetramer, – 2 H	
4-Br-guaiacol	3.9	139.04	$C_7H_6O_3$	Monomer +1 O - 2 H; 2-MeOBQ	*a, b*
	7.1	277.07	$C_{14}H_{12}O_6$	Dimer +2 OH -2 Br, 2 H	
	8.5	261.08	$C_{14}H_{12}O_5$	Dimer +1 OH -2 Br, 2 H	
	9.7	308.98	$C_{13}H_9O_4Br$	Dimer - 1 CH_3, 1 Br, 1 H	
	12.0	461.02	$C_{21}H_{17}O_7Br$	Trimer + 1 OH - 2 Br, 1 H	
	12.1	431.01	$C_{20}H_{15}O_6Br$	Trimer + 1 H - 1 CH_3, 2 Br	
4-Cl-guaiacol	3.9	139.04	$C_7H_6O_3$	Monomer +1 O - 2 H; 2-MeOBQ	*a, b*
	7.1	277.07	$C_{14}H_{12}O_6$	Dimer +2 OH -2 Cl, 2 H	
	8.4	261.08	$C_{14}H_{12}O_5$	Dimer +1 OH -2 Cl, 2 H	
	9.4	265.03	$C_{13}H_9O_4Cl$	Dimer - 1 CH_3, 1 Cl, 1 H	
	11.8	417.07	$C_{21}H_{17}O_7Cl$	Dimer + 1 O, 2 Cl	
	11.9	387.06	$C_{20}H_{15}O_6Cl$	Trimer - 1 CH_3, 2 Cl,	
	13.3	509.10	$C_{27}H_{21}O_8Cl$	Tetramer + 2 H - 1 CH_3, 3 Cl	
4-F-guaiacol	3.9	139.04	$C_7H_6O_3$	Monomer +1 O - 2 H; 2-MeOBQ	*a, b*
	7.1	277.07	$C_{14}H_{12}O_6$	Dimer +2 OH -2 F, 2 H	
	7.1	575.12	$C_{28}H_{21}O_9F_3$	Tetramer + 1 O - 1 F, 1 H	
	8.4	261.08	$C_{14}H_{12}O_5$	Dimer +1 OH -2 Br, 2 H	
	10.9	383.11	$C_{21}H_{18}O_7$	Trimer + 1 OH - 3 F	

[a] Compared to an authentic (commercial) sample of 2-MeOBQ.
[b] Only product observed when monitored via HPLC (UV/vis spectroscopic detection).

Table S2.2. Guaiacol reaction products detected using LC-MS (negative ion mode).

Substrate	Product t_R (min)	*m/z*	Molecular Formula	Description	Footnotes
5-Br-guaiacol	9.5	400.09	$C_{14}H_{12}O_4Br_2$	Dimer	
	11.6	600.85	$C_{21}H_{17}O_6Br_3$	Trimer	
	12.2	520.92	$C_{21}H_{16}O_6Br_2$	Trimer - 1 Br, 1 H	
	13.8	720.87	$C_{28}H_{21}O_8Br_3$	Tetramer - 1 Br, 1 H	
	13.0	800.8	$C_{28}H_{22}O_8Br_4$	Tetramer	
6-Br-guaiacol	8.4	336.97	$C_{14}H_{11}O_5Br$	Dimer + 1 OH - 1 Br	
	10.1	658.96	$C_{28}H_{22}O_9Br_2$	Tetramer + 1 OH - 2 Br, 1 H	
	10.4	400.9	$C_{14}H_{12}O_4Br_2$	Dimer	
	11.5	736.87	$C_{28}H_{21}O_9Br_3$	Tetramer + 1 OH - 1 Br	
	11.7	506.91	$C_{20}H_{14}O_6Br_2$	Trimer - 1 CH_3, 1 Br	
	11.7	706.86	$C_{27}H_{18}O_8Br_3$	Tetramer - 1 CH_3, 1 Br	
	12.7	600.85	$C_{21}H_{17}O_6Br_3$	Trimer	
	12.9	722.89	$C_{28}H_{23}O_8Br_4$	Tetramer + 1 H - 1 Br	
	14.4	800.8	$C_{28}H_{22}O_8Br_4$	Tetramer	
4-NO_2-guaiacol	3.8	139.04	$C_7H_6O_3$	Monomer +1 O - 2 H; 2-MeOBQ	*a*
	6.5	168.03	$C_7H_7NO_4$	Monomer	
	8.1	304.05	$C_{14}H_{11}NO_7$	Dimer + 1 O - 1 NO_2, 1 H	
	8.6	276.05	$C_{13}H_{11}NO_6$	Dimer + 1 OH, 1 H - 1 NO_2, 1 OCH_3	
	9.6	335.05	$C_{14}H_{12}N_2O_8$	Dimer	
	10.5	443.07	$C_{20}H_{16}N_2O_{10}$	Trimer + 2 H - 1 NO_2, 1 CH_3	
	10.7	441.06	$C_{20}H_{14}N_2O_{10}$	Trimer - 1 NO_2, 1 CH_3	
	11.2	457.09	$C_{21}H_{18}N_2O_{10}$	Trimer - 1 NO_2	
	11.6	518.07	$C_{21}H_{17}N_3O_{13}$	Trimer + 1 O	
	11.8	288.02	$C_{13}H_7NO_7$	Dimer + 1 O - 1 NO_2 - 1 CH_3 - 2 H	
4-MeO-guaiacol	3.7	323.04	$C_{14}H_{12}O_9$	Dimer +3 OH - 2 CH_3, 3 H	
	3.8	139.04	$C_7H_6O_3$	Monomer +1 O - 2 H; 2-MeOBQ	*a*
	4.4	289.04	$C_{14}H_{10}O_7$	Dimer + 1 OH -2 CH_3, 2 H	
	6.2	425.05	$C_{21}H_{14}O_{10}$	Trimer + 1 OH - 3 CH_3, 2 H	
	6.4	275.05	$C_{14}H_{12}O_6$	Dimer - 2 CH_3	
	6.0	445.11	$C_{22}H_{22}O_{10}$	Trimer + 1 OH, 2 H - 2 CH_3, 1 H	
	6.7	427.10	$C_{22}H_{20}O_9$	Trimer - 2 CH_3	
	6.2	443.13	$C_{23}H_{24}O_9$	Trimer + 1 H - 1 CH_3	
	8.5	425.09	$C_{22}H_{16}O_9$	Trimer - 2 CH_3, 4 H	
	8.6	305.1	$C_{16}H_{18}O_6$	Dimer	
	9.1	579.15	$C_{30}H_{28}O_{12}$	Tetramer - 2 CH_3	

[a] Detected in positive ion mode.

Table S2.2 (continued).

Substrate	Product t_R (min)	*m/z*	Molecular Formula	Description	Footnotes
4-Me-guaiacol	5.2	305.1	$C_{16}H_{18}O_6$	Dimer + 2 OH - 2 H	
	6.2	303.09	$C_{16}H_{16}O_6$	Dimer + 2 OH - 4 H	
	7.5	289.11	$C_{16}H_{18}O_5$	Dimer + 1 OH - 1 H	
	7.8	273.08	$C_{15}H_{14}O_5$	Dimer + 1 OH - 1 CH_3, 2 H	
	10.0	439.14	$C_{24}H_{24}O_8$	Trimer + 2 OH - 4 H	
	13.0	273.11	$C_{16}H_{18}O_4$	Dimer	
	13.9	409.16	$C_{24}H_{25}O_6$	Trimer	

[a] Detected in positive ion mode.

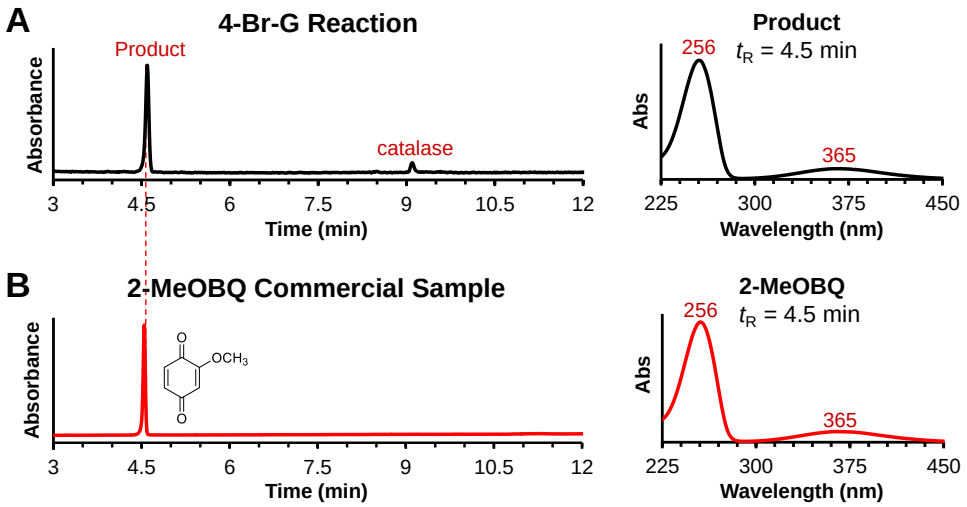

Figure S2.2. A) HPLC chromatogram (260 nm) of the reaction of 500 µM 4-Br-guaiacol with 10 µM DHP B in the presence of 500 µM H_2O_2 at 25 °C in 5 % MeOH/100 mM KP_i (v/v) at pH 7, and the corresponding UV-visible spectrum of the reaction product (t_R = 4.5 min). The reaction was quenched after 5 minutes with the addition of excess catalase (t_R = 9 min). B) An authentic sample of 2-MeOBQ under identical elution conditions as panel A, and its corresponding UV-visible spectrum.

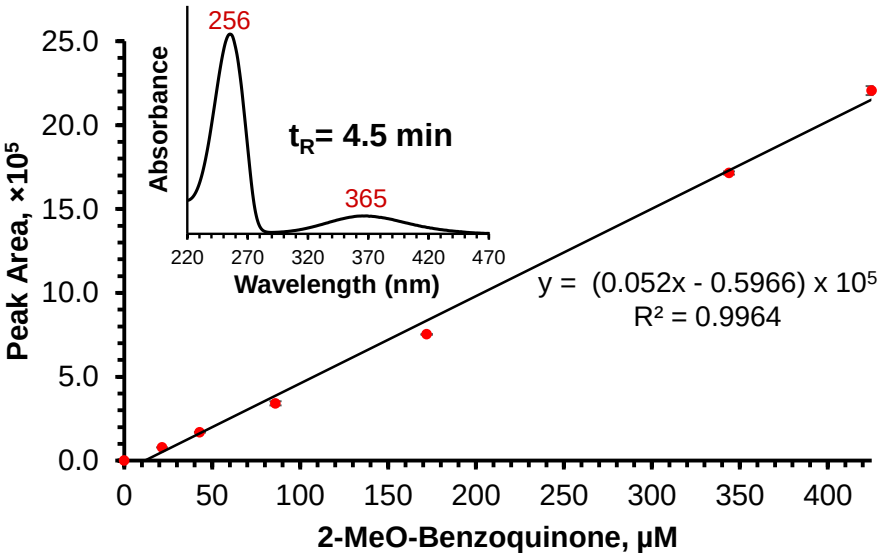

Figure S2.3. HPLC calibration curve for quantification of 2-MeOBQ (0 – 425 µM); inset: UV-visible spectrum of 2-MeOBQ obtained from the HPLC chromatogram (t_R = 4.5 min).

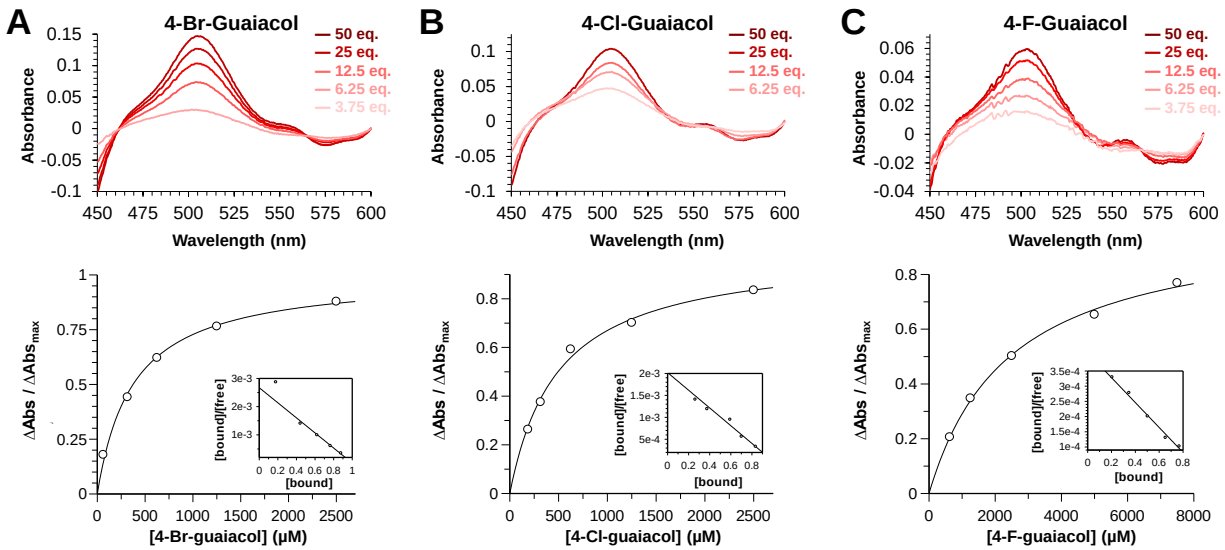

Figure S2.4. Optical difference spectra (top) and titration curves (bottom) of 4-X-guaiacol binding (3.75-50 eq) to 25 μM DHP B in 5 % MeOH / 100 mM KP_i (v/v) at pH 7 for A) 4-Br-guaiacol, B) 4-Cl-guaiacol, and C) 4-F-guaiacol. *Insets*: corresponding Scatchard plots (ratio of concentrations of bound ligand to unbound ligand versus the bound ligand concentration).

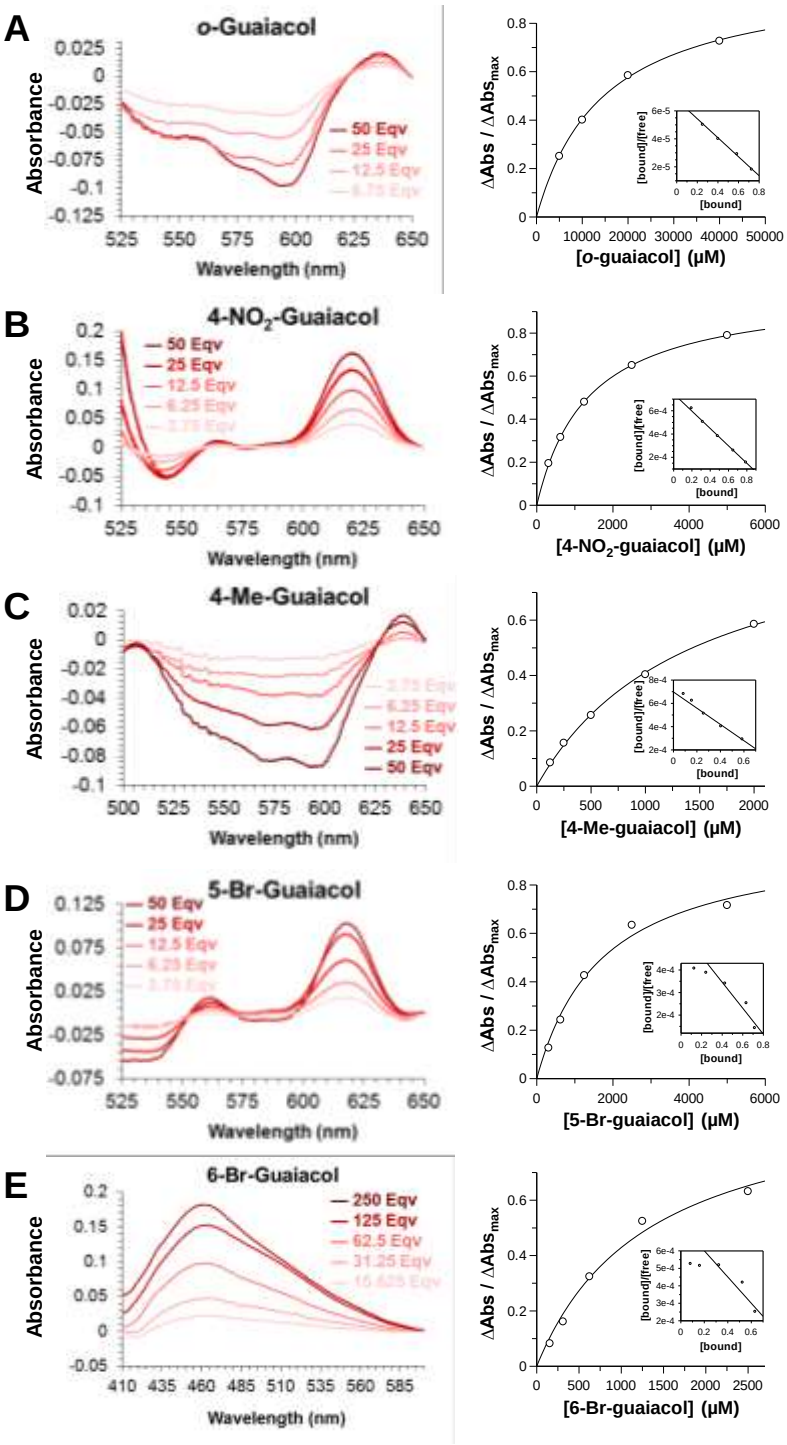

Figure S2.5. Optical difference spectra (left) and titration curves (right) of guaiacol binding (3.75-250 eq) to 25 μM DHP B in 5 % MeOH / 100 mM KPi (v/v) at pH 7 for A) *o*-guaiacol, B) 4-NO_2-guaiacol, C) 4-Me-guaiacol, D) 5-Br-guaiacol, and E) 6-Br-guaiacol. *Insets*: corresponding Scatchard plots (ratio of concentrations of bound ligand to unbound ligand versus the bound ligand concentration).

Table S2.3. X-ray data collection and refinement statistics for DHP B in complex with 4-bromo-*o*-guaiacol, (6CKE), 5-bromo-*o*-guaiacol, (6CRE), 6-bromo-*o*-guaiacol, (6CO5), 4-nitro-*o*-guaiacol (6CH5) and 4-methoxy-*o*-guaiacol (6CH6).

	4-Br-G	**5-Br-G**	**6-Br-G**	**4-NO_2-G**	**4-MeO-G**
PDB Entry	6CKE	6CRE	6CO5	6CH5	6CH6
Data Collection					
Wavelength (Å)	1.00	1.00	1.00	1.00	1.00
Temperature (K)	100	100	100	100	100
Space Group	$P2_12_12_1$	$P2_12_12_1$	$P2_12_12_1$	$P2_12_12_1$	$P2_12_12_1$
Unit-cell parameters (Å)					
a	59.40	59.22	59.52	59.65	59.79
b	66.45	66.19	66.14	66.37	66.35
c	68.21	68.20	68.39	68.22	68.29
Unique reflections	57,274 (2,821)[a]	36,635 (1,809)	30,799 (1,511)	31,440 (2,214)	29,059 (2,117)
Completeness (%)	99.9 (100)	97.8 (99.1)	99.4 (99.0)	99.3 (96.8)	99.97 (99.86)
R_{merge} (%)[b]	7.5 (66.2)	12.9 (86.3)	11.9 (79.6)	7.6 (37.3)	11.1 (64.0)
R_{pim} (%)[c]	3.7 (33.9)	6.2 (42.9)	6.0 (41.6)	4.1 (17.9)	5.6 (32.5)
$CC_{1/2}$[d]	0.746	0.642	0.553	0.906	0.776
$I/\sigma_{(I)}$	22.4 (1.9)	13.7 (2.0)	14.1 (1.9)	19.8 (3.3)	16.9 (2.7)
Redundancy	4.8 (4.7)	4.9 (4.8)	4.8 (4.7)	4.3 (3.9)	4.8 (4.8)
Refinement					
Resolution (Å)	1.37	1.58	1.69	1.65	1.70
R_{work} (%)[e]	17.42 (25.19)	16.34 (21.99)	16.68 (19.95)	15.26 (24.1)	16.2 (34.1)
R_{free} (%)[f]	19.27 (27.84)	21.17 (25.77)	20.89 (24.91)	20.56 (28.7)	22.73 (41.4)
No. of protein atoms	2,470	2,294	2,339	2,721	2,676
No. of solvent atoms	413	392	406	260	289
R.m.s.d from ideal geometry[g]					
Bond lengths (Å)	0.007	0.007	0.007	0.013	0.015
Bond angles (°)	0.916	0.910	0.922	1.697	1.71
Ramachandran plot (%)[h]					
Most favored region	98.49	97.78	98.50	99.1	98.5
Addl allowed region	1.13	2.22	1.50	0.9	1.5
Outliers	0.38	----	----	0	0

[a]Values in parentheses are for the highest resolution shell. [b]$R_{merge} = \sum_{hkl}\sum_i[|I_i(hkl) - \langle I(hkl)\rangle| / \sum_{hkl}\sum_i I(hkl)] \times 100$, where $I_i(hkl)$ is the i^{th} measurement and $\langle I(hkl)\rangle$ is the weighted mean of all measurements of I(hkl). [c]$R_{pim} = \sum_{hkl}\sqrt{1/n-1}\sum_i[|I_i(hkl) - \langle I(hkl)\rangle| / \sum_h\sum_i I(hkl)] \times 100$. [d]$CC_{1/2} = \sum(x - \langle x\rangle)(y - \langle y\rangle) / [\sum(x - \langle x\rangle)^2 \sum(y - \langle y\rangle)^2]^{1/2}$. [e]$R_{work} = \sum|F_O - F_C|/\sum F_O \times 100\%$, where F_O and F_C are the observed and calculated structure factors, respectively. [f]R_{free} is the R factor for the subset (5-10 %) of reflections selected before and not included in the refinement. [g]Root-mean-square deviation. [h]Ramachandran plot created via MolProbity.

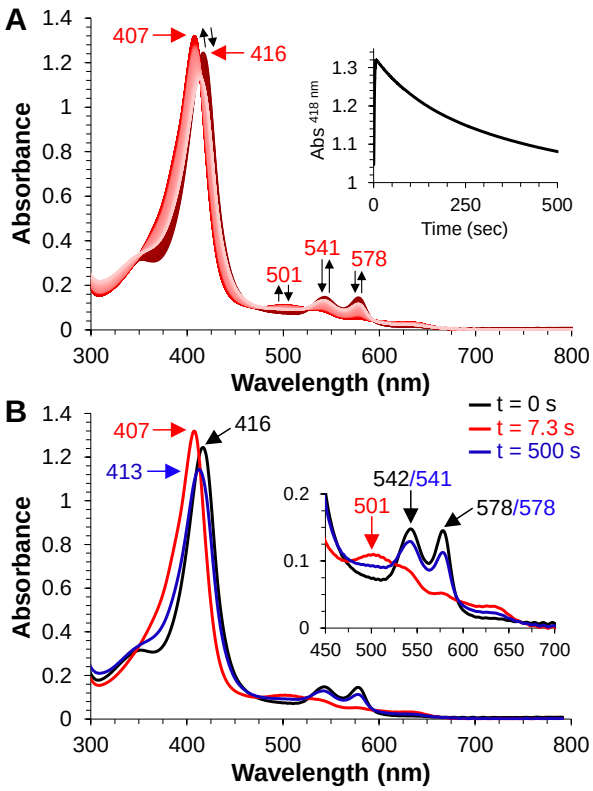

Figure S2.6. Kinetic data for the reaction of oxyferrous DHP B with 4-Br-guaiacol. A) Stopped-flow UV−visible spectra of the double-mixing reaction between oxyferrous DHP B (10 µM) premixed with 10 eq. of H_2O_2 (500 ms) and then reacted with 10 eq. 4-Br-guaiacol at pH 7.0 (900 scans over 500 s); inset: the single wavelength (418 nm) dependence on time obtained from the raw data. B) Experimentally obtained spectra of oxyferrous DHP B (black, t = 0 s) reacted with 4-Br-guaiacol, resulting in ferric DHP B (red, t = 7.3 s) and further reduction to oxyferrous DHP B (blue, t = 500 s).

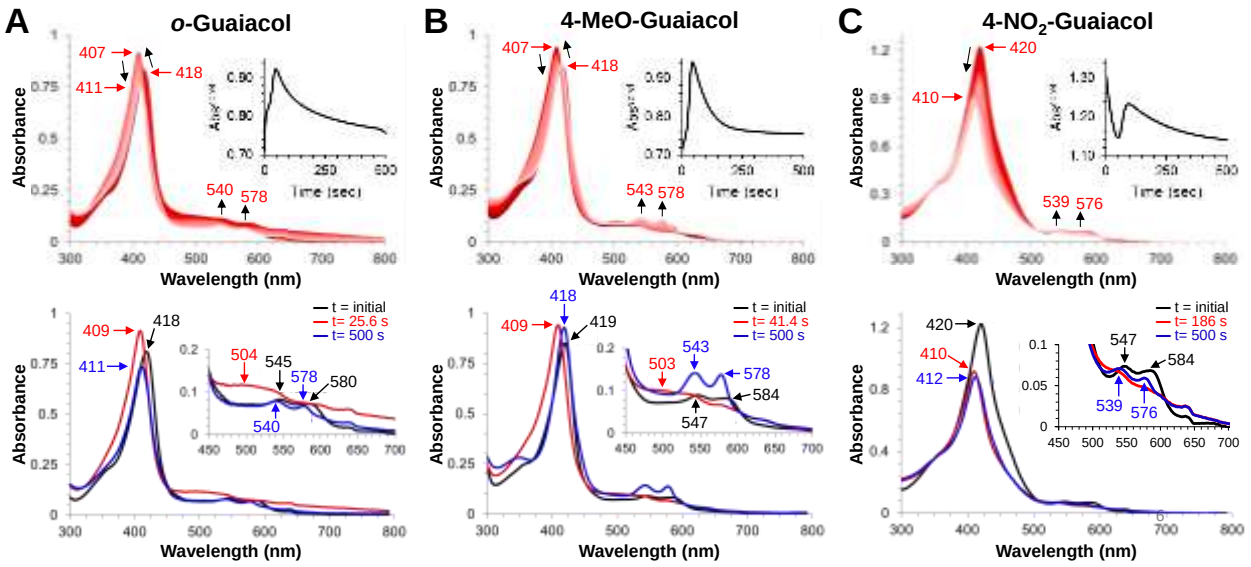

Figure S2.7. Kinetic data for the reaction of preformed DHP B Compound ES with o-G, 4-MeO-G and 4-NO_2-G. **A) *o*-Guaiacol:** *top panel*, stopped-flow UV−visible spectra of the double-mixing reaction between ferric DHP B (10 µM) premixed with 10 eq. of H_2O_2 (500 ms) and then reacted with 10 eq. *o*-guaiacol at pH 7.0 (900 scans over 500 s); inset: the single wavelength (408 nm) dependence on time obtained from the raw data; *bottom panel*, experimentally obtained spectra of Compound ES (black, t = 0 s) reacted with *o*-guaiacol, resulting in ferric DHP B (red, t = 25.6 s) and further reduction to oxyferrous DHP B (blue, t = 500 s). **B) 4-MeO-guaiacol:** *top panel*, stopped-flow UV−visible spectra of the double-mixing reaction between ferric DHP B (10 µM) premixed with 10 eq. of H_2O_2 (500 ms) and then reacted with 10 eq. 4-MeO-guaiacol at pH 7.0 (900 scans over 500 s); inset: the single wavelength (408 nm) dependence on time obtained from the raw data; *bottom panel*, experimentally obtained spectra of Compound ES (black, t = 0 s) reacted with 4-MeO-guaiacol, resulting in ferric DHP B (red, t = 41.4 s) and further reduction to oxyferrous DHP B (blue, t = 500 s). **C) 4-NO_2-guaiacol:** *top panel*, stopped-flow UV−visible spectra of the double-mixing reaction between ferric DHP B (10 µM) premixed with 10 eq. of H_2O_2 (500 ms) and then reacted with 10 eq. 4-NO_2-guaiacol at pH 7.0 (900 scans over 500 s); inset: the single wavelength (408 nm) dependence on time obtained from the raw data; *bottom panel*, experimentally obtained spectra of Compound ES (black, t = 0 s) reacted with 4-MeO-guaiacol, resulting in ferric DHP B (red, t = 186 s) and further reduction to oxyferrous DHP B (blue, t = 500 s).

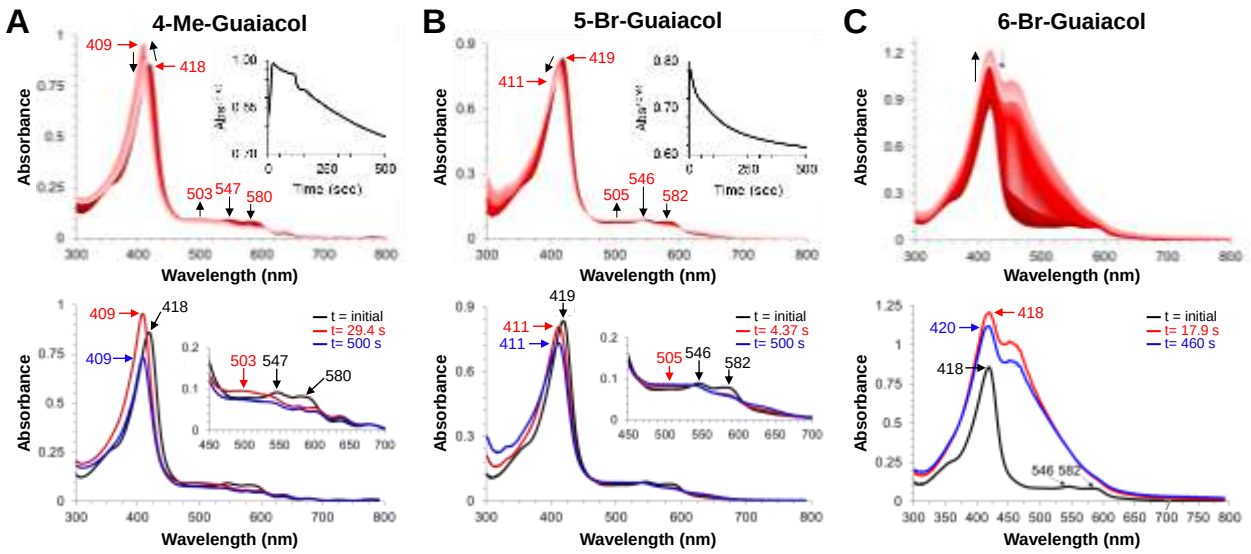

Figure S2.8. Kinetic data for the reaction of preformed DHP B Compound ES with 4-Me-G, 5-Br-G, and 6-Br-G. **A) 4-Me-guaiacol:** *top panel*, stopped-flow UV−visible spectra of the double-mixing reaction between ferric DHP B (10 μM) premixed with 10 eq. of H_2O_2 (500 ms) and then reacted with 10 eq. 4-Me-guaiacol at pH 7.0 (900 scans over 500 s); inset: the single wavelength (408 nm) dependence on time obtained from the raw data; *bottom panel*, experimentally obtained spectra of Compound ES (black, t = 0 s) reacted with 4-Me-guaiacol, resulting in ferric DHP B (red, t = 29.4 s) that was slowly reduced and approached a Compound RH-like species (blue, t = 500 s). **B) 5-Br-guaiacol:** *top panel*, stopped-flow UV−visible spectra of the double-mixing reaction between ferric DHP B (10 μM) premixed with 10 eq. of H_2O_2 (500 ms) and then reacted with 10 eq. 5-Br-guaiacol at pH 7.0 (900 scans over 500 s); inset: the single wavelength (408 nm) dependence on time obtained from the raw data; *bottom panel*, experimentally obtained spectra of Compound ES (black, t = 0 s) reacted with 5-Br-guaiacol, resulting in ferric DHP B (red, t = 4.37 s) and further reduction to a Ferric/Compound RH mixture (blue, t = 500 s). **C) 6-Br-guaiacol:** *top panel*, stopped-flow UV−visible spectra of the double-mixing reaction between ferric DHP B (10 μM) premixed with 10 eq. of H_2O_2 (500 ms) and then reacted with 5 eq. 6-Br-guaiacol at pH 7.0 (900 scans over 500 s); inset: the single wavelength (408 nm) dependence on time obtained from the raw data; *bottom panel*, experimentally obtained spectra of Compound ES (black, t = 0 s) reacted with 6-Br-guaiacol, resulting in an increase of absorbance at 460 nm disrupting both the Soret band and Q-band regions.

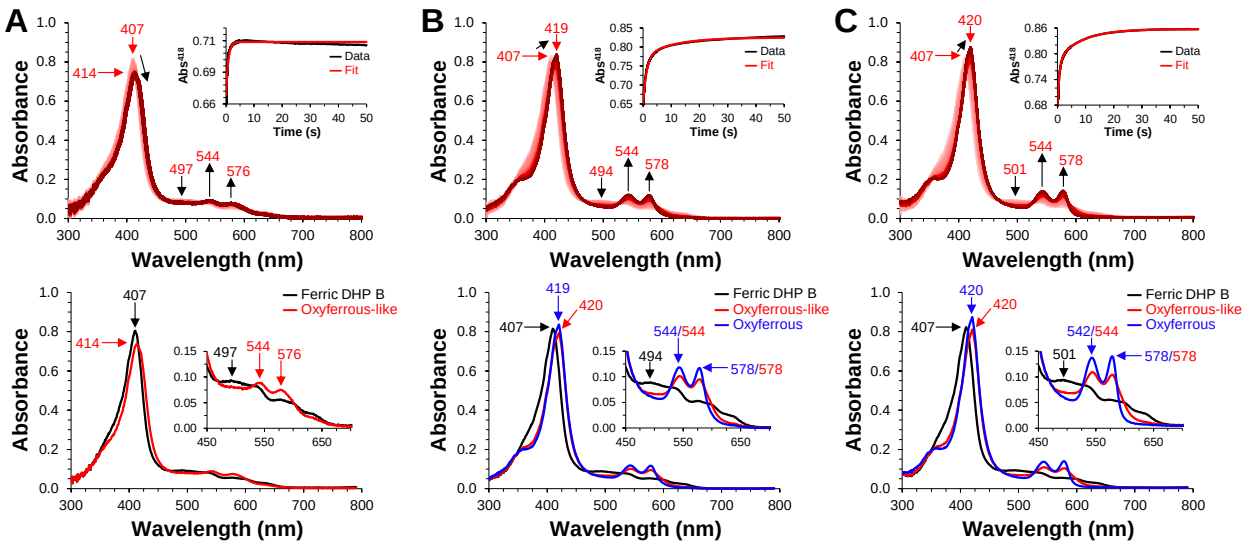

Figure S2.9. Stopped-flow spectroscopic monitoring of the reaction of ferric DHP B with 2-MeOBQ. **A) 0.625 µM 2-MeOBQ:** *top panel*, stopped-flow UV−visible spectra of the single-mixing reaction between ferric DHP B (8 µM) reacted with 0.625 µM 2-MeOBQ at pH 7.0 (900 scans over 50 s); inset: the single wavelength (418 nm) dependence on time obtained from the raw data (black) and fit (red); *bottom panel*, Calculated spectra of the two reaction components derived from the SVD analysis: Ferric DHP B (black) and oxyferrous-like DHP B (red). **B) 6.25 µM 2-MeOBQ:** *top panel*, stopped-flow UV−visible spectra of the single-mixing reaction between ferric DHP B (8 µM) reacted with 6.25 µM 2-MeOBQ at pH 7.0 (900 scans over 50 s); inset: the single wavelength (418 nm) dependence on time obtained from the raw data (black) and fit (red); *bottom panel*, Calculated spectra of the three reaction components derived from the SVD analysis: Ferric DHP B (black), oxyferrous-like DHP B (red), and oxyferrous DHP B (blue). **C) 625.0 µM 2-MeOBQ:** *top panel*, stopped-flow UV−visible spectra of the single-mixing reaction between ferric DHP B (8 µM) reacted with 625.0 µM 2-MeOBQ at pH 7.0 (900 scans over 50 s); inset: the single wavelength (418 nm) dependence on time obtained from the raw data (black) and fit (red); *bottom panel*, Calculated spectra of the three reaction components derived from the SVD analysis: Ferric DHP B (black), oxyferrous-like DHP B (red), and oxyferrous DHP B (blue).

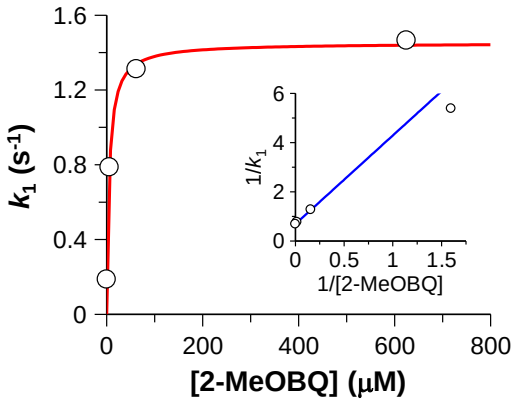

[2-MeOBQ], μM	k_1	k_2
0.625	0.186 (±0.006)	N/A
6.25	0.786 (±0.005)	0.093 (±0.003)
62.5	1.311 (±0.004)	0.227 (±0.001)
625.0	1.465 (±0.004)	0.117 (±0.001)

N/A = not applicable, data fit to a single exponential

Figure S2.10. *Top*: plot of k_{obs} vs [2-MeOBQ] using the data obtained from Figure S9 for the reduction of WT ferric DHP B by 2-MeOBQ (0.625-625 μM) yielding the oxyferrous-like DHP species; inset: corresponding double-reciprocal plot ($1/k_{obs}$ vs 1/[2-MeOBQ]). *Bottom*: rate constants determined from the SVD analysis data of the presented in Figure S9.

Chapter 3

Nonnative Heme Incorporation into Multifunctional Globin Increases Peroxygenase Activity an Order and Magnitude Compared to Native Enzyme

Ashlyn H. McGuire, Alexandra R. Pettit, Jihye Kang, Talita Malewschik, Nikhila K. Dhanvantari Madhuresh, Vesna de Serrano, Leiah M. Carey and Reza A. Ghiladi

Department of Chemistry, North Carolina State University, Raleigh, North Carolina, 27695

Author Contributions: Ashlyn H. McGuire is responsible for all work excluding crystallographic work (Vesna de Serrano and Leiah M. Carey), Mn-DHP HPLC and substrate binding studies (Alexandra R. Pettit), Deu-DHP HPLC studies (Jihye Kang), Meso-DHP Binding Studies (Talita Malewschik) and spectroelectrochemical workup (Nikhila K. Dhanvantari Madhuresh)

ABSTRACT

Nonnative cofactor exchange was performed on the hemoenzyme Dehaloperoxidase (DHP) in attempt to increase the enzyme's reactivity. The native enzyme is capable of oxidizing a wide range of substrates, encompassing halophenols, haloindoles, pyrroles, and haloguaiacols, by utilizing multiple substrate-directed oxidation mechanisms catalyzed by the cosubstrate, H_2O_2 or O_2. The versatility and robust nature of DHP provides an unprecedented multifunctional protein scaffold. By use of the Teale heme extraction method, the original iron protoporphyrin IX (Fe-PPIX) was exchanged with M-PPIX (M = Mn, Co, Cu) or Fe-R-PIX (R = meso, deutero). UV-visible spectroscopic methods and X-ray crystallography determined that the nonnative porphyrins were successfully incorporated and retain the similar positions as the original cofactor. The reactivities of the modified enzymes were determined by using substrates with known reactivity with native DHP (indoles, phenols, and guaiacols) and quantified by biochemical assays monitored using UV-visible and liquid/gas chromatographic techniques. The benchmark trihalophenol peroxidase assay demonstrated a turnover number increase of 6-fold with the nonnative enzyme, while maintaining its catalytic efficiency. Peroxygenase activity was compared by the oxidation

of Russig's Blue; both the turnover number and the catalytic efficiency were increased by 11-fold and 8-fold, respectively, for Meso-DHP. By probing the reactivity of DHP and its cofactor variants we will provide insight on whether 'nature's selected' Fe-PPIX or the novel nonnative-DHP variants will lead to optimal reactivity and selectivity. The successful incorporation of nonnative cofactors into DHP and resulting enzymatic activity provides important understanding towards selectively tuning the enzymatic function of a unique multifunctional scaffold.

INTRODUCTION

Metalloenzymes provide a useful platform to conduct specific chemical reactions with a high degree of chemoselectivity and catalyst turnover, while being economically and environmentally favorable when compared to traditional catalytic methods. Though there are be natural limitations to these biocatalysts, new methods are emerging which enable the enhancement of native enzyme reactivity and discovery of new functionalities; techniques such as amino acid mutagenesis and in applicable cases nonnative cofactor incorporation in metalloenzymes are approaches utilized that push the boundaries of protein engineering. Hemoproteins are an optimal candidate as they are ubiquitous in nature and can accomplish a variety of reactions and functions by way of its cofactor including: radical chemistry, O-atom insertion, C-H activation. The canonical enzymes of the peroxidase class include horseradish peroxidase, cytochrome *c*, and globins to a lesser extent. Thoroughly-studied enzymes of the (per)oxygenase class are cytochrome P450s. These hemoproteins have evolved to accomplish their required functions to a sufficient/high degree, yet scientists have shown through protein and cofactor engineering that it is possible to further improve the native activity.

An obvious example on probing enzymatic mechanisms include incorporating a nonnative metal. Heme enzymes have regularly swapped iron for Mn as the are many examples of manganese metalloproteins such as superoxide dismutase (mitochondrial prokaryotic) and some catalases. Both classes are known to prevent oxidation damage from O_2 and H_2O_2, respectively.[1] Manganese porphyrins can be used to probe reactivity in myoglobin and hemoglobin as it is incapable of binding dioxygen species.[2] Conversely, Co-porphyrins have high affinities to O_2 and have been incorporated in globins, horseradish peroxidase (HRP), and cytochrome C to measure oxygen bindings and characterize 6cLS heme species.[3–6] These discoveries are ground breaking and

expansive, but all the previous enzymes share an attribute, they are monofunctional. We explored a unique multifunctional system that can accomplish most of the reactivities of the canonical enzymes listed above through a robust and unique hemoprotein, dehaloperoxidase (DHP).

First discovered as a coelomic hemoglobin from the marine worm *Amphitrite ornata*, DHP was found to possess peroxidase reactivity against halophenolic compounds.[7,8] As the substrate scope expanded the multifunctionality of DHP was revealed. These catalytic activities include H_2O_2/O_2-catalyzed radical electron transfer (peroxidase/oxidase) and direct O-atom insertion (peroxygenase/oxygenase).[9–11] The specific activity used by the hemoenzyme is determined by the structure of the substrate demonstrating a clear structure-function relationship between enzyme and substrate. The substrate scope of dehaloperoxidase currently includes halophenols,[7,12–14] nitrophenols,[10] methoxyphenols (guaiacols),[15] methylphenols (cresols),[16] indoles,[9] pyrroles,[11] and select catechols[10] and quinones[15,17] (Figure. 1). The diverse list of substrates are of environmental importance as many of these compounds have been labeled as priority organic pollutants (POPs) by organizations such as the Environmental Protection Agency (EPA-Clean Water Act) and World Health Organization (WHO) [18,19]

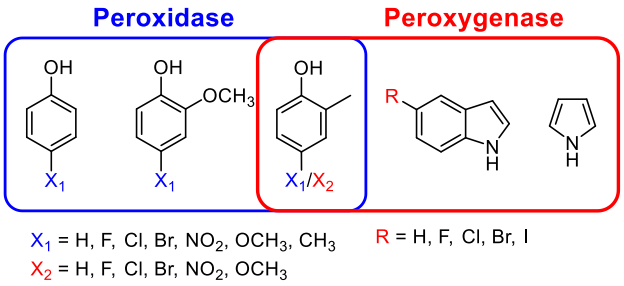

Figure 3.1. A selection of the substrate scope of DHP

The versatility and robustness of this enzyme allows it to be used as a platform to further improve it as a biocatalyst. Previously, our lab has attempted rationally-designed point mutagenesis,[20] but as a promising alternative, cofactor exchange is optimal as DHP has an accommodating active site large enough for iron protoporphyrin IX (Fe-PPIX). In attempt to tune

and enhance the reactivity of DHP, different metals could be exchanged with iron and new protoporphyrin-like cofactors, such as Deu-PPIX and Meso-PPIX could be completely exchanged via a heme acid-butanone extraction (Figure 2).[21] This relatively simple procedure allows for the reactivity and mechanistic investigation of an unprecedented biocatalyst.

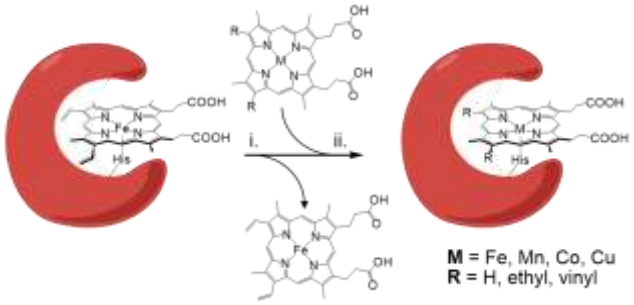

Figure 3.2. Teale Butanone-Heme extraction scheme. Steps include (i) decreasing pH to 2.5 and addition of three volumes of 2-butanone (ii) nonnative porphyrin is then added in molar excess at pH 7.

EXPERIMENTAL PROCEDURES

Materials. Ferric samples of WT DHP B were expressed and purified as previously reported.[12] Oxyferrous DHP B was prepared by the aerobic addition of excess ascorbic acid to ferric DHP B, followed by removal of the reducing agent via a PD-10 desalting column.[22] The WT enzyme concentration was determined spectrophotometrically using an ε_{Soret} of 116400 M^{-1} cm^{-1}. Solutions of H_2O_2 (in 100 mM KP_i, pH 7) and *m*CPBA (in MeOH) were prepared fresh daily and kept on ice until they were needed. Nonnative porphyrins were purchased from Frontier Scientific or VWR. Stock solutions of substrates were prepared in MeOH and stored in the dark at −80 °C until they were needed. Porphyrins were purchased from Frontier Scientific. Acetonitrile (MeCN) was high-performance liquid chromatography (HPLC) grade, and all other reagent grade chemicals were purchased from VWR, Sigma-Aldrich, or Fisher Scientific and used without further purification.

Nonnative Cofactor DHP Preparation. Following a modified Teale-Butanone extraction method,[21,23] DHP B dissolved in 100 mM KP_i was adjusted to pH 2.3 - 2.5 by dropwise additions of 0.1 M HCl and immediately mixed with an equal volume of ice-cold 2-butanone. The mixture was vigorously shaken for 30 s and allowed to stand at 0 ℃ for 1 min until the deeply colored upper layer of butanone phase (heme-containing) separated from the colorless lower layer of aqueous phase (apoenzyme). The butanone phase was siphoned off. The remaining aqueous phase was treated twice more with 2-butanone and dialyzed against 10 mM KP_i in quadruplicate to remove the dissolved butanone. The dialyzed solution was centrifuged to remove insoluble material and stored at 4 ℃. The apoenzyme in 10 mM KPi (pH 7.0) was mixed with excess of the desired porphyrin (2-4 mg) in 400 µL 0.1 M NaOH and allowed to stand at 0 ℃ for 30-60 min. The mixture was then passed through a carboxymethyl cellulose column equilibrated with 10 mM KPi (pH 7.0). The complex was absorbed on the column, whereas the unbound porphyrin passed through the column. The column was washed with of 10 mM KPi (pH 7.0). The absorbed complex was slowly eluted with 40 mM KPi (pH 7.0) and stored in 40% (v/v) glycerol at -80 ℃. Molar absorptivities of the enzyme with substituted cofactors were determined via ICP-OES.

Spectroelectrochemical Analysis of Meso-DHP. A spectroelectrochemical (SEC) cell was bought from BASi which contained a 0.5 mm pathlength quartz cuvette, a platinum mesh working electrode, platinum wire counter electrode and Ag/AgCl (3 M NaCl) reference electrode. The working electrode was activated before every experiment by scanning from -0.25 V to +1.4 V Ag/AgCl reference in 0.5M sulfuric acid until a clean and reproducible cyclic voltammogram was achieved. Simultaneous spectral measurement and application of potential were performed using an Agilent 8453 UV−visible spectrophotometer and a Pine-WaveNow potentiostat coupled with AfterMath 1.4.8245 software package (AfterMath.Ink). The sample was prepared in a supporting

electrolyte consisting of 500 mM potassium chloride and 100 mM KPi. Electron transfer mediators TMPD and BCB were added to the sample at DHP/mediator ratio 2:1. Final concentration of the protein in the sample was 50 μM. Small volumes of stock solutions were degassed with argon gas for 1-2 hours and transferred into the glovebox in sealed containers. The SEC cell was stored in the glovebox for at least 2 hours before the experiment. WT-DHPB and Meso-DHPB were used in the experiment. All the reported potentials are against Ag/AgCl reference. 210mV is added to the applied potentials against Ag/AgCl to convert to standard hydrogen electrode (SHE) scale

Substrate Binding Studies. The substrate dissociation constants (K_d) were determined in triplicate for DHP in 100 mM KP_i (pH 7) containing 5% MeOH at 25 °C using a Cary 50 ultraviolet−visible (UV−vis) spectrophotometer per previously published protocols.[9,24] The UV−vis spectrometer was referenced with 25 μM WT DHP B in 100 mM KP_i (pH 7) in 5% MeOH. Spectra were acquired in the presence of phenolic substrate concentrations (3.75−50 equiv) while constant DHP B (25 μM) and methanol concentrations were maintained. Analyses of the Q-band region (450−600 nm) were performed using the ligand binding function in Grafit (Erithacus Software Ltd.).

UV-Visible Spectroscopic Peroxidase and Peroxygenase Assays. Optical spectra were recorded using quartz microcuvettes (1 cm pathlength) on a Cary 50 UV-visible spectrophotometer. The 1 mL reaction mixture contained 1 μM enzyme (WT and nonnative cofactor), 150 μM trihalophenol (TXP) or 400 μM 1-methoxynaphthalene (1-MeON),[25,26] and varying H_2O_2 concentrations in 100 mM potassium phosphate buffer at pH 7. The apparent values of K_m and k_{cat} for DHP B and the nonnative derivatives and the cosubstrate with variable concentrations of H_2O_2 were calculated by triplicate measurements of initial rates at each H_2O_2 concentration. The experimental data were fitted to the Michaelis-Menten model using the enzyme kinetics software GraFit (Erithacus

Software). The peroxidase enzymatic activity was assayed on the basis of the disappearance of cosubstrate (trichlorophenol, 312 nm; tribromophenol, 316 nm) monitored for 5 min at 25 °C. The peroxygenase activity was assayed on the basis of the appearance of product (Russig's Blue, 600 nm) monitored for 5 min at 25 °C.

HPLC Activity Studies. Reactions were performed in triplicate at pH 7 (unless otherwise indicated) in 100 mM KP_i containing 5% MeOH at 25 °C. Assay components (250 μL final volume) included 10 μM enzyme and 500 μM substrate (in MeOH), and the reaction was initiated by the addition of 500 μM oxidant (H_2O_2 or *m*CPBA). The reactions were quenched after 5 min with excess catalase. A 200 μL aliquot was diluted 4-fold with 600 μL of 100 mM KP_i (pH 7). The samples were analyzed using a Waters 2796 Module coupled with a Waters 2996 photodiode array detector and equipped with a Thermo Fisher Scientific ODS Hypersil (150 mm × 4.6 mm) 5 μm particle size C_{18} column. Separation was performed using a linear gradient of binary solvents (solvent A, H_2O and 0.1% TFA; solvent B, acetonitrile and 0.1% TFA). The elution consisted of the following conditions: (1.5 mL/min A:B) 95:5 to 5:95 linearly over 12 min, 5:95 isocratic for 2 min, 5:95 to 95:5 over 1 min, and then isocratic for 3 min. Data analysis was performed using the Waters Empower software package.

Stopped-Flow UV−Vis Spectroscopy Studies. Optical spectra were recorded using a Bio-Logic SFM-400 triple- mixing stopped-flow instrument coupled to a rapid scanning diode array UV−vis spectrophotometer. Protein and hydrogen peroxide solutions were prepared in 100 mM KP_i (pH 7), and the substrates were dissolved in buffer containing 10% methanol. Single- and double-mixing data were collected (900 scans total) over a three-time domain (1.5, 15, and 150 ms) using the Bio-Kine 32 software package (Bio-Logic). All data were evaluated using the Specfit Global Analysis System software package (Spectrum Software Associates) and fit with SVD analysis as

either one-step, two-species or two-step, three-species irreversible mechanisms, where applicable. For data that did not properly fit these models, experimentally obtained spectra at selected time points detailed in the figure legends are shown. Kinetic data were baseline-corrected using the Specfit autozero function when appropriate. Double-mixing experiments were performed using an aging line prior to the second mixing step to observe Compound ES reactivity with the substrates (10 eq). Compound ES was pre-formed by reaction of ferric DHP B with 10 equiv of H_2O_2 in an aging line for 500, 900, 2900 ms, for WT, Deu-, and Meso-DHP, respectively.[40]

Protein Crystallization and X-ray Diffraction Studies. Non-His-tagged ferric DHP B variants were used for crystallization experiments, and was overexpressed and purified, as previously reported.[15,27–29] Nonnative proteins were prepared as explained above (heme-butanone extraction). The proteins were oxidized to ferric form, equilibrated at 4° C for several hours in order to reduce heme disorder,[30] and were crystallized using hanging-drop vapor diffusion method. WT DHP crystals normally grow from 30-32% MPEG 2000, 0.2 M ammonium sulfate and 0.02 M sodium cacodylate (pH 6.5), and all of the heme substituted proteins crystallized under these same crystallization conditions. Crystallization drops (2-5 µL) were set up by mixing protein at 10 mg/mL in 20 mM sodium cacodylate (pH 6.5) and crystallizing solution at 1:1, 1.5:1 or 2:1 of protein:reservoir solution, and the crystals for all heme variant proteins appeared after 3-5 days of incubation at 4° C. All the substrate derivatizations were performed by overnight soaking of crystals in solutions containing 34% MPEG 2000, 0.2 M ammonium sulfate, supplemented with varying concentrations of substrate dissolved in DMSO, adding 5% DMSO to the final soaking solution. The crystals were subsequently cryoprotected by dipping in soaking solution supplemented with 25% ethylene glycol and flash cooled in liquid nitrogen before data collection. X-ray diffraction data were collected remotely on BM-22 beamline at the SER-CAT, Advanced

Photon Source, Argone National Laboratories. The data sets were collected at 100 K, in a single wavelength mode at 1.0000 Å, employing a shutterless detector Rayonix MX300HS, and the data were processed using iMosfilm, Pointeless and Aimless within CCP4 program suite and HKL2000 program suite.[27,31] Molecular replacements were performed with Phaser-MR[27,32] using 3IXF coordinates as a search model.[33] The resulting models were refined using REFMAC5[34] in the CCP4 suite, using ccp4i graphical interface[27,35] and phenix.refine in the PHENIX suite of programs[27,36,37] and inspection and manual model building was performed in COOT.[27,32] Final models were validated using COOT[38] and MolProbity, and the data collection and refinement information is summarized in Table 2. Illustrations were generated using PyMol (Schrodinger).

RESULTS

Cofactor Replacement

The native heme cofactor was removed by Teale acid-butanone extraction, the heme content was determined spectroscopically by monitoring the decrease of the Soret band as demonstrated by the yellow trace in Figure 3A and 3B.[2,21] The apo-enzyme was incubated with an excess amount of the desired metallated porphyrin after which the free porphyrin was removed by ion exchange chromatography. After purification the spectroscopic profiles (200-800 nm) were characterized by UV-vis spectroscopy to ensure complete cofactor incorporation and free-cofactor removal. The enzyme cofactor variants were also compared spectroscopically with WT DHP (Figure 3). Panels A and B compare the ferric and oxyferrous oxidation states, respectively. A hypsochromic Soret shift is observed as the 2,4 porphyrin substituents are changed from vinyl > ethyl > hydrogen groups with minor q-band shifts. In panel C oxy-WT DHP is compared to the metal-exchanged protoporphyrin IX. The spectra of Co-DHP and Cu-DHP are reminiscent of molecular oxygen-

bound Fe(II) (6cLS). The reduced 5-coordinate heme (ferrous) and Mn(II) species were analyzed in an oxygen free environment (Figure S1 and S2). Both Meso-DHP [422 (Soret), 545, red] and Deu-DHP [422 (Soret), 542, black] had very similar UV-visible characteristics, demonstrating a hypsochromic shift in the Soret and q-bands compared to WT [433 (Soret), 554].[12] The molar absorptivities were obtained with a combination of absorption spectroscopy and inductively coupled plasma optical emission spectrometry (ICP-OES): ε = 116400 (WT-), 175745 (meso-), 143210 (deu-), 97240 (Mn-), 231645 (Co-), 190356 M^{-1} cm^{-1} (Cu).

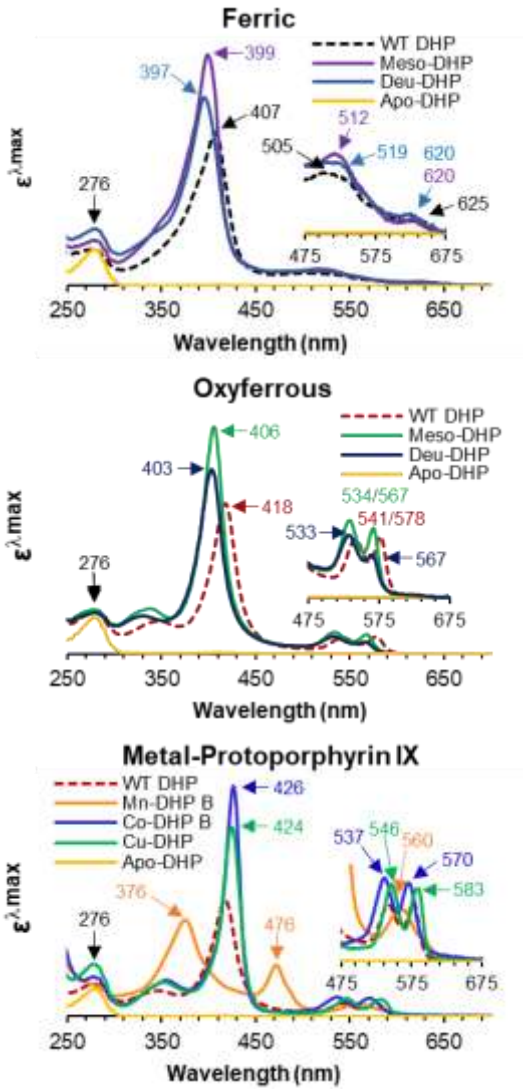

Figure 3.3. Spectroscopic features of all DHP cofactor variants: (A) Fe(III) proto-, meso-, deutero-porphyrin IX with DHP scaffold, (B) Fe(II)-O_2 proto-, meso-, deutero-DHP, and (C) metal exchanged protoporphyrin IX-DHP (Fe, Mn, Co, Cu)

Spectroelectrochemical Properties of Meso-DHP

The Fe(III) and Fe(II) Meso-DHP were allowed to attain equilibrium, anaerobically, while under a series of applied potentials (+500 to -500 mV) and the [ox]/[red] ratio was determined by monitoring the Soret shift from 399 to 422 nm in quadruplicate. Under an oxidizing potential like E_{app}= +230 mV, observed Soret peak at 407nm indicates meso-DHP in its ferric from and deoxyferrous form is seen at 422 nm under limiting reduction potential such as E_{app}= -470mV. The total number of electrons transferred was calculated to be n = 0.90 ± 0.9, as expected for a one electron redox process. The formal reduction potential (Eo') of this redox system from the Nernst plot was determined to be -100.21 ± 5.57 mV (vs Ag/AgCl reference electrode) ; through a conversion of +210 mV, the Eo' was determined to be +109.79 ± 5.57 mV versus standard hydrogen electrode (SHE), a more negative potential when compared to WT DHP (+206 ± 6 mV). The study was attempted using Deu-DHP, but due to long periods of time at high temperatures (25 °C) and high salt concentrations leading to protein denaturation, reproducible results could not be obtained.

Enzymatic Kinetic Activity Studies

The activity of the nonnative cofactor-DHP variants was tested using a benchmark TCP/TBP bioassay (Figure 4). Co-DHP, Cu-DHP and Mn-DHP not react in this presence of H_2O_2, but the Fe-containing porphyrins demonstrated very high reactivity against TXP substrates in the presence of H_2O_2. Michaelis Menten kinetic parameters were derived by monitoring the decrease of the 312 (TCP) and 315 nm (TBP) bands. The catalytic reaction resulted in 2,6-dihalo-1,4-benzoquinone (279 / 290 nm) formation. In the absence of either enzyme or H_2O_2, product formation was not observed in agreement with previous results.[12,13] The oxidative reaction of TCP with the three enzymes was monitored a period of 5 min by UV-vis (Figure 4A). The black trace indicates 1 min

of time passing, at that time point Meso-DHP had nearly reacted with TCP to completion to the oxidatively dehalogenated product. Deu-DHP was only slightly faster than WT DHP (Figure S4A). The catalytic efficiency (k_{cat} / K_m) of each reaction show little change, but most notably the turnover number of Meso-DHP had a 6.3-fold increase from the WT-DHP reaction when initiated from both the ferric and oxyferrous oxidation state (Figure 4C). The initial rate of reactivity of Meso-DHP with the brominated analog was also faster than the WT reaction which was fairly similar to Deu-DHP (Figures 4B and S4B). Meso-DHP again had a ~6-fold increase in k_{cat} when compared to WT DHP.

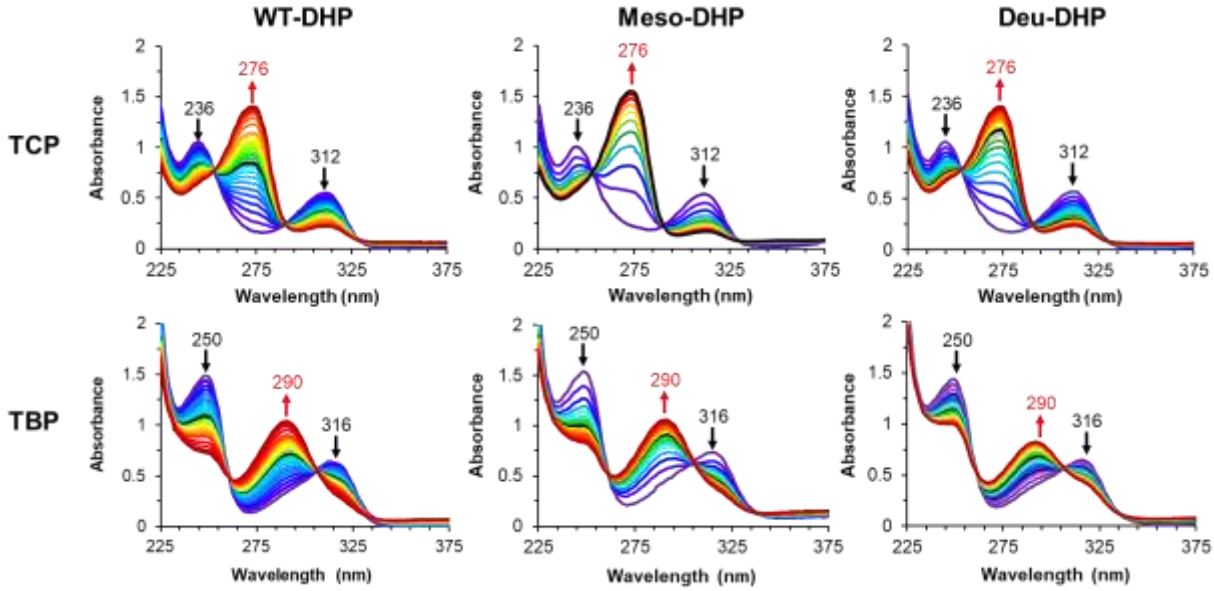

Figure 3.4. Kinetic data for the oxidative reactions of different cosubstrates, TCP and TBP, with 1 μM DHP (WT, Meso- and Deu-) and 150 μM corresponding cosubstrates and varying H_2O_2 concentrations in 100 mM KP_i, pH 7, black trace represents 1 min into reaction: (A) Trichlorophenol reactivity with WT, Meso-, and Deu-DHP, monitored by TCP (236, 312 nm - decrease) and dichlorobenzoquinone (276 nm - increase), (B) Tribromophenol reactivity with WT, Meso-, and Deu-DHP, monitored by TBP (250, 315 nm - decrease) and dibromobenzoquinone (290 nm - increase), (C) Michaelis Menten parameters of all three enzymes with cosubstrates TXP's and H_2O_2.

Table 3.1. Kinetic parameters of trihalophenol oxidation by DHP variants

	Ferric Enzyme				Oxyferrous Enzyme			
Cosubstrate	**Enzyme**	**k_{cat} (s^{-1})**	**K_m^{H2O2} (μM)**	**k_{cat}/K_m^{H2O2} ($\mu M^{-1} s^{-1}$)**	**Enzyme**	**k_{cat} (s^{-1})**	**K_m^{H2O2} (μM)**	**k_{cat}/K_m^{H2O2} ($\mu M^{-1} s^{-1}$)**
TCP	WT DHP B	1.28 ± 0.057	19 ± 3	0.0674	WT DHP B	1.17 ± 0.05	35 ± 6	0.0334
	Meso-DHP B	8.23 ± 1.532	109 ± 38	0.0755	Meso-DHP B	7.22 ± 0.312	104 ± 9	0.0694
	Deu-DHP B	0.86 ± 0.163	141 ± 36	0.0061	Deu-DHP B	2.39 ± 0.089	35 ± 5	0.0682
TBP	WT DHP B	0.82 ± 0.024	12 ± 2	0.0683	WT DHP B	1.15 ± 0.026	17 ± 1	0.0676
	Meso-DHP B	4.80 ± 0.715	141 ± 36	0.0340	Meso-DHP B	10.49 ± 2.75	351 ± 122	0.0299
	Deu-DHP B	1.22 ± 0.145	42 ± 11	0.0290	Deu-DHP B	1.57 ± 0.064	94 ± 4	0.0167

A second method to determine the differences in the enzyme reaction rates was a colorimetric assay utilizing the formation of Russig's Blue from the enzymatic oxidation of 1-methoxynaphthalene. The reactions were initiated upon the addition of varying concentrations of H_2O_2 and monitored for 5 mins. The initial reaction rates were determined by extracting the absorbance data at 610 nm (Figure S5), the formation rate was plotted against the increasing concentration of peroxide to demonstrate the extremely enhanced activity of Meso- and Deu-DHP (Figure 5). The concentration of Russig's Blue was found using the molar absorptivity 14500 $M^{-1} cm^{-1}$ (610 nm).[26] The kinetic parameters of Meso-DHP were drastically improved from WT DHP, presenting an 11.4-fold increase in turnover and an 8.1-fold increase in catalytic efficiency. Deu-DHP resulted in a lesser improvement compared to Meso-DHP but the kinetic parameters were still greatly enhanced from the wildtype enzyme, the turnover and catalytic efficiency were increased 6.0-fold and 4.8-fold, respectively. The increase between Meso- and Deu-DHP was about 2-fold, indicating the order of reactivity to be Meso > Deu > WT (Table 2).

Table 3.2. Kinetic Parameter of H_2O_2 dependent oxidation of 1-Methoxynaphthalene to Russig's Blue

	K_M^{H2O2} (μM)	k_{cat} (min^{-1})	k_{cat} / K_M^{H2O2} (μM^{-1} min^{-1})
WT-DHP	26.1 ± 19.2	1.6 ± 0.3	0.0613
Meso-DHP	36.7 ± 8.7	18.2 ± 1.3	0.496
Deu-DHP	32.3 ± 12	9.5 ± 0.6	0.294

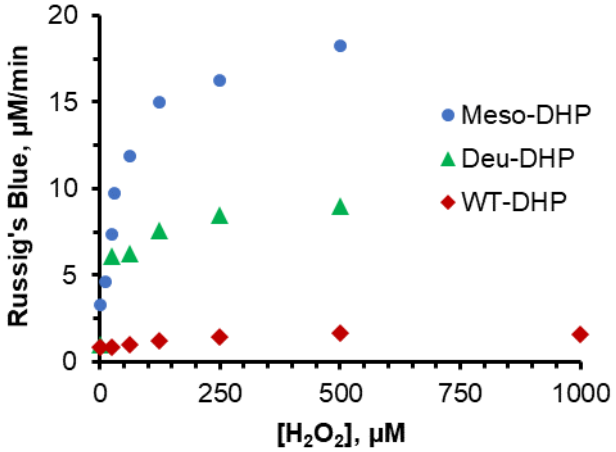

Figure 3.5. Peroxide dependent rate of Russig's Blue formation for WT, Meso-, and Deu-DHP.

Nonnative DHP Reactivity Studies

To further examine the substrate scope of the nonnative enzymes, previously studied substrates of WT DHP were reacted with the new enzymes and the reaction conversions were compared. These 5 min endpoint assays were conducted using previously published conditions and the reactivity was measured by HPLC/UV-vis. A panel of substituted phenols, indoles, pyrroles were examined, and substrate conversions were calculated (Table 3). The Co and Cu enzyme variants did not exhibit H_2O_2-catalyzed substrate reactivity. Mn-DHP was greatly inhibited (Table S1) compared to the native reaction and resulted in near yields 0 (2,4-DNP) -17.8% (4-BG) of the native reactions with the WT enzyme with H_2O_2 as an oxidant and 0 (2,4-DNP) – 68.9% (2,4,6-TBP) with *m*CPBA as the oxidant. Although reactivity was increase in the presence of the stronger oxidant, reactivity was not able to be restored to the initial conversion.

Table 3.3. H_2O_2-dependent substrate conversion using dehaloperoxidase with differ Fe-containing porphyrins: protoporphyrin, IX mesoporphyrin IX, deuteroporphyrin IX.

Substrate	WT-DHP	Meso-DHP	Deu-DHP
4-BP	35.5 ± 0.9	60.2 ± 3.5	28.9 ± 1.3
2,4,6-TCP	>99	>99	94.7 ± 3.6
2,4,6-TBP	97 ± 1	>99	99 ± 13
2,3,4,5,6-PCP	11.0 ± 2.1[a]	21.7 ± 8.8	27.8 ± 1.7
4-NP	34.0 ± 0.1[b]	42.8 ± 1.0	29.5 ± 1.0
2,4-dNP	n.d[b]	16.6 ± 1.7	2.2 ± 1.1
o-guaiacol	67.6 ± 0.2[c]	99.0 ± 0.1	86.3 ± 1.7
4-Br-G	99.7 ± 0.2[c]	>99	99.5 ± 1.2
o-cresol	31.6 ± 6.2[a]	60.6 ± 9.4	49.8 ± 6.0
4-Br-*o*-cresol	27.5 ± 3.5[a]	46.7 ± 4.0	52.2 ± 3.6
Indole	24.1 ± 2.3[d]	72.3 ± 2.3	39.4 ± 2.7
5-Br-I (pH 7)	48.1 ± 2.3[d]	85.7 ± 1.0	47.8 ± 4.5
1-MeO-Naphthlene	25.4 ± 0.7	62.4 ± 2.1	65.6 ±1.5
Pyrrole	31.7 ± 2.5[e]	54.4 ± 0.3	25.8 ± 0.9
N-Methylpyrrole	40.8 ± 2.2[e]	61.3 ± 0.6	35.0 ± 4.1

Although limited conversion was demonstrated with the three previous enzymes, in general, Fe-containing Meso- and Deu-DHP had similar or increased reactivity compared to the native enzyme. The peroxidase substrates, TCP, TBP, and 4-Br-*o*-guaiacol originally have high reactivity with WT-DHP, this trend remained with the nonnative iron-containing DHP enzymes. The (peroxygenase) substrate classes containing pyrroles, indoles and cresols resulted in greatly increased reactivity with Meso-DHP ranging from a 1.5-2-fold (pyrrole, n-Me-pyrrole, *o*-cresol, 4-Br-*o*-cresol and 5-Br-I) to a 3-fold (indole) increase, but remained the same in the presence of Deu-DHP (with the exception of the cresol class).

The remaining phenolic substrates, 4-BP, PCP, 4-NP, 2,4-dNP, and *o*-guaiacol, exhibited increased or equivalent reactivity with Deu-DHP, and heightened reactivity in the presence of Meso-DHP demonstrated by substrate conversion increases of up to 2-fold higher. A notable observation was the presence of 2,4-dinitrophenol reactivity by Meso-DHP (16%), which was unreactive in the presence of WT DHP in pH 7 conditions. The pKa of 2,4-dNP (4.07[39]) is lower

than 4-NP (7.15[39]) which supports the diminished activity of 2,4-dNP compared to 4-NP in these conditions. As a way to further probe the substrate's oxidation a pH dependence study was conducted using both of the nitrophenols as well as pyrrole as it also has a lower pKa (-3.8[40]). These reactions were conducted using the same conditions, with the exception of pH, (5, 6, 7, and 8) and the substrates conversion was measured by HPLC UV-vis.

In Figure 6A WT-DHP has no reactivity at pH 8, but increases as the pH in decreased (up to 44.9% conversion).[41] Deu-DHP demonstrated limited reactivity at pH 8 (5.8%) but has similar reactivity to the native enzyme as the pH is lowered. The major difference observed was Meso-DHP's enhanced activity at higher pH's, in pH 8 conditions, there is already 35.9% conversion, as the conditions become more acidic Meso-DHP and WT-DHP have similar reactivities. The trend for 2,4-dNP remained the same, WT-DHP had no reactivity against the substrate at pH 7 and 8 but reached 24.6% at the lowest pH (Figure 6B). Deu-DHP had limited reactivity start at pH 7 (2.1%) yet had similar conversions as the WT enzyme at lower pH's. The most drastic difference is a feature of Meso-DHP, at pH 7 and 8 there is moderate activity, 16.5% and 8.8%, respectively. At the lower pH's, 5 and 6, Meso-DHP reaches ~30% substrate conversion. Pyrrole's pH studies also demonstrated the expected results, as the pH decreased all three enzymes had increasing activity, Meso-DHP consistently lead to higher activity (Figure 6C).

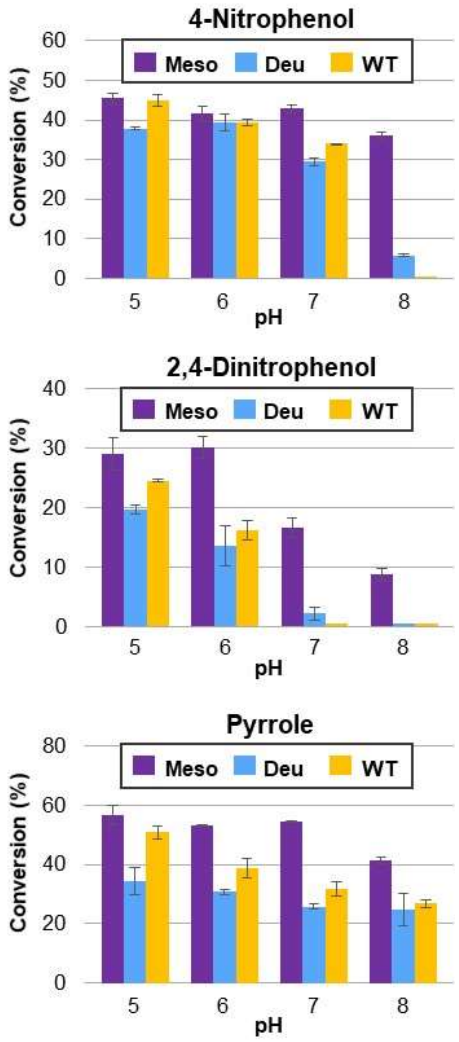

Figure 3.6. pH dependent reactions of 4-NP, 2,4-dNP, and pyrrole

To further examine the differences in reactivity and rate in the enzyme variants timed-reactions (0 - 60 min) of enzyme-catalyzed 1-MeON conversion were studied (Figure 7). At the final endpoint the substrate conversion was measured to be similar for all three enzymes, yet the early time points (0-10 mins) of the enzyme variants demonstrate a huge substrate conversion rate increase. For reactions quenched at 30 s, Meso-DHP had reacted with 55% of the substrate, Deu-DHP with 32% and WT with 3%. These results combined with the previously discussed sections

demonstrate that nonnative enzymes have enhanced reaction, initial reaction rate, and Meso-DHP has a lesser pH dependence for its optimal activity.

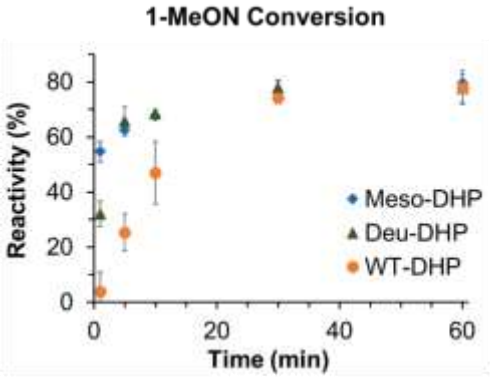

Figure 3.7. Time Dependence of DHP reactivity with 1-MeON (0-60 min).

Stopped-Flow UV-Visible Characterization of Nonnative DHP B Reactions

Formation of the H_2O_2-activated heme species was investigated by single-mixing stopped-flow UV-visible spectroscopy at pH 7 (Figure 8 and 9). Each ferric enzyme [Meso-DHP: 399 (Soret), 520, 630 nm; Deu-DHP: 397 (Soret), 518, 630 nm, black] was rapidly mixed with 10 eq. H_2O_2 to form Compound ES [Meso-DHP: 407 (Soret), 534, 575 nm; Deu-DHP: 407 (Soret), 530, 567(sh) nm, blue]. The formation time of Compound ES was interpolated by SVD analysis to be 2900 and 900 ms, for Meso-DHP and Deu-DHP, respectively. The lifetime of the transient species was measured in seconds (20-50 s) before degradation. Compound ES was observed to be a transient species and the resultant heme species was observed after 500 secs (900 scans; Figure S6). The final species of Meso-DHP did not return to the ferric heme state [402 (Soret) and 580 nm, blue]; the Soret's intensity decreased 1.5-fold due to heme-bleaching and a major band at 580 nm within the q-band region was formed. Deu-DHP underwent a less drastic bleaching and the final species was reminiscent of the initial ferric starting species.

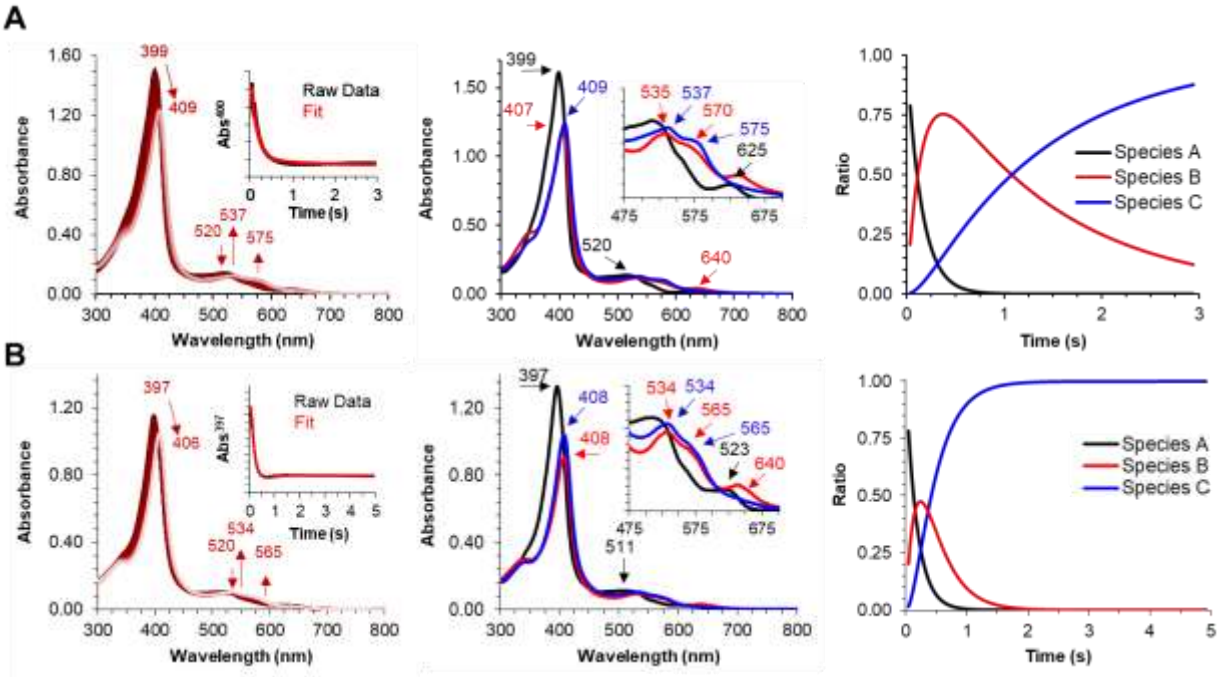

Figure 3.8. Kinetic data for the reaction of Meso-DHP and Deu-DHP with 10 eq. H_2O_2 at pH 7. **(A)** Left: Raw data of Meso-DHP and H_2O_2 reacting over 3 s to form Compound ES. The inset shows the raw data wavelength trace and SVD fit at 400 nm. Middle: calculated spectra of the three reaction components derived from the SVD analysis: Ferric Meso-DHP (black), a preactivated species of Compound ES (red) and Compound ES (blue). Right: time dependences of the relative concentrations for the three components shown in the middle panel as determined from the fitting of the spectra in the top panel. **(B)** Kinetic data for the reaction of Deu-DHP with 10 eq. H_2O_2 at pH 7. Left: raw data of Deu-DHP and H_2O_2 reacting over 5 s to form Compound ES. The inset shows the raw data wavelength trace and SVD fit at 397 nm. Middle: calculated spectra of the three reaction components derived from the SVD analysis: Ferric Deu-DHP (black), a preactivated species of Compound ES (red) and Compound ES (blue), Right: time dependences of the relative concentrations for the three components shown in the middle panel as determined from the fitting of the spectra in the top panel.

Substrate reactivity of the DHP variants were analyzed by double-mixing stopped-flow UV-visible spectroscopy at pH 7. Four substrates, 4-bromocresol, 5-bromoindole, 4-nitrophenol and 1-methoxynaphthalene, previously demonstrated reactivity with WT DHP[16] were used to compare the new DHP variants. For all figures and data, as well as Mn-DHP data, see the supporting information (Figures S7-9).

Meso-DHP: Compound ES, formed in an aging line for 2.9 s, reacted with each of the four substrates. Raw data and calculated spectra derived by SVD analysis (Figures 9 and S7) identified

a typical heme reduction pathway in which Compound ES was reduced to the ferric oxidation state and a consequent reduction the oxyferrous globin resting state in all cases with the exception of 4-BC which remained in a ferric-like peroxidase resting state. For 4-BC, the formation of the ferric state [398 (Soret), 520, 630nm] (Figure 9A and B) was complete after 225 ms, faster than WT's formation time of 368 nm. The ferric species was short lived and a new species was formed [398 (Soret), 486, 530, 592, 630], these results slightly differ from the results published in Malewschik *et.al.*[16] as the final species in Meso- are less indicative of an Fe-Br adduct in the WT reaction. Additionally, The SVD calculated species demonstrate that the enzymes return to the resting ferric state was faster for the Meso-DHP (225 ms) compared to 368 ms for WT.

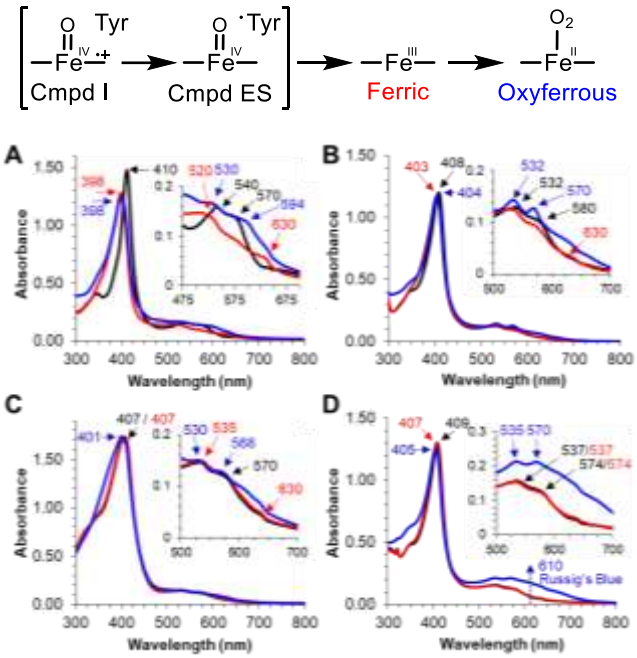

Figure 3.9. (A) Calculated spectra of the three reaction components derived from the SVD analysis: Meso-DHP Compound ES (black), ferric Meso-DHP B (red) and the final resting species (blue). **(B)** calculated spectra of the three reaction components, Meso-DHP Compound ES (black), a ferric/oxyferrous mixture (red) and oxyferrous (blue). **(C)** calculated spectra of the three reaction components, Meso-DHP Compound ES (black), ferric (red) and oxyferrous species(blue). **(D)** calculated spectra of the three reaction components, Meso-DHP Compound ES (black), ferric (red) and oxyferrous species (blue).

Analysis of the other DHP substrates reactivity was conducted with the two previously published substrates, 5-BI[9] and 4-NP[10], and 1-MeON, a substrate presented within the work (Figure S7 A-C). The reactivity with Meso-DHP Compound ES and 5-BI follow a similar trend as the WT enzyme. The calculated species demonstrated that Compound ES [408 (Soret), 532, 580 nm, black] was reduced quickly to a ferric/oxyferrous mixture [403 (Soret), 535, 580, 630(sh) nm, red] and then further reduced to an oxyferrous state [404 (Soret), 532, 570 nm, blue] with the formation of the blue product, 5,5′-Br_2-indigo [600s nm]. The reactivity with 4-NP (λ_{max} = 360 nm) was much slower than 5-BI, Compound ES [407 (Soret), 535, 570 nm, black] was slowly reduced to a ferric/oxyferrous mixture [401 (Soret), 530, 568 nm, blue] and at the end of the 50 s reaction, this species was only present in ~66%, comparatively to 5-BI's final abundance of nearly 100%. Meso-DHP and 1-MeON reacted similarly to 5-BI as Compound ES [409 (Soret), 537, 574, black] was reduced completely to the oxyferrous state. [405 (Soret), 535, 570, blue]. The product, Russig's blue, was observed at 610 nm.

Deu-DHP: The reactivities of the four previously discussed substrates with Deu-DHP Compound ES were then compared (Figures 10 and S8). SVD analysis was only able to be performed with 4-BC and 5-BI as the two other substrate oxidations' data (4-NP and 1-MeON) did not properly fit one-step, two species or two-step, three species irreversible mechanisms, and as such, experimentally obtained spectra at selected time points detailed in the figure legends are shown. The oxidation of 4-BC demonstrated similar results compared to Meso-DHP, Compound ES [410 (Soret), 538, 565, black] was reduced back to ferric [397 (Soret), 524, 625, red], and then further reacted to a final resting species [404 (Soret), 526, blue]. SVD analysis calculated the time from Compound ES to ferric was between the two other iron-containing enzymes WT (368 s) < Deu (275 s) < Meso (225 s).

For 5-BI the calculated 3-species demonstrated that Compound ES [407 (Soret), 534, 565, 636 nm, black] was reduced to a ES/ferric mixture [406 (Soret), 535, 564, 636 nm, red] and then further reduced to a ferric/oxyferrous state [404 (Soret), 526 nm, blue] with the limited formation of the blue product, 5,5′-Br_2-indigo [600s nm]. Similar to the reactivity with Meso-DHP, Deu-DHP reacted slowly with 4-NP (λ_{max} = 360 nm) from Compound ES [407 (Soret), 535, 565 nm, black; t = 0 s] was slowly reduced to a ES/ferric mixture [406 (Soret), 536, 568 nm, red; t = 110 s] and then to a convoluted ferric mixture [404 (Soret), 606 nm, blue; t = 500 s]. Deu-DHP Compound ES [407 (Soret), 535, 565 nm, black; t = 0 s] reacted with 1-MeON reduced the heme to a ES/Ferric mixture [406 (Soret), 535, 560 nm, red; t = 45 s] and then completely reduced to the oxyferrous state [404 (Soret), 531, 554, blue; t = 500] with a shoulder at 610 nm representing Russig's Blue formation.

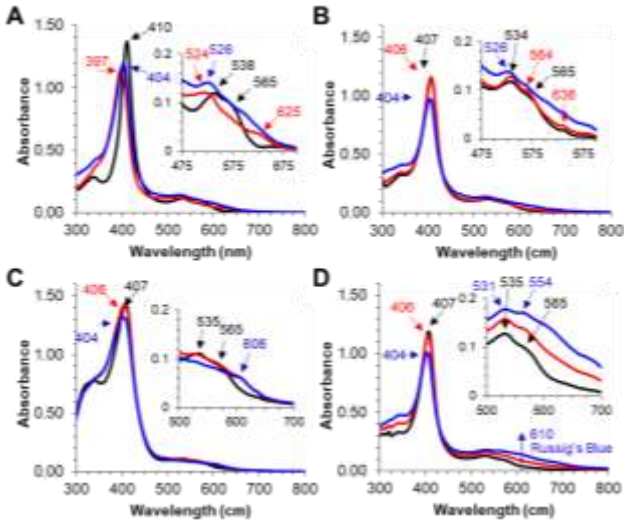

Figure 3.10. (A) Calculated spectra of the three reaction components derived from the SVD analysis: Deu-DHP Compound ES (black), ferric Deu-DHP (red) and a ferric-like final resting species (blue). **(B)** Calculated spectra of the three reaction components derived from the SVD analysis Deu-DHP Compound ES (black), oxyferrous (red) and oxyferrous/heme bleaching (blue, t = 500 s). **(C)** Selected time point traces of three reaction components Deu-DHP Compound ES (black, t = 0 s), ferric/ES mixture (red, t = 110 s) and ferric/bleached heme species (blue, t = 500 s). **(D)** Selected time point traces of three reaction components Deu-DHP Compound ES (black, t = 0 s), ferric (red, t = 45 s) and oxyferrous species (blue, t = 500 s).

Mn-DHP: As previously discussed, Mn-DHP was much less active at substrate oxidation in the presence of H_2O_2. Stopped-flow UV-vis experiments (Figure S9) were used to determine the mechanistic reasons. In Figure S9A, the single mixing experiment between Mn-DHP and 50 eq H_2O_2 demonstrate that peroxide is not a strong enough oxidant to fully oxidize Mn(III)-DHP to Compound ES, as only a small portion of the enzyme is oxidized (Soret = 410 nm). Conversely, the stronger oxidant *m*CPBA (5 eq., Figure S9B), fully oxidized the enzyme to Compound ES in 150 ms. This activated species was short lived as seen by the return to the resting Mn(III) state complete after 15 seconds. The reactivity of "*m*CPBA activated" Mn-DHP Compound ES (mixing time = 150 ms) with 5-BI (Figure S9C) demonstrated a 6-fold enzyme reduction rate increase as seen by the return to the Mn(III) after 2.5 s.

Binding Studies

The electronic absorption spectra of DHP B in the presence of guaiacol substrates were recorded in 100 mM KPi (pH 7) containing 5 % (v/v) MeOH. The Soret band and/or the Q-band region, showed well-behaved optical difference spectra (Figures S10-14) upon titration of the phenolic substrates (< 250 equiv), enabling the determination of the corresponding apparent dissociation constants (Kd values; Table 4). The binding coefficients demonstrated no obvious trend among the DHP variants. The substrate with the highest affinity was consistently 4-BC (< 90 μM), and the weakest substrate binding was either 4-NP (Meso- and WT DHP) or 2,4,6-TCP (Deu-DHP).

Table 3.4. K_d Values for Substrate Binding to DHP B Variants at pH 7

Substrate	WT-DHP	Meso-DHP	Deu-DHP	Mn-DHP
4-BP	305 ± 15	182 ± 8	438 ± 30	149 ± 6
4-BC	86 ± 14[16]	39 ± 3	90 ± 9	19 ± 1
4-NP	262 ± 23	1332 ± 282	291 ± 52	880 ± 53
2,4,6-TCP	208 ± 13	111 ± 7	532 ± 81	649 ± 26

X-ray crystallographic studies of DHP B in complex with heme variants.

The structure of the nonnative enzyme, Meso-, Deu-, and Mn-DHP were determined individually and in complex with 4-nitrophenol (4-NP), 4-bromophenol (4-BP), 4-bromo-*o*-cresol (4-BrC) and/or 2,4,6-trichlorophenol (TCP). The protein/heme variants crystallized in $P2_12_12_1$ space group, were found to be isomorphous with two molecules to the asymmetric unit, protomer A and B, under conditions consistent with the previously reported structures for WT DHP B [15,20,42]. The resolution for each of the obtained structures are listed in Table S2 and were found to vary from 1.32 Å (Mn-DHP) to 1.98 Å (Deu-DHP complexed with TCP). The protein variants showed the presence of substrates in the active site of both monomers present in the asymmetric unit, with the exception of Deu-DHP in complex with 4-NP (4-NP bound only in protomer A). Accordingly, the figures and selected distances (Table S3) are presented for the protomer A.

Heme environments for Mn-, Deu- and Meso-DHP (two alternate positions in the binding cavity, Figure X1) structures in the absence of the substrate are shown in Figure 11 (A-C), respectively. In general, Mn-DHP structures superpose very closely with the native DHP B, with rmsd of 0.35 Å in absence of substrate, and rmsd 0.19 Å and 0.39 Å in the presence of 4-NP and TCP structures respectively. In the case of Meso- and Deu-DHP, differences in heme positioning were observed in the binding cavity in the absence of the bound ligand when compared to WT DHP (Figures 11A-C).

As a marker for the heme position we have shown distances from CG1 and CG2 atoms of residue V59, which are equidistant from heme atoms C4A and C1B in WT and Mn-DHP structures (numbers for Mn-DHP, protomer A are given in Table S3), as well as residues L83, L92, F24 F35 and F97 as markers for the positions 2 (p2) and 4 (p4) of the heme macrocycle. From Figure (Figure 11A and B) it can be seen that the cofactor in Mn-DHP and Deu-DHP occupy distinct

positions within the heme cavity. Mn-PIX is positioned approximately 4 Å deeper into the cavity, relative to Deu-PIX, the latter being shifted toward the entrance of the cavity and therefore more exposed to solvent. In fact, the protein buried heme surface for the two proteins, in absence of a ligand, amounting to an average 87% for Mn-PIX surface area, and 62% for Deu-PIX, resulting in a difference of about 25%, as calculated by PISA software (Krissinel & Henrick (2007)).

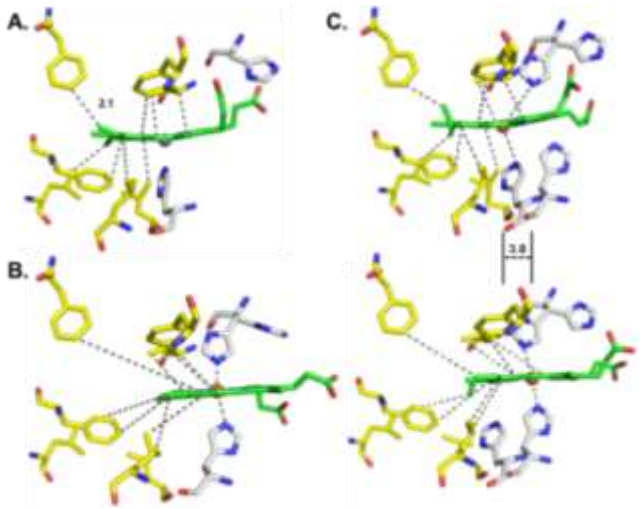

Figure 3.11. Cofactor displacement of Deu-PPIX in the DHP scaffold. A) Mn-DHP, a model for WT DHP B. B) Deu-DHP in Bis-Histidine extended conformation. C) Cofactor displacement of Meso-PPIX in the DHP scaffold

The observed heme binding differences are likely due to fewer hydrophobic contacts that are available in Deu-PIX, since the vinyl side groups in the 2,4-positions of the porphyrin macrocycle are substituted for hydrogen atoms. Additionally, different heme binding positions are likely facilitated by the flexibility of the proximal loop that contains residue H89 which coordinates the heme metal center. In the structures of WT, Mn and Meso-DHP, H89 is located on a tight helical turn comprising residues 87-89. In Deu-DHP in the absence of ligand, and even when 4-BP is bound, this helical turn is in a relaxed conformation, making the entire loop more flexible. This state could be facilitating the movement of the proximal heme binding side, allowing the formation

of a bis-histidine ligation state of the heme iron, shown in Figure 12, which likely stabilizes the binding of this cofactor variant in the heme cavity and could potentially explain the more exposed positioning of the Deu-PIX compared to the other cofactors.

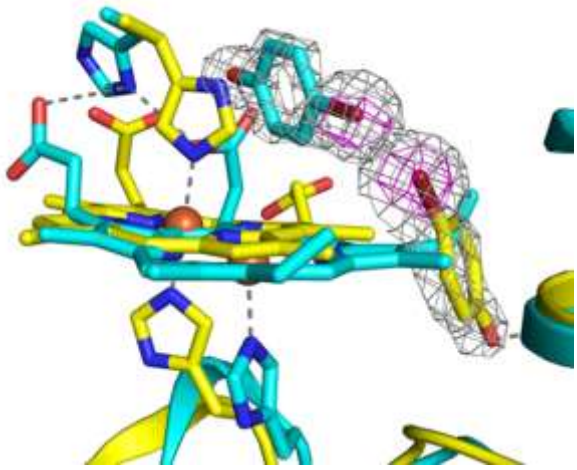

Figure 3.12. Cofactor displacement of Deu-PIX (yellow, bis-His ligation) superimposed with Meso-PIX (teal) with 4-BP substrate.

In our studies of non-native heme variants, we have tried to focus on comparing structures the non-native enzyme complexed with: a known WT DHP inhibitor (4-BP), a peroxidase substrate (TCP), a peroxygenase substrate (4-NP), and a substrate of both activities (4-BC). The relevant binding constants and hydrogen bonding interactions for the complex of substrates with Deu-, Meso- and Mn-DHP, compared to WT DHP, are listed in Table 3.

4-bromophenol: The observed binding mode of Meso-DHP and Mn-DHP with 4-BP (Figure 13A and C) is virtually identical to what was previously observed for WT-DHP. The substrate is positioned above the heme in the distal cavity, showing a hydrogen bonding interaction between the hydroxyl group of 4-BP and the carboxylic group of heme propionate D (2.99 Å for Mn-DHP, 2.94 Å for Meso-DHP and 2.82 Å for WT). The distal histidine, H55, assumes its external conformation, which is also observed in the Mn-DHP structure and was observed for WT DHP.

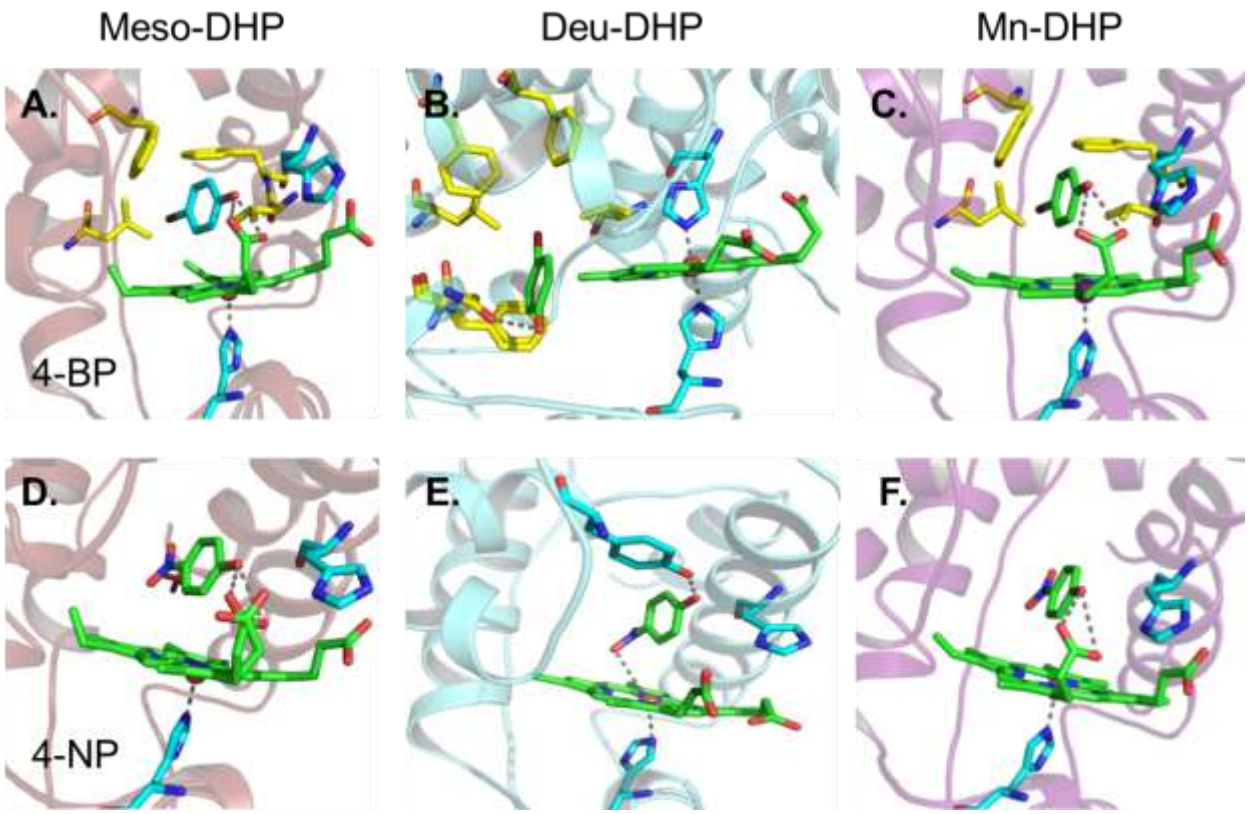

Figure 3.13. Substrate interaction in 3 DHP variant active sites. A) Meso-DHP/4-BP, B) Deu-DHP/4-BP, C) Mn-DHP/4-BP, D) Meso-DHP/4-NP, E) Deu-DHP/4-NP, and F) Mn-DHP/4-NP
In the case of Deu-DHP (Figure 13B), the observed binding mode was significantly different in the compared to Meso-DHP complex. The substrate binds in a distinct internal location, positioned between the δ edge and backbone of residues N96 and F97. The bromine atom is surrounded by hydrophobic residues F21, F24, V59, L100, with the closest residues being F21 and F24 at a distance of 3.81 and 4.14 Å, respectively. Moreover, there are two important hydrogen bonding interactions, which further stabilize the protein-substrate interaction i) hydroxyl of 4-BP and oxygen atom of the N96 side chain and ii) peptide bond N of T93 (Table 3). Additionally, in order to verify the position of 4-BP, we have also calculated anomalous difference map[43,44] and a bromine peak was found to be located precisely at the position found for the bromine atom in the 4-BP structure (data not shown).

As mentioned before, Deu-PIX has decreased hydrophobic interactions with the protein within the heme binding cavity, so the cofactor can slide out toward the entrance of the heme cavity. The distance between CB of residue N96 and methyl group CMF of the 4-BP bound orientation of Deu-PIX is 7.10 Å. In comparison, for Deu-DHP complexed with 4-NP, this distance is 3.50 Å. Thus, in the presence of 4-BP, the substrate molecule most likely generates and fills this cavity,

pushing the Deu-PIX cofactor to this external position. The overall binding of 4-BP involves a clockwise rotation of the Deu-PIX moiety by approximately 50^{o}, positioning the CMF at a distance of 3.28 Å from Br atom and 3.35 Å from C3 atom of the substrate, which maintains the hydrophobic environment needed for this interaction. This is in agreement with mutation attempts in Cytochrome $P450_{BM3}$ (Reynolds et al, 2016) to strengthen the binding of Deu-PIX affected by generation of 'holes' due to absence of vinyl groups normally present native heme molecule.

4-nitrophenol: The position observed for this compound complexed with the non-native proteins (Figure 13 D-F) is virtually identical to what was previously observed for WT-DHP.[10] The nitro group in the *para*-position of the ring does not interact with a hydrophobic environment, as such this substrate is positioned closer to the entrance of the heme binding cavity, with the hydroxyl group interacting with propionate D and Y38 residues, listed in Table 3. In this complex, Deu-DHP aligns well with both Meso-DHP and with Mn-DHP, rmsd values of 0.31 and 0.34 Å, respectively, whereas these values were 0.74 and 0.78 Å for 4-BP structures, respectively.

4-bromo-o-cresol: For the 4-BC complex with Meso-DHP the substrate binds in the same position and orientation as in WT protein (PDB Entry: 6ONX), shown in superposition of the active site for the two structures in Figure S15, (average rmsd value of 0.21 Å). However, in protomer A, this substrate is found in two different conformations (data not shown), one of which (occupancy of 0.2), is identical to the only conformation present in protomer B. The other conformation, with the occupancy of 0.7, shows substrate interactions similar to those encountered for 4-methyl-*o*-cresol and 4-fluoro-*o*-cresol two of the most reactive of *para*-substituted *o*-cresol substrates (PDB Entry: 6ONR and 6ONG, respectively), where the substrate hydroxyl group interacts with Y38 via a water molecule, and directly interacts with residue T56.

2,4,6-trichlorophenol: The complex of the peroxidase substrate TCP with WT DHP B was recently solved by our group, and the position of the substrate was found to be virtually identical to previously published structure of the complex of TCP with DHP A mutant Y34N[45] (PDB Entry 4KMW), shown in Figure S16A. In the TCP complex structures with Deu- and Mn-DHP, the TCP ligand is observed to bind very similarly as observed for WT DHP, as shown in Figure S16B. Since Meso-DHP structures were shown to be similar to the Mn-DHP structures, the TCP-Mn-DHP complex may also be regarded as a good representative for TCP-Meso-DHP complex. The substrate is bound at the entrance to the heme cavity, displacing the heme propionate D side chains by being in close proximity to the region occupied by this group. The hydroxyl group of the substrate has strong hydrogen bonding interaction with residues Y38 and H55 (external conformation), as depicted in Figures S16B and listed in Table 3.

Overall, the panel of substrates chosen to be complexed with the non-native variants of DHP seem to interact with Meso- and Mn-DHP in similar fashion compared with the structures previously obtained for WT DHP (Figure S17). The interaction with Deu-DHP with the substrates, specifically with 4-BP, affects the mobility and disorder of the Deu-PIX in the heme binding cavity, potentially due to weakened hydrophobic interactions because of replacement of the vinyl groups for hydrogens (Figure S18)

DISCUSSION

The data presented herein, support that the multifunctional enzyme DHP is an optimal candidate for swapping nonnative porphyrin cofactors as it can readily accept different metallated protoporphyrin IX's (Mn, Cu, Co) and also structurally different porphyrin cofactors such as Meso-PIX and Deutero-PIX. The nonnative DHP variants possess similar stability and, when

applicable, equal or increased activity against peroxidase and peroxygenase substrates. The iron-porphyrin incorporated enzymes demonstrated moderate to excellent activity against the substrates analyzed within this study. The activity of wildtype DHP (Fe-PPIX-substituted) has been well characterized since its initial discovery in 1996,[7] demonstrating activity against toxic compounds such as halogenated and nitrosylated phenols,[10,12,13] guaiacols,[15] cresols,[16] indoles,[9] and pyrroles.[11] The mechanism of oxidation of the compound classes vary dependent on the substrates' structure, including H_2O_2- and O_2-activated electron transfer or direct O-atom incorporation into the oxidized product. The multiple activities of this small globin are reminiscent of monofunctional peroxidases, peroxygenases, and oxidases, but all can be conducted in the active site of DHP. An enzyme with these multifunctional characteristics provides an excellent scaffold for a tunable biocatalyst.

The unreactive/low reactivity synthetic DHP enzymes were determined to be Co-, Cu-, Mn-PPIX incorporated into the activity pocket. Co-PPIX when bound to DHP is in a low spin d^6 state, it is expected to be stable and inert to oxidation/reduction. As such, the lack of reactivity was justified. Previous research with synthetic Co-globins have reported O_2-binding 50-100(myoglobin) and 10-25 (hemoglobin) times higher than the corresponding Fe-containing native proteins.[4] Loss of peroxidase activity in HRP was also reported due to the high binding affinity of O_2 and low affinity towards H_2O_2.[5] Cu-DHP had close to zero percent reactivity with all substrates analyzed. Mn-DHP exhibited weak activity towards DHP's known substrates. For the nine substrates analyzed the native oxidant of DHP, H_2O_2, saw a decrease of 90 ± 7% reactivity on average, and *m*CPBA resulted in an average decrease of 66 ± 28%. Mechanistic investigations demonstrated that Mn-DHP Compound ES is auto-reduced to Mn(III) quickly, this process

competes with substrate oxidation which is supported by the reduced substrate reactivity. Overall, the incorporation of Mn-PPIX was not beneficial to the enzyme's oxidative function.

Within this study two Fe-porphyrins structurally similar to Fe-PPIX were compared. The 2 and 4 porphyrin positions were modulated from vinyl to ethyl to hydrogens. In previous research, Yonetani et. al. found that the mutant 2,4 positions when incorporated into cytochrome C peroxidase did not diminish the peroxidase activity towards ascorbate (1968) and within the scaffold of horseradish peroxidase, guaiacol oxidation was only slightly diminished (1972). Peroxidase activity was greatly affected by removal of the 6,7-propionate groups.[46,47] Tamura (1972) concluded that DHP's structurally similar horse-heart myoglobin required the 2,4 positions for O_2-transport, but the propionates were unnecessary.[48] These observations remain true when analyzing DHP, but in the case of deutero and meso incorporation into DHP activity is not only retained, it is in most situations greatly enhanced, as demonstrated in the HPLC and enzyme kinetics section above. Although as seen in the crystal structures, some porphyrin dissociation occurs in Deu-DHP and thus some efficiency may be lost, it is expected that if the vinyl 'holes' are filled by amino acid point substitution, some of the lost activity could be retained.

DHP is a unique globin/enzyme, known as the first globin with biologically relevant peroxidase activity,[7,49–51] later, discovered to also possess peroxygenase activity.[9,11,16,41] Trihalophenol peroxidase assays demonstrated that both meso- and deutero-PPIX-incorporated DHP could increase turnover numbers and initial rates. while maintaining the native enzyme catalytic efficiency. As this enzyme is multifunctional, an assay to determine peroxygenase activity was required. To obtain that data, an assay developed by Shoji and coworkers to monitor the hydroxylation of 1-methoxynaphthalene was applied to compare the iron-porphyrin containing enzymes.[25] The formation of the product, Russig's Blue, allowed for the colorimetric

determination of kinetic data. Most notably, the catalytic efficiencies and turnover numbers of the synthetic variants were drastically increased from the WT globin, Meso > Deutero >>> WT.

The reactivity difference between WT DHP and Meso-DHP can be attributed to the heme structure differences (vinyl to ethyl groups), the additional sp^3 hybridized carbons in the MPIX increase the electron donation towards the Fe-center which assists in stabilizing the ferric state. This can be supported experimentally by monitoring the auto-oxidation over time, contrasting with the WT PPIX auto-reduction properties.[12] Previous research of substituted myoglobins have demonstrated a 2,4- pK_a dependence of Meso (9.2) > Deu (8.8) > Proto (8.7) as well as the same general trend for these cofactors in HRP.[47,48] The basicity of those groups in the cofactor also affected the redox potential in myoglobin, Meso (-170 mV) > Deu (-162 mV) > Proto (-140 mV) (reference electrode is Ag/AgCl).[30] We demonstrated a similar trend in DHP with WT DHP (206 ± 6 mV; standard hydrogen electrode reference; SHE) and Meso-DHP having ~ 2-fold more negative potential (+109.79 ± 5.57 mV vs SHE). As peroxidase enzymes that have a more negative redox potential (vs SHE) typically have enhanced peroxidase activity,[52] these data provide insight on why Meso-DHP provides enhanced catalytic activity.

CONCLUSION

Dehaloperoxidase's catalytic capabilities are drastically enhanced upon the incorporation of Fe Meso-PIX, and moderately enhanced upon the addition of Fe Deu-PIX when exchanged for the native Fe PPIX, while maintaining the globin's multifunctionality. The TXP and 1-MeON activity studies demonstrated accelerated peroxidase and peroxygenase reactivity in the presence of iron nonnative porphyrins as a result of increased electron donation towards the iron center by altering the 2,4-positions. These results demonstrate that DHP is an exceptional candidate for cofactor exchange and as it is the first enzyme with biologically relevant multifunctionality, which is an unprecedented scaffold. Utilizing DHP's previously

existing versatility and robustness against POP's affecting the ecosystem, this engineered biocatalyst is the first of its kind. We can improve on nature's design by incorporating nonnative cofactors to further design this biological catalyst to increase the ability of this natural bioremediation agent against common small molecule pollutants.

REFERENCES

1. Christianson, D. W. Structural chemistry and biology of manganese metalloenzymes. *Progress in Biophysics and Molecular Biology* **67**, 217–243 (1997).
2. Bond, W. C., Stone, K. L., Hua, J. & Choudhry, H. Manganese-Substituted Myoglobin: Characterization and Reactivity of an Oxidizing Intermediate towards a Weak C-H Bond. *Inorganics* **3**, 219–229 (2015).
3. Zaki, C. *et al.* Crystal Structures of Manganese-and Cobalt-substituted Myoglobin in Complex with NO and Nitrite Reveal Unusual Ligand. doi:10.1016/j.jinorgbio.2007.08.002
4. Yonetani, T., Yamamoto, H. & Woodrow, G. V. Studies on Cobalt Myoglobins and Hemoglobins I. PREPARATION AND OPTICAL PROPERTIES OF MYOGLOBINS AND HEMOGLOBINS CONTAINING COBALT PROTO-, MESO-, AND DEUTEROPORPHYRINS AND THERMODYNAMIC CHARACTERIZA- TION OF THEIR REVERSIBLE OXYGENATION*. *J. Biol. Chem.* **249**, 682–690 (1974).
5. Wang, M.-Y., Hoffman, B. & Hollenberg, P. Cobalt-substituted Horseradish Peroxidase. *J. Biol. Chem.* **252**, 6268–6275 (1977).
6. Ikeda-Saito, M., Iizuka, T., Yamamoto, H., Kayne, F. J. & Yonetani, T. Studies on Cobalt Myoglobins and Hemoglobins. *J. Biol. Chem.* **252**, 4882–4887 (1977).
7. Chen, Y. P., Woodin, S. A., Lincoln, D. E. & Lovell, C. R. An unusual dehalogenating peroxidase from the marine terebellid polychaete Amphitrite ornata. *J. Biol. Chem.* **271**, 4609–4612 (1996).
8. Roach, M. P. *et al.* Notomastus lobatus chloroperoxidase and amphitrite ornata dehaloperoxidase both contain histidine as their proximal heme iron ligand. *Biochemistry* **36**, 2197–2202 (1997).
9. Barrios, D. A. *et al.* Peroxygenase and oxidase activities of dehaloperoxidase-hemoglobin from Amphitrite ornata. *J. Am. Chem. Soc.* **136**, 7914–7925 (2014).
10. McCombs, N. L., D'Antonio, J., Barrios, D. A., Carey, L. M. & Ghiladi, R. A. Nonmicrobial nitrophenol degradation via peroxygenase activity of dehaloperoxidase-hemoglobin from amphitrite ornata. *Biochemistry* **55**, 2465–2478 (2016).
11. McCombs, N., Smirnova, T. & Ghiladi, R. Oxidation of Pyrrole by Dehaloperoxidase-Hemoglobin: Chemoenzymatic Synthesis of Pyrrolin-2-Ones. *Catal. Sci. Technol.* (2017). doi:10.1039/C7CY00781G
12. D'Antonio, J. *et al.* Spectroscopic and mechanistic investigations of dehaloperoxidase B from amphitrite ornata. *Biochemistry* **49**, 6600–6616 (2010).
13. Feducia, J. *et al.* Characterization of dehaloperoxidase compound ES and its reactivity with trihalophenols. *Biochemistry* **48**, 995–1005 (2009).
14. Belyea, J. *et al.* Enzyme Function of the Globin Dehaloperoxidase from Amphitrite ornata Is Activated by Substrate Binding †. **44**,
15. McGuire, A. H., Carey, L. M., De Serrano, V., Dali, S. & Ghiladi, R. A. Peroxidase versus Peroxygenase Activity: Substrate Substituent Effects as Modulators of Enzyme Function in the Multifunctional Catalytic Globin Dehaloperoxidase. *Biochemistry* **57**, 4455–4468 (2018).
16. Malewschik, T., de Serrano, V., McGuire, A. H. & Ghiladi, R. A. The multifunctional globin dehaloperoxidase strikes again: Simultaneous peroxidase and peroxygenase mechanisms in the oxidation of EPA pollutants. *Arch. Biochem. Biophys.* **673**, 108079

(2019).
17. Zhao, J., Zhao, J. & Franzen, S. The Regulatory Implications of Hydroquinone for the Multifunctional Enzyme Dehaloperoxidase-Hemoglobin from Amphitrite ornata. (2013). doi:10.1021/jp407663n
18. Title 40 - Protection of Environment, Code of Federal Regulations, Section 423, Appendix A, U.S. Environmental Protection Agency, Washington, D.C.,. (2013).
19. Title 15 U.S. Code Chapter 53 - Toxic Substances Control Act. (1976).
20. Carey, L. M., Gavenko, R., Svistunenko, D. A. & Ghiladi, R. A. How nature tunes isoenzyme activity in the multifunctional catalytic globin dehaloperoxidase from Amphitrite ornata. (2017). doi:10.1016/j.bbapap.2017.11.004
21. Teale, F. W. J. Cleavage of the haem-protein link by acid methylethylketone. *BBA - Gen. Subj.* **35**, 543 (1959).
22. D'Antonio, J. & Ghiladi, R. A. Reactivity of deoxy- and oxyferrous dehaloperoxidase B from Amphitrite ornata: Identification of Compound II and Its ferrous-hydroperoxide precursor. *Biochemistry* **50**, 5999–6011 (2011).
23. Yonetani, T. Studies on cytochrome c peroxidase. X. Crystalline apo-and reconstituted holoenzymes. *J. Biol. Chem.* **242**, 5008–13 (1967).
24. Chenprakhon, P., Sucharitakul, J., Panijpan, B. & Chaiyen, P. Measuring binding affinity of protein-ligand interaction using spectrophotometry: Binding of neutral red to riboflavin-binding protein. *J. Chem. Educ.* **87**, 829–831 (2010).
25. Shoji, O. *et al.* Aromatic C-H bond hydroxylation by P450 peroxygenases: A facile colorimetric assay for monooxygenation activities of enzymes based on Russig's blue formation. *J. Biol. Inorg. Chem.* **15**, 1109–1115 (2010).
26. Erman, J. E., Kilheeney, H., Bidwai, A. K., Ayala, C. E. & Vitello, L. B. Peroxygenase activity of cytochrome c peroxidase and three apolar distal heme pocket mutants: hydroxylation of 1-methoxynaphthalene. *BMC Biochem.* **14**, (2013).
27. The CCP4 suite: Programs for protein crystallography. *Acta Crystallogr. Sect. D Biol. Crystallogr.* **50**, 760–763 (1994).
28. Evans, P. R. & Murshudov, G. N. How good are my data and what is the resolution? *Acta Crystallogr. Sect. D Biol. Crystallogr.* **69**, 1204–1214 (2013).
29. Otwinowski, Z. & Minor, W. Processing of X-ray diffraction data collected in oscillation mode. *Methods Enzymol.* **276**, 307–326 (1997).
30. Galinato, M. G. I., Fogle, R. S., Stetz, A. & Galan, J. F. Modulating the nitrite reductase activity of globins by varying the heme substituents: Utilizing myoglobin as a model system. *J. Inorg. Biochem.* **154**, 7–20 (2016).
31. McCoy, A. J. *et al.* Phaser crystallographic software. *J. Appl. Crystallogr.* **40**, 658–674 (2007).
32. Murshudov, G. N., Vagin, A. A. & Dodson, E. J. Refinement of macromolecular structures by the maximum-likelihood method. *Acta Crystallogr. D. Biol. Crystallogr.* **53**, 240–55 (1997).
33. Potterton, E., Briggs, P., Turkenburg, M. & Dodson, E. A graphical user interface to the CCP4 program suite. *Acta Crystallogr. - Sect. D Biol. Crystallogr.* **59**, 1131–1137 (2003).
34. Afonine, P. V. *et al.* Towards automated crystallographic structure refinement with phenix.refine. *Acta Crystallogr. Sect. D Biol. Crystallogr.* **68**, 352–367 (2012).
35. Emsley, P., Lohkamp, B., Scott, W. G. & Cowtan, K. Features and development of Coot. *Acta Crystallogr. Sect. D Biol. Crystallogr.* **66**, 486–501 (2010).

36. Davis, I. W. *et al.* MolProbity: all-atom contacts and structure validation for proteins and nucleic acids. *Nucleic Acids Res.* **35**, W375-83 (2007).
37. Krissinel, E. & Henrick, K. Inference of Macromolecular Assemblies from Crystalline State. *J. Mol. Biol.* **372**, 774–797 (2007).
38. Adams, P. D. *et al.* PHENIX: a comprehensive Python-based system for macromolecular structure solution. *Acta Crystallogr. D. Biol. Crystallogr.* **66**, 213–21 (2010).
39. *CRC Handbook of Chemistry and Physics*. (CRC Press (Taylor and Francis Group), 2010).
40. Jones, R. A. & Bean, G. P. *Organic Chemisry: A Series of Monographs*. (Academic Press, 1977).
41. McCombs, N. L., D'Antonio, J., Barrios, D. A., Carey, L. M. & Ghiladi, R. A. Nonmicrobial nitrophenol degradation via peroxygenase activity of dehaloperoxidase-hemoglobin from amphitrite ornata. *Biochemistry* **55**, 2465–2478 (2016).
42. De Serrano, V., D'Antonio, J., Franzen, S. & Ghiladi, R. A. Structure of dehaloperoxidase B at 1.58 Å resolution and structural characterization of the AB dimer from Amphitrite ornata. *Acta Crystallogr. Sect. D Biol. Crystallogr.* **66**, 529–538 (2010).
43. Hendrickson, W. A. Anomalous diffraction in crystallographic phase evaluation. *Q. Rev. Biophys.* **47**, 49–93 (2014).
44. Choe, J. *et al.* Anomalous differences of light elements in determining precise binding modes of ligands to glycerol-3-phosphate dehydrogenase. *Chem. Biol.* **9**, 1189–97 (2002).
45. Wang, C., Lovelace, L. L., Sun, S., Dawson, J. H. & Lebioda, L. Complexes of Dual-Function Hemoglobin/Dehaloperoxidase with Substrate 2,4,6-Trichlorophenol Are Inhibitory and Indicate Binding of Halophenol to Compound I. *Biochemistry* **52**, 6203–6210 (2013).
46. Yonetani, T. & Asakura, T. Studies on cytochrome c peroxidase. XII. Crystalline synthetic enzymes containing unnatural heme prosthetic groups. *J. Biol. Chem.* **243**, 4715–4721 (1968).
47. Tamura, M., Asakura, T. & Yonetani, T. Heme-Modification studies on Horseradish Peroxidase. *Biochim. Biophys. Acta* **268**, 292–304 (1972).
48. Tamura, M., Woodrow, G. V. & Yonetani, T. Heme-modification studies of myoglobin. II. Ligand binding characteristics of ferric and ferrous myoglobins containing unnatural hemes. *BBA - Protein Struct.* **317**, 34–49 (1973).
49. Zhang, E. *et al.* Crystallization and initial spcctroscopic characterization of the heme-containing dehaloperoxidase from the marine polychaete Amphitrite ornata. *Acta Crystallogr. Sect. D Biol. Crystallogr.* **52**, 1191–1193 (1996).
50. Du, J. *et al.* Amphitrite ornata Dehaloperoxidase (DHP): Investigations of Structural Factors That Influence the Mechanism of Halophenol Dehalogenation Using 'Peroxidase-like' Myoglobin Mutants and 'Myoglobin-like' DHP Mutants. (2011). doi:10.1021/bi2009129
51. Franzen, S., Ghiladi, R. A., Lebioda, L. & Dawson, J. Chapter 10: Multi-functional hemoglobin dehaloperoxidases. *RSC Met.* **2016-Janua**, 218–244 (2016).
52. Hosseinzadeh, P. & Lu, Y. Design and fine-tuning redox potentials of metalloproteins involved in electron transfer in bioenergetics. *Biochim. Biophys. Acta - Bioenerg.* (2016). doi:10.1016/j.bbabio.2015.08.006

Supporting Information for

Chapter 3: Nonnative Heme Incorporation into Multi-functional Globin Increases Peroxygenase Activity an Order and Magnitude Compared to Native Enzyme

Ashlyn H. McGuire, Alexandra R. Pettit, Jihye Kang, Talita Malewschik, Nikhila K. Dhanvantari Madhuresh, Vesna de Serrano, Leiah M. Carey and Reza A. Ghiladi

Department of Chemistry, North Carolina State University, Raleigh, North Carolina, 27695

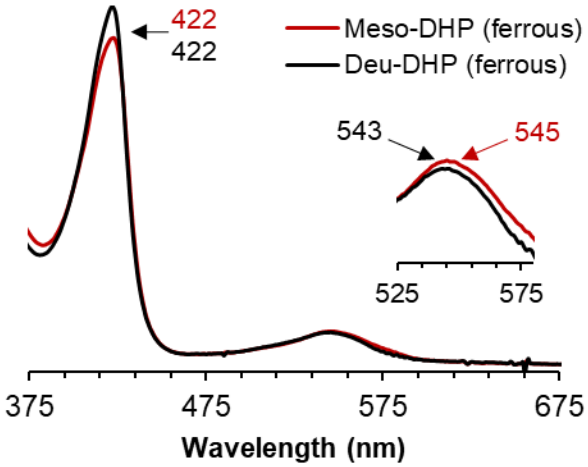

Figure S3.1. Ferrous Meso- and Deu-DHP

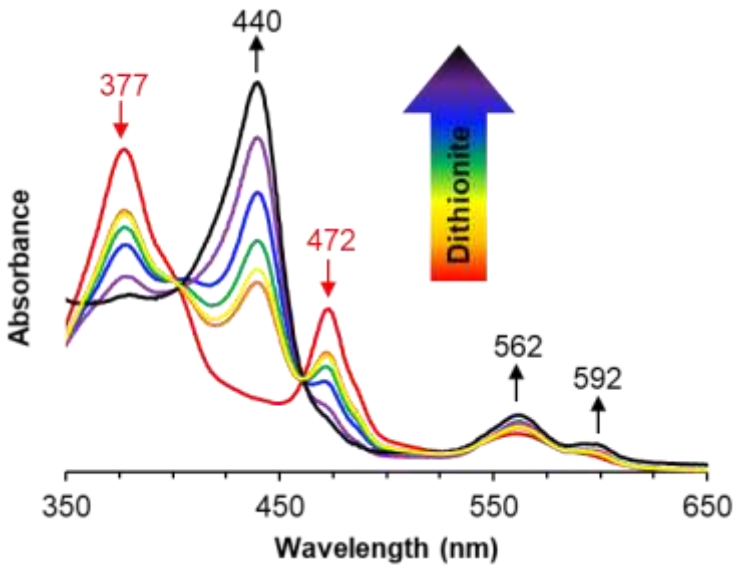

Figure S3.2. Mn-DHP reduction titration with sodium dithionite

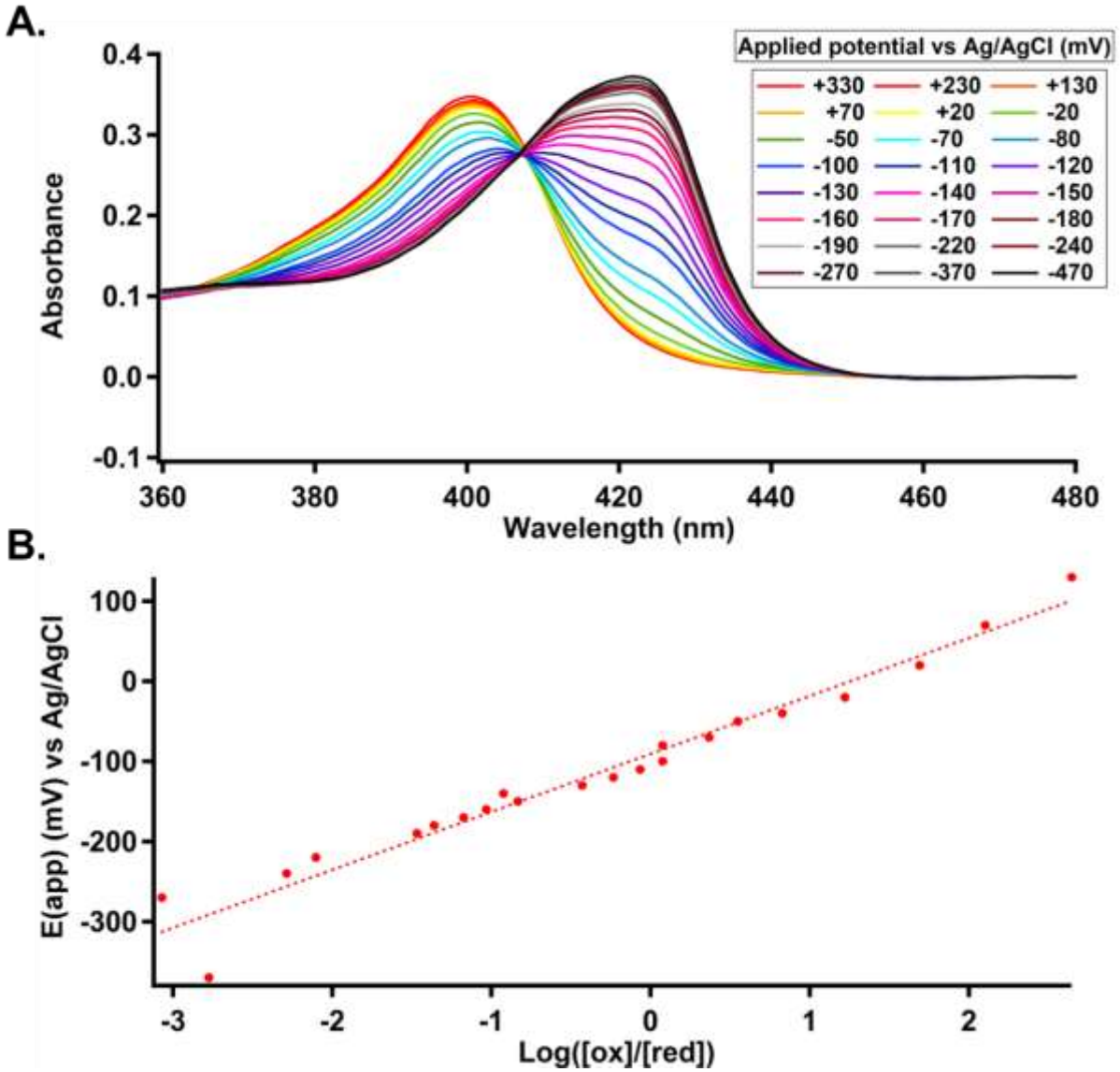

Figure S3.3. Spectroelectrochemical properties of Meso-DHP. A) Soret shift as a function of applied potential. B) Nerst plot of oxidized and reduced enzyme ratio

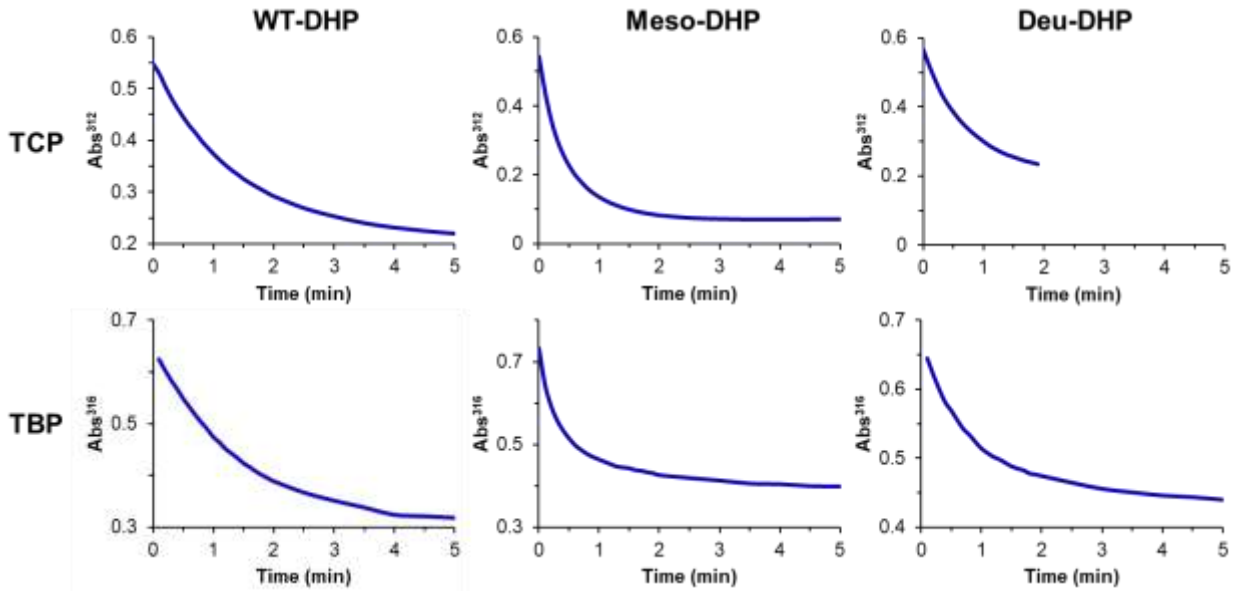

Figure S3.4. UV-visible monitoring of TCP and TBP decrease over 5 min to extract rate constants

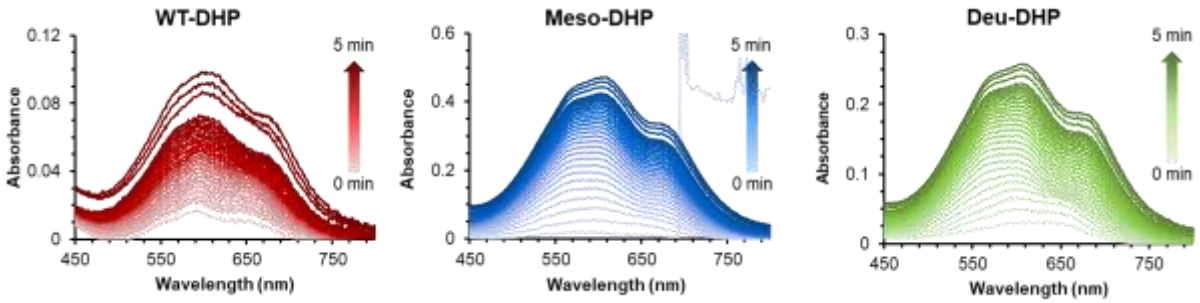

Figure S3.5. Russig's Blue formation at 610 nm

Table S3.1. Mn-DHP reactivity with a panel of 9 representative substrates with H_2O_2 and *m*CPBA

	Mn-DHP		WT DHP B	
Substrate	H_2O_2	mCPBA	H_2O_2	mCPBA
TBP	15.7 ± 1.4	68.9 ± 1.9*	100	76.8 ± 10.1
o-G	4.5 ± 1.3	33.4 ± 3.3	67.6 ± 0.2	46.4 ± 3.4
4-BG	17.8 ± 3.2	52.9 ± 2.9	100	68.1 ± 3.6
6-BG	14.9 ± 5.1	48.8 ± 6.6	88.8 ± 0.2	54.9 ± 1.8
4-CG	15.2 ± 5.7	12.4 ± 6.9	100	75.2 ± 12.9
4-NP	0	14.1 ± 1.0*	39.4 ± 0.7	59.1 ± 2.5
2,4-DNP	0	0	16.2 ± 1.6	2.0 ± 1.4
indole	2.2 ± 1.6	22.5 ± 3.3*	24.1 ± 2.3	27.6 ± 1.3
5-BI	3.9 ± 2.8	12.5 ± 2.1*	48.1 ± 2.3	30.0 ± 3.3

* < 5% substrate reactivity with *m*CPBA

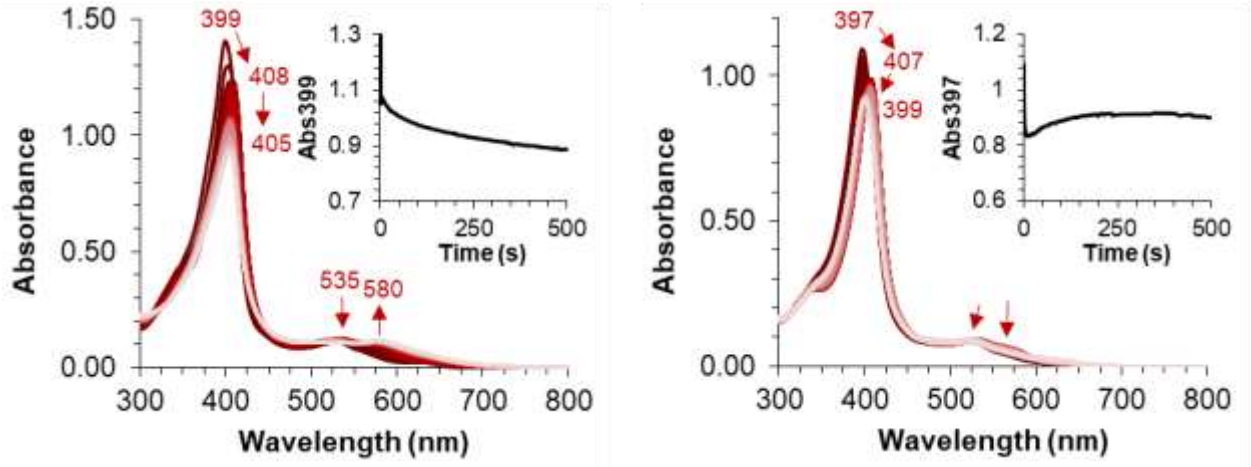

Figure S3.6. Kinetic data of Meso-DHP (left) and Deu-DHP (right) when reacted with H_2O_2 for 500 s. Insets show raw data trace at the soret maximum wavelengths

Figure S3.7. Kinetic data for the reaction of Meso-DHP with 10 eq. H_2O_2 and substrates 4-BC, 5-Br-I, 4-NP and 1-MeON at pH 7. **(A)** *Left*: Raw data of Meso-DHP Compound ES reacting with 4-BC over 50 s (900 scans). The inset shows the raw data wavelength trace and SVD fit at 409 nm. *Middle*: Calculated spectra of the three reaction components derived from the SVD analysis: Meso-DHP Compound ES (black), ferric Meso-DHP B (red) and the final resting species (blue). *Right*: Time dependences of the relative concentrations for the three components shown in the middle panel as determined from the fitting of the spectra in the top panel. **(B)** *Left*: Raw data of Meso-DHP Compound ES and 5-BI reacting over 50 s (900 scans). The inset shows the raw data wavelength trace and SVD fit at 409 nm. *Middle*: calculated spectra of the three reaction components derived from the SVD analysis Meso-DHP Compound ES (black), a ferric/oxyferrous mixture (red) and oxyferrous (blue). *Right*: time dependences of the relative concentrations for the three components shown in the middle panel as determined from the fitting of the spectra in the top panel. **(C)** *Left*: Raw data of Meso-DHP Compound ES and 4-NP reacting over 50 s (900 scans). The inset shows the raw data wavelength trace and SVD fit at 409 nm. *Middle*: calculated spectra of the three reaction components derived from the SVD analysis Meso-DHP Compound ES (black), ferric (red) and oxyferrous species(blue). *Right*: time dependences of the relative concentrations for the three components shown in the middle panel as determined from the fitting of the spectra in the top panel. **(D)** *Left*: Raw data of Meso-DHP Compound ES and 1-MeON reacting over 50 s (900 scans). The inset shows the raw data wavelength trace and SVD fit at 409 nm. *Middle*: calculated spectra of the three reaction components derived from the SVD analysis Meso-DHP Compound ES (black), ferric (red) and oxyferrous species (blue). *Right*: time dependences of the relative concentrations for the three components shown in the middle panel as determined from the fitting of the spectra in the top panel.

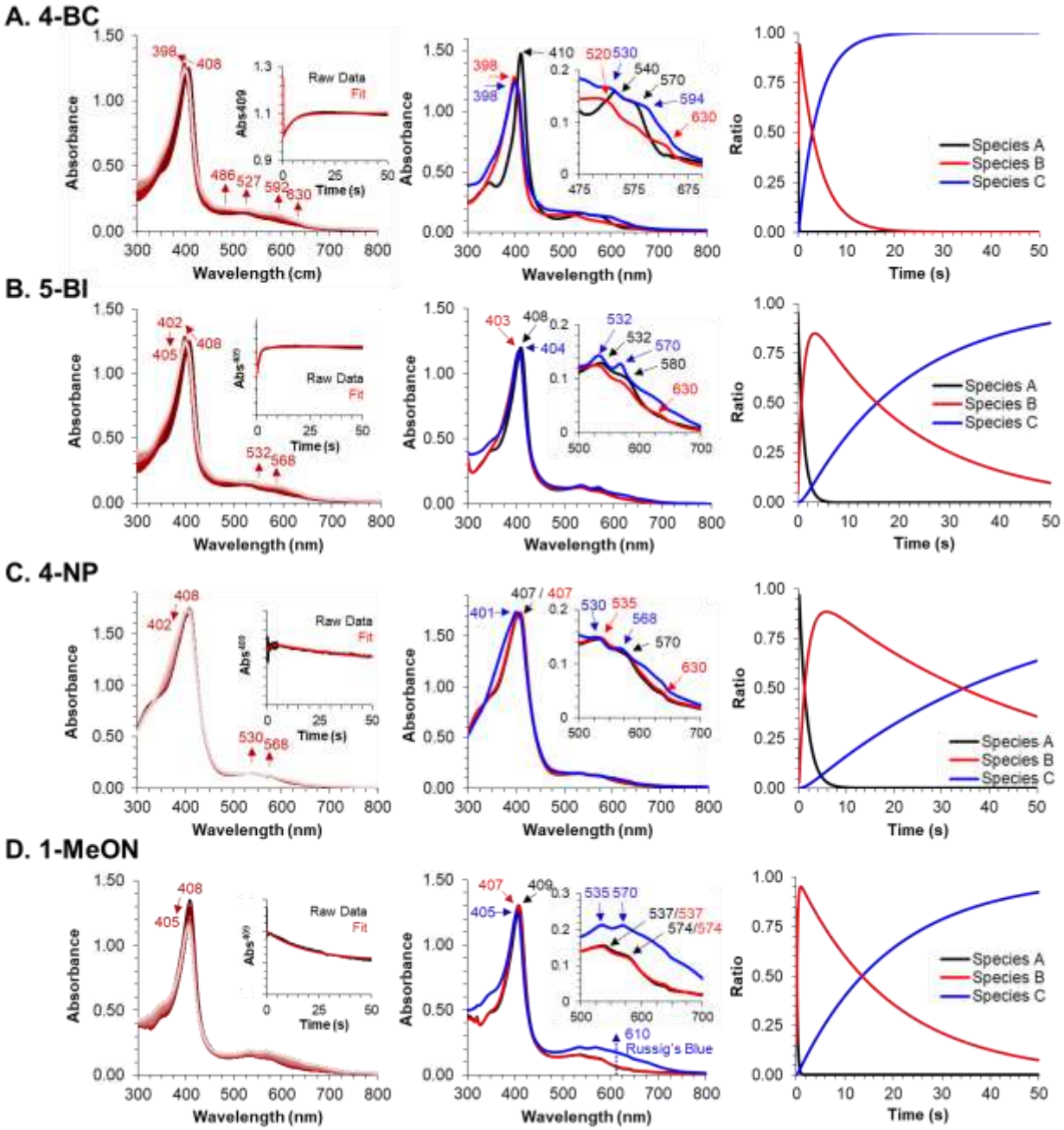
A. 4-BC
B. 5-BI
C. 4-NP
D. 1-MeON
Absorbance
Wavelength (cm)
Wavelength (nm)
Raw Data
Fit
Time (s)
Ratio
Species A
Species B
Species C
Russig's Blue

Figure S3.8. Kinetic data for the reaction of Deu-DHP with 10 eq. H_2O_2 and substrates 4-BC, 5-Br-I, 4-NP and 1-MeON at pH 7. **(A)** *Left*: Raw data of Deu-DHP Compound ES reacting with 4-BC over 50 s (900 scans). The inset shows the raw data and SVD fit at 409 nm. *Middle*: Calculated spectra of the three reaction components derived from the SVD analysis: Deu-DHP Compound ES (black), ferric Deu-DHP (red) and a ferric-like final resting species (blue). *Right*: Time dependences of the relative concentrations for the three components shown in the middle panel as determined from the fitting of the spectra in the top panel. **(B)** *Left*: Raw data of Deu-DHP Compound ES and 5-BI reacting over 500 s (900 scans). The inset shows the raw data wavelength trace and SVD fit at 403 nm. *Middle*: calculated spectra of the three reaction components derived from the SVD analysis Deu-DHP Compound ES (black), oxyferrous (red) and oxyferrous/heme bleaching (blue). *Right*: time dependences of the relative concentrations for the three components shown in the middle panel as determined from the fitting of the spectra in the top panel. **(C)** *Left*: Raw data of Deu-DHP Compound ES and 4-NP reacting over 500 s (900 scans). The inset shows the raw data wavelength trace at 409 nm. *Middle*: selected time point traces of three reaction components Deu-DHP Compound ES (black, t = 0 s), ferric/ES mixture (red, t = 110 s) and ferric/bleached heme species (blue, t = 500 s). *Right*: intentionally left blank **(D)** Top: Raw data of Deu-DHP Compound ES and 1-MeON reacting over 50 s (900 scans). The inset shows the raw data wavelength trace and SVD fit at 409 nm. Middle: selected time point traces of three reaction components Deu-DHP Compound ES (black, t = 0 s), ferric (red, t = 45 s) and oxyferrous species (blue, t = 500 s). Bottom: intentionally left blank.

A. 4-BC

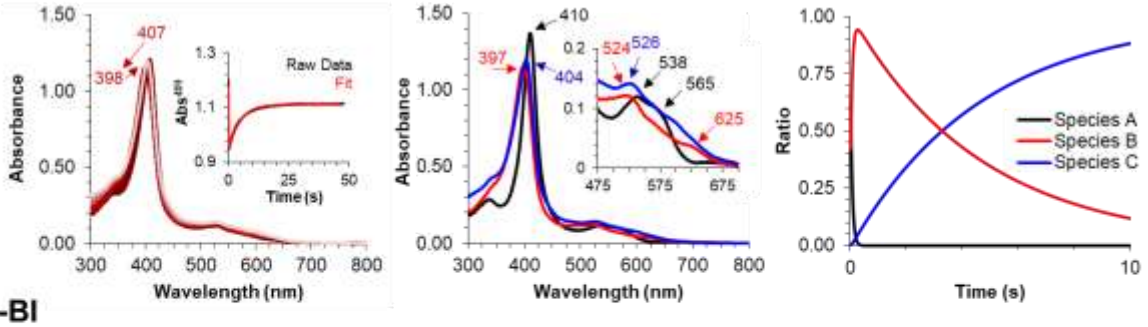

B. 5-BI

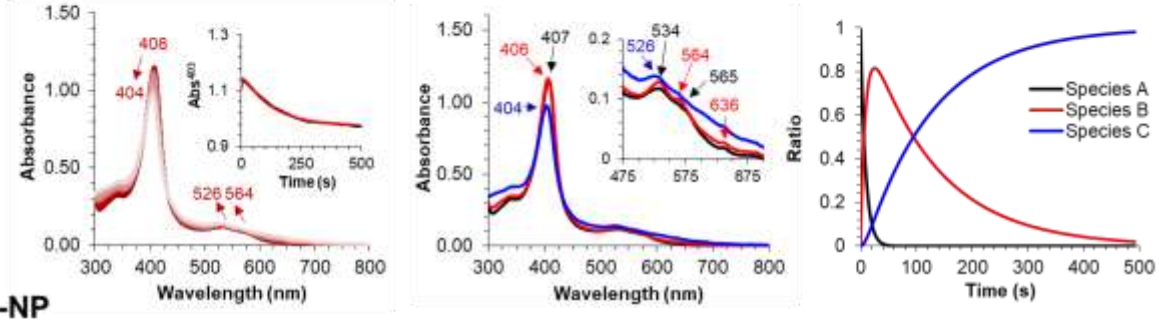

C. 4-NP

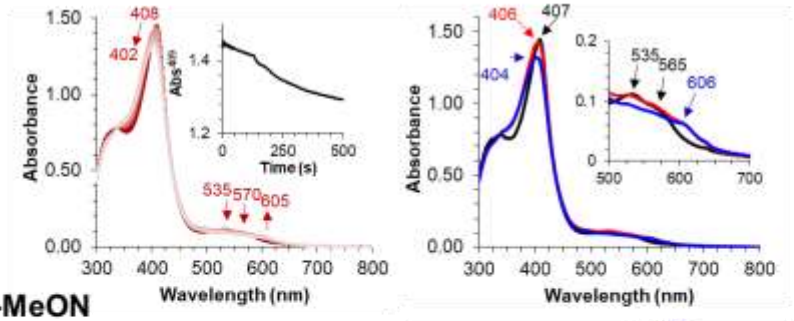

D. 1-MeON

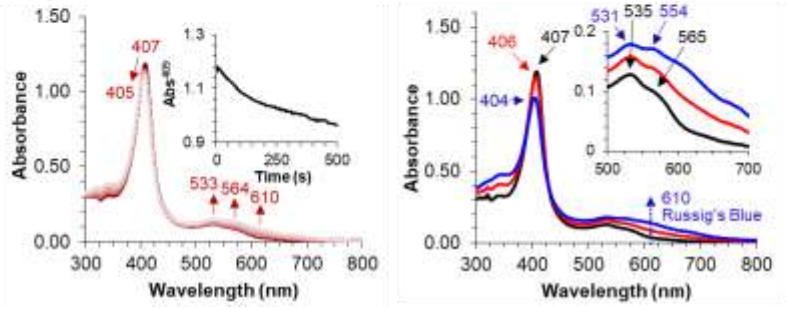

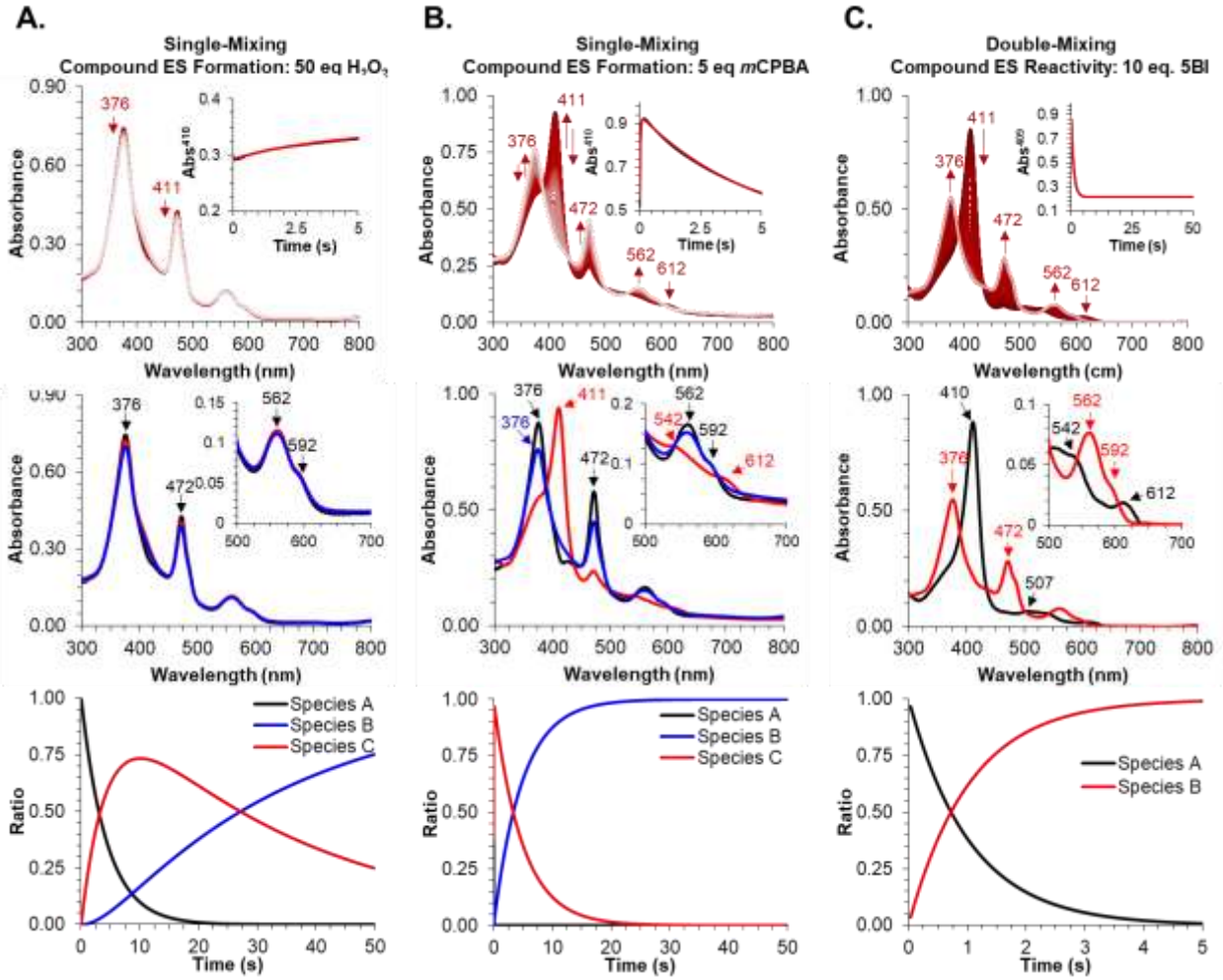

Figure S3.9. Kinetic data for the activation and reaction of 8 µM Mn-DHP with oxidants and the substrate 5BI at pH 7. **(A)** *Top*: Raw data of Mn-DHP reacting with 50 eq. H_2O_2 to form Compound ES over 50 s (900 scans). The inset shows the raw data and SVD fit at 410 nm. *Middle*: Calculated spectra of the three reaction components derived from the SVD analysis: Mn(III)-DHP (black, red, blue). *Top*: Time dependences of the relative concentrations for the three components shown in the middle panel as determined from the fitting of the spectra in the top panel. **(B)** *Top*: Raw data of Mn-DHP and 5 eq. *m*CPBA to form Compound ES reacting over 50 s (900 scans). The inset shows the raw data wavelength trace and SVD fit at 410 nm. *Middle*: calculated spectra of the three reaction components derived from the SVD analysis Mn-DHP Compound ES (black) and Mn(III)-DHP (red, blue). *Bottom*: time dependences of the relative concentrations for the three components shown in the middle panel as determined from the fitting of the spectra in the top panel. **(C)** *Top*: Raw data of Mn-DHP Compound ES (activated with 5 eq. *m*CPBA) and 10 eq. 5BI reacting over 50 s (900 scans). The inset shows the raw data wavelength trace at 410 nm. *Middle*: calculated spectra of the two reaction components derived from the SVD analysis Mn-DHP Compound ES (black) and Mn(III)-DHP (red).

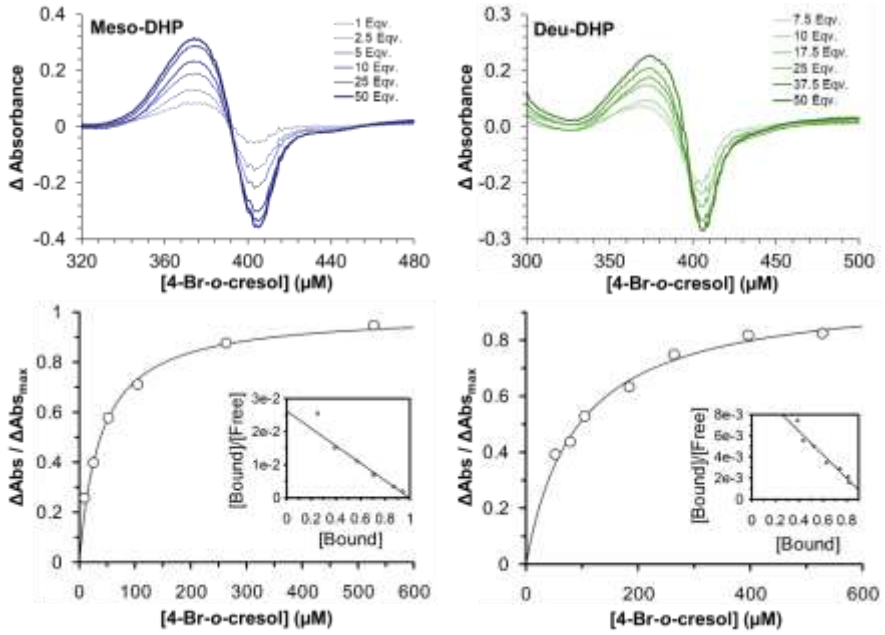

Figure S3.10. Optical difference spectra (top) and titration curves (bottom) of substrate binding to 10 µM Meso- and Deu-DHP in 5 % MeOH / 100 mM KPi (v/v) at pH 7 for 4-BC. Insets: corresponding Scatchard plots (ratio of concentrations of bound ligand to unbound ligand versus the bound ligand concentration).

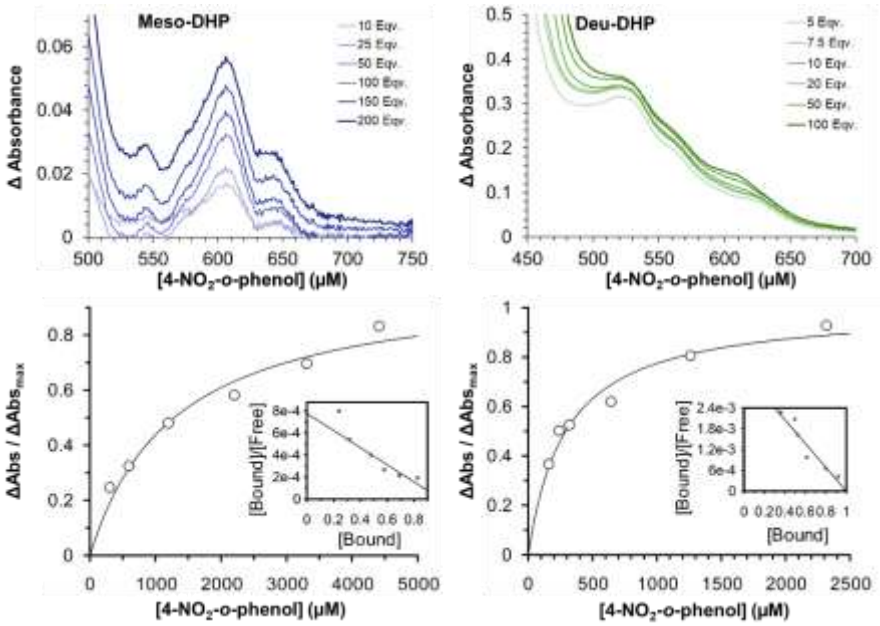

Figure S3.11. Optical difference spectra (top) and titration curves (bottom) of substrate binding to 25 µM Meso- and Deu-DHP B in 5 % MeOH / 100 mM KPi (v/v) at pH 7 for 4-NP. Insets: corresponding Scatchard plots (ratio of concentrations of bound ligand to unbound ligand versus the bound ligand concentration).

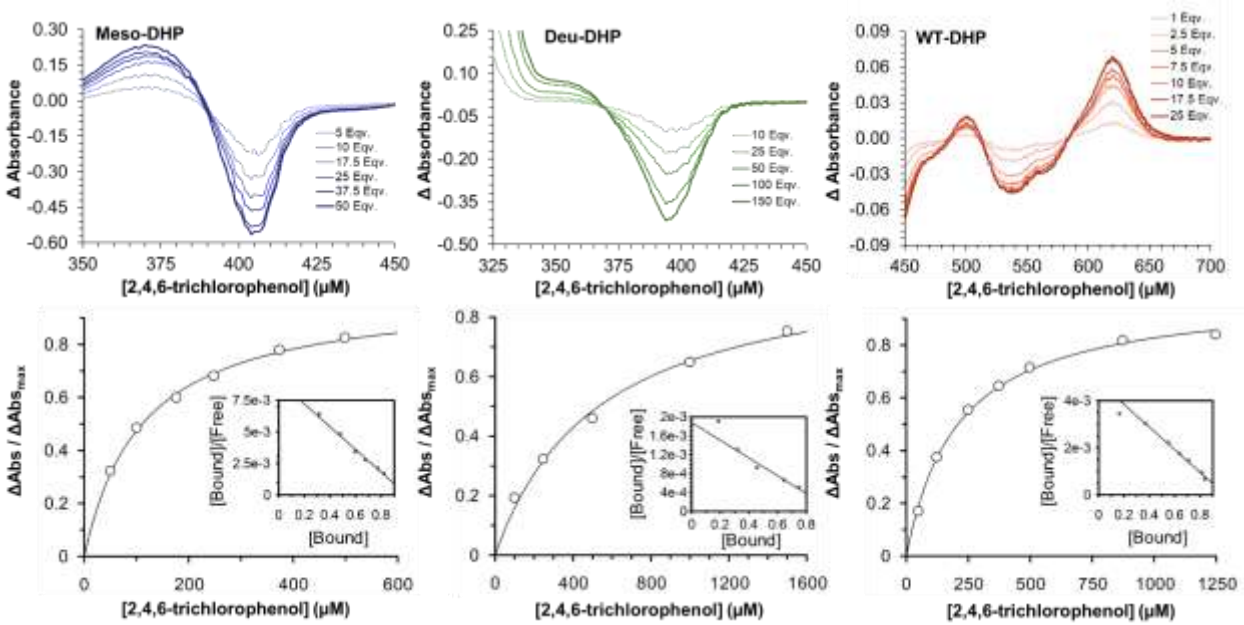

Figure S3.12. Optical difference spectra (top) and titration curves (bottom) of substrate binding to 10 µM Meso-DHP and 25 µM Deu-DHP and WT DHP in 5 % MeOH / 100 mM KPi (v/v) at pH 7 for 2,4,6-TCP. Insets: corresponding Scatchard plots (ratio of concentrations of bound ligand to unbound ligand versus the bound ligand concentration).

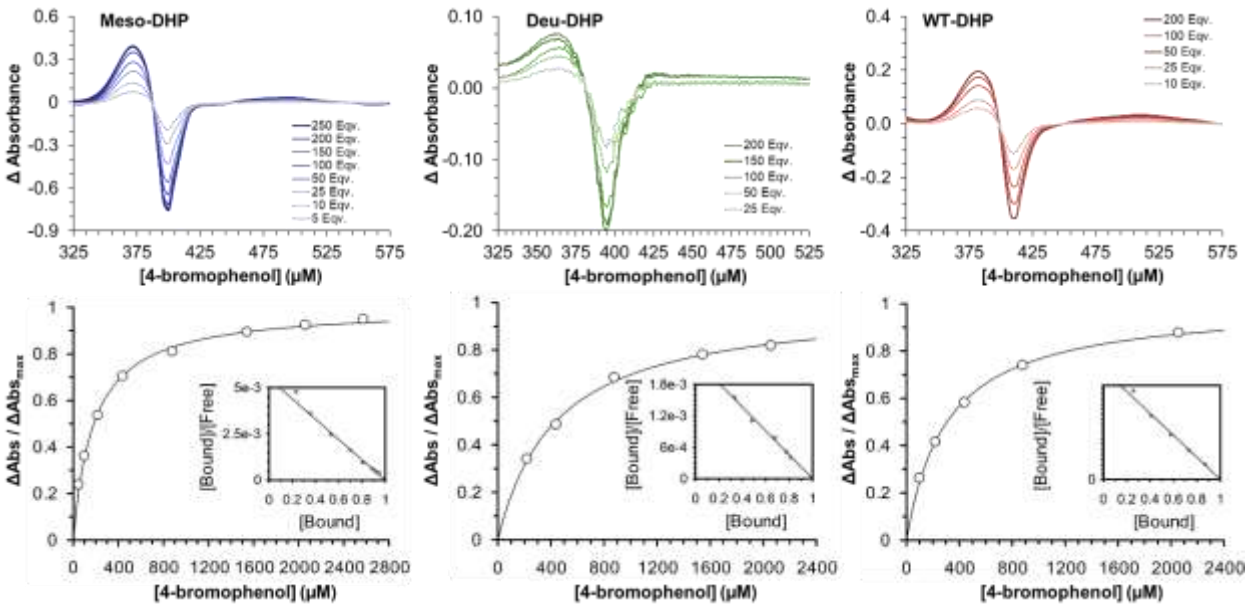

Figure S3.13. Optical difference spectra (top) and titration curves (bottom) of substrate binding to 10 µM Meso-DHP and 25 µM Deu-DHP at WT DHP in 5 % MeOH / 100 mM KPi (v/v) at pH 7 for 4-BP. Insets: corresponding Scatchard plots (ratio of concentrations of bound ligand to unbound ligand versus the bound ligand concentration).

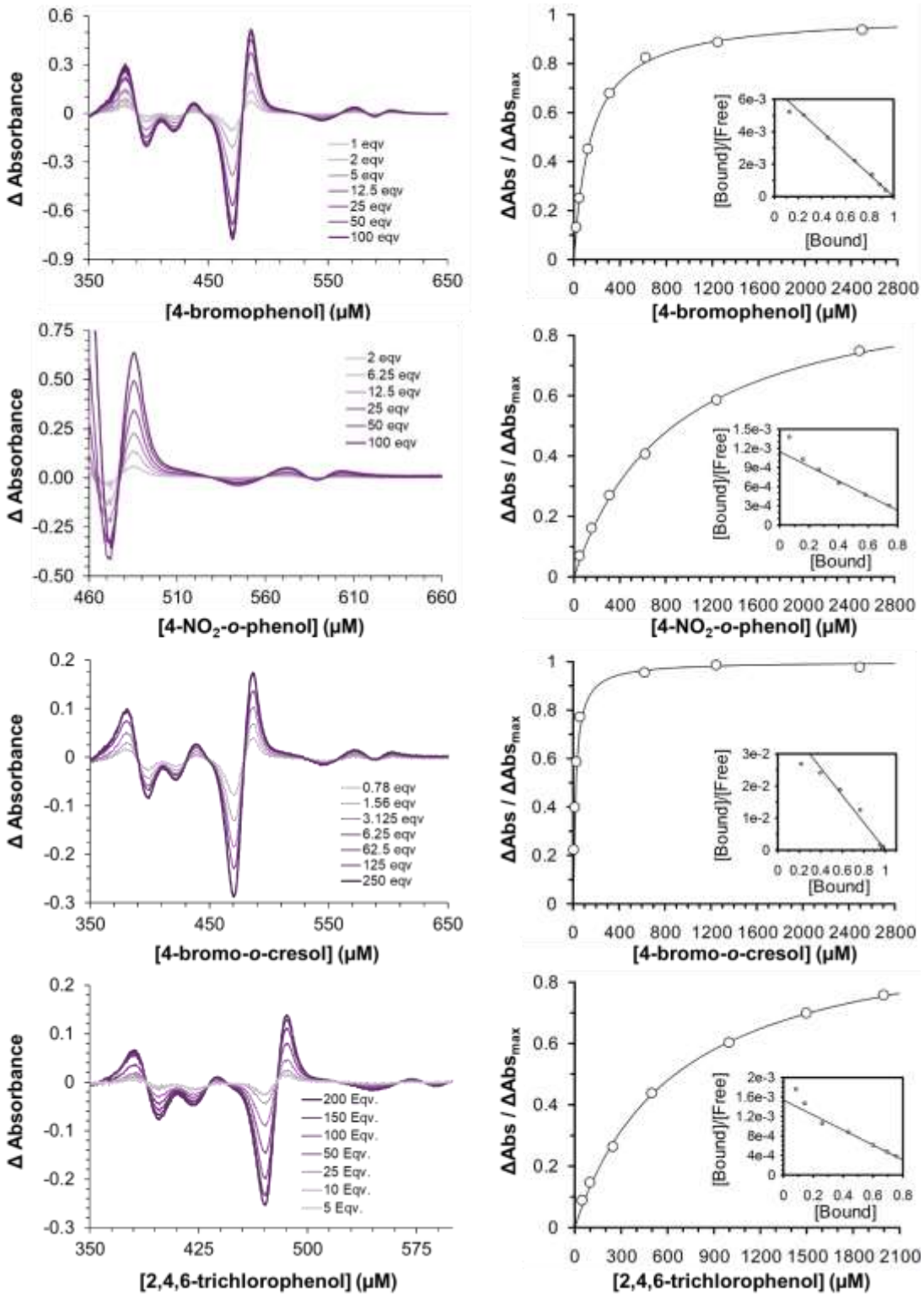

Figure S3.14. Optical difference spectra (left) and titration curves (right) of substrate binding to 25 μM Mn-DHP in 5 % MeOH / 100 mM KPi (v/v) at pH 7 for A) 4-BP, B) 4-NP, C) 4-BC and D) 2,4,6-TCP. Insets: corresponding Scatchard plots (ratio of concentrations of bound ligand to unbound ligand versus the bound ligand concentration).

Table S3.2. Data Table and refinement statistics for substrate-bound Meso-, Deu-, Mn- and WT-DHP.

	Deutero-DHP				Meso-DHP			
	4-Br-phenol	4-Br-o-cresol	4-nitro-phenol	TCP	4-Br-phenol	4-Br-o-cresol	4-nitro-phenol	TCP
PDB Entry	6VDR	6VDS	6VDT	6VDU	6VD3	6VD4	6VD6	6VD5
Data Collection								
Wavelength (Å)	1	1	1	1	1	1	1	1
Temperature (K)	100	100	100	100	100	100	100	100
Space Group	$P2_12_12_1$	$P2_12_12_1$	$P2_12_12_1$	$P2_12_12_1$	$P2_12_12_1$	$P2_12_12_1$	$P2_12_12_1$	$P2_12_12_1$
Unit-cell parameters (Å)								
a	59.4	59.6	58.5	59.2	60.7	58.9	59.1	59.2
b	67.6	67.5	67.6	67.9	67.4	67.6	67.8	68
c	67.6	68	68	67.9	67.6	68.1	67.9	68
Unique Reflections	21411	18217	23728	18367	29651	19160	35281	33761
Completeness (%)	97.6 (78.1) [a]	98.3(89.3)	94.4 (77.94)	98.7 (93.4) [a]	94.7 (88.6)	99.4 (96.3)	94.5 (78.0) [a]	98.9 (98.9)
R_{meas} (%) [b]	7.0 (46.7)	16.2(95.4)	8.1 (75.8)	8.5 (63.9)	6.2 (42.9)	9.6 (66.7)	4.3 (50.8)	6.9 (98.9)
R_{pim} (%) [b]	2.2 (28.5)	5.2 (35.2)	3.7 (39.7)	3.8 (29.1)	2.7 (21.0)	6.0 (41.9)	2.1 (27.6)	2.0 (38.4)
$CC_{1/2}$ [b]	0.997 (0.819)	0.994 (0.646)	0.998 (0.631)	0.997 (0.777)	0.997 (0.805)	0.995 (0.650)	0.998 (0.741)	0.999 (0.673)
$I/s_{(I)}$	32.7 (1.8)	22.3 (1.6)	20.9 (1.7)	20.8 (1.9)	28.6 (2.1)	12.0 (1.3)	29.4 (1.98)	40.0 (1.5)
Multiplicity	9.6 (2.9)	9.1 (7.5)	4.2 (2.9)	4.7 (4.5)	4.4 (3.7)	2.4 (2.3)	3.8 (2.7)	11.6 (7.0)
Refinement								
Resolution Range (Å)	47.83-1.87	47.89-1.98	47.95-1.78	44.65-1.98	33.77-1.67	30.42-1.95	37.3-1.56	48.08-1.64
R_{work} (%) [c]	20.97	22.88	23.67	20.2	16.91	19.52	15.35	17.7
R_{free} (%) [d]	25.9	26.25	28.77	25.19	18.74	24.18	22.08	21.8
No. of Protein Atoms	2554	2507	2567	2457	2617	2408	2408	2462
No. of Solvent Atoms	111	47	97	87	158	118	169	166
R.m.s. deviations [e]								
Bond lengths (Å)	0.0084	0.0086	0.0124	0.008	0.009	0.011	0.011	0.006
Bond angles (°)	2.07	2.187	2.292	1.455	1.789	1.795	1.858	0.847
Ramachandran Statistics (%) [f]								
Preferred	95.5	91.3	94.7	94	97.9	97.5	99	98.5
Allowed	3.2	6.4	2.6	4.8	2.1	2.5	1	1.5

Table S3.2 (cont.). Data Table and refinement statistics for substrate-bound Meso-, Deu-, Mn- and WT-DHP.

		Mn-DHP		**WT-DHP**
	4-Br-phenol	4-Br-o-cresol	4-nitro-phenol	TCP
PDB Entry	6VDV	6VDW	6VDX	6VDY
Data Collection				
Wavelength (Å)	1	1	1	1
Temperature (K)	100	100	100	100
Space Group	$P2_12_12_1$	$P2_12_12_1$	$P2_12_12_1$	$P2_12_12_1$
Unit-cell parameters (Å)				
a	60.5	59.3	59.4	59.2
b	67.7	67.6	67.6	67.5
c	67.8	67.8	67.6	68.1
Unique Reflections	20150	36097	34684	28809
Completeness (%)	91.0 (62.6) [a]	99.9 (100)	99.8 (100)	98.8 (98.7) [a]
R_{meas} (%) [b]	11.7 (63.8)	11.3 (50.7)	5.4 (65.2)	5.2 (50.9)
R_{pim} (%) [b]	4.4 (27.0)	4.9 (27.0)	2.5 (32.1)	2.3 (21.8)
$CC_{1/2}$ [b]	0.999 (0.992)	0.990 (0.910)	1.001 (0.588)	0.998 (0.848)
$I/s_{(I)}$	18.2 (2.4)	19.5 (3.0)	28.1 (1.8)	35.5 (2.5)
Multiplicity	6.4 (4.8)	5.4 (4.7)	4.5 (3.9)	5.4 (3.2)
Refinement				
Resolution Range (Å)	47.85-1.88	44.62-1.58	44.64-1.60	37.29-1.70
R_{work} (%) [c]	19.58	18.09	22.6	19.39
R_{free} (%) [d]	23.6	20.95	25.66	24.62
No. of Protein Atoms	2538	2552	2454	2582
No. of Solvent Atoms	118	169	144	150
R.m.s. deviations [e]				
Bond lengths (Å)	0.0083	0.013	0.011	0.014
Bond angles (°)	2.377	2.576	2.556	1.845
Ramachandran Statistics (%) [f]				
Preferred	95.2	96.9	91.2	97.3
Allowed	4.8	3.1	4.4	2.7

Table S3.3. Selected distances

	WT-DHP				Hydrogen bond length (Å)		
Complex	K_d (mM)	PDB Entry	Metal-His89 distance	Metal-substrate hydroxyl distance	Propionate-substrate hydroxyl	Tyr38-substrate hydroxyl	His55-substrate[c] hydroxyl
4-BP	305 (± 15)	3LB2	2.1	6.5	2.5	3.5	[int] d 3.00/[ext] d 4.20
4-Br-*o*-cresol	86 (± 14)	6ONX	2.1	4.8	5.6	6.9	[int] d 4.50/ [ext] d 7.30
4-NP	262 (± 23)	5CHQ	2.3	6.7	3.3	3.3	[ext] d 3.80
TCP	208 (± 13)	6VDY	2.4	8	n.d., 6.7[d]	2.4	[ext] d 2.79
	Mn-DHP						
4-BP	150 (± 5)	6VDV	2.3	6.9	2.8	3.1	[ext] d 3.91
4-Br-*o*-cresol	23 (± 2)	n.d.					
4-NP	873 (± 55)	6VDW	2.27	7	2.53	2.8	[ext] d 3.72
TCP	652 (± 41)	6VDX	2.3	8.1	n.d., 6.73[d]	2.49	[ext] d 3.03
	Meso-DHP						
4-BP	182 (± 8)	6VD3	2.2	6.3	2.97	4.55	[ext] d 4.10
4-Br-*o*-cresol[a]	38 (± 4)	6VD4	2.5	4.7	6.2	7.2	[int]ε 2.44, δ 4.2[f]/[ext] d 8.40
4-NP	1288 (± 318)	6VD6	2.1	6.7	2.6	3.4	[ext] d 3.86
TCP	111 (± 7)	6VD5	n.d.[e]	7.8	n.d., 6.1[d]	2.5	[ext] d 2.70
	Deu-DHP						
4-BP	438 (± 30)	6VDR	2.1	9.6	10.7	12.5	Asn96/Thr93N-substrate[b] 2.86/3.12
4-Br-*o*-cresol	90 (± 9)	6VDS	2.1	8.5	11.3	12.6	Asn96/Thr93N-substrate[b] 2.96/2.98
4-NP	291 (± 97)	6VDT	2.7[g]	6.7	6	2.5	[ext] d 4.06
TCP	532 (± 81)	6VDU	n.d.[e]	7.8[h]	n.d.[h]	2.6	[ext] d 2.72

n.d. not determined.

[a] Numbers reported for Meso-DHP complex with 4-Br-o-cresol from protomer B.

[b] Hydrogen bond distance reported for the nitrogen of the amide of Asn96 and amine of Thr92 to the hydroxyl group of the substrate.

[c] Only the values for δN of His55 are reported, due to closer proximity to substrates.

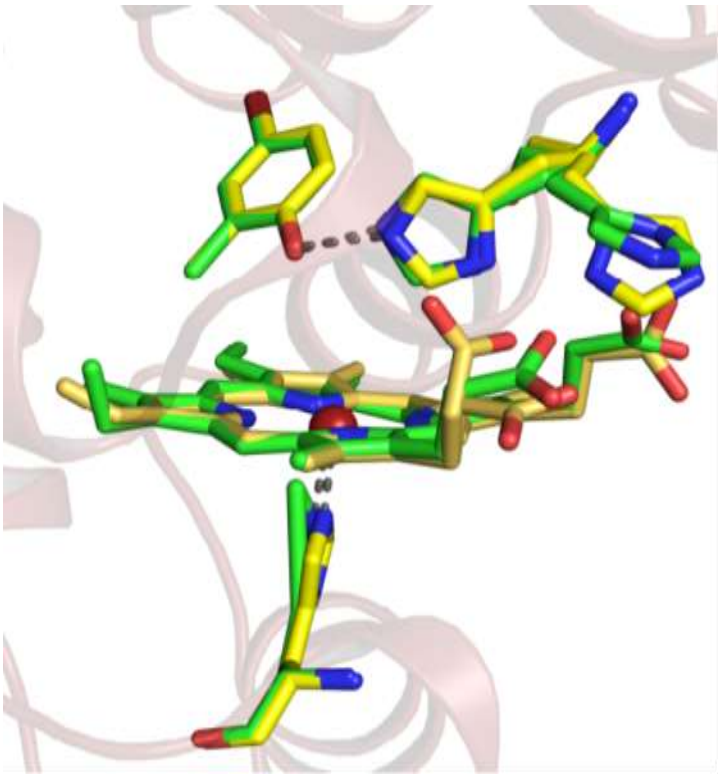

Figure S3.15. Overlay 4-BC bound Meso-DHP (green) and WT-DHP (yellow)

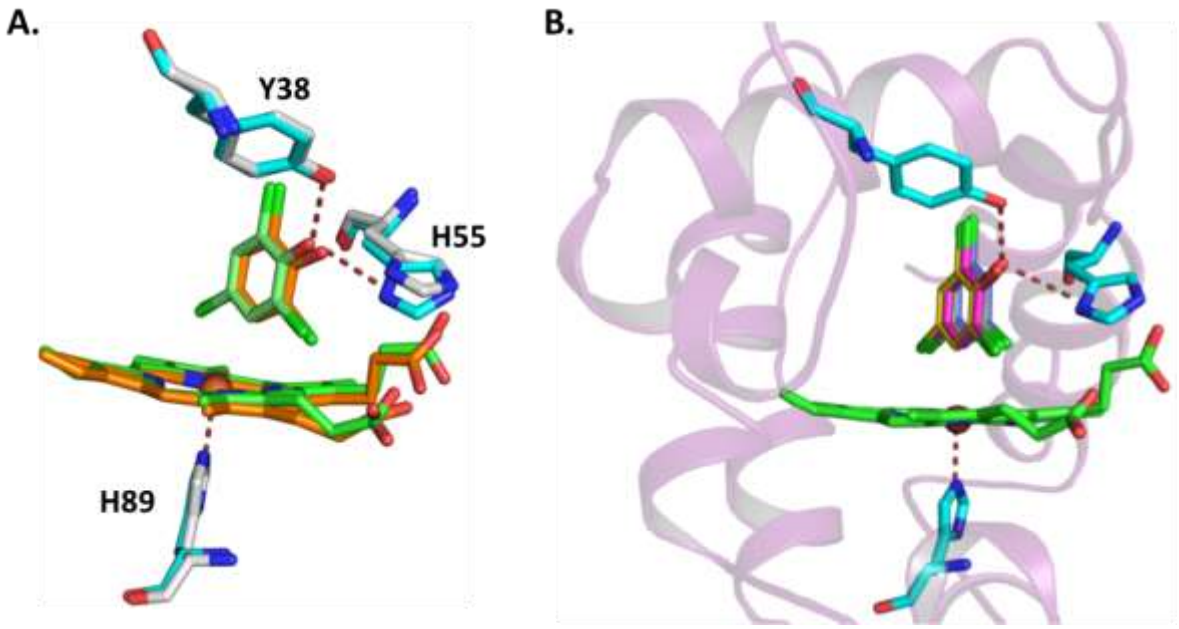

Figure S3.16. Superposition of the active site for the TCP bound complexes. (A) Active site structures for the overlayed WT (green) and DHPa Y34N mutant, PDB entry 4KWM (orange). (B) Active site structure for the overlayed Deu-DHP (yellow), meso-DHP (violet), WT (green) and Mn-DHP(purple). Only protein residues that stabilize the TCP binding by engaging in hydrogen bonding interactions with hydroxyl of TCP are shown, namely Y38 and H55 in its solvent exposed conformation. The overlayed TCP complexes are shown in background of Mn-heme-TCP complex protein scaffold, as well as its H89 proximal residue that coordinates the heme metal center is also shown

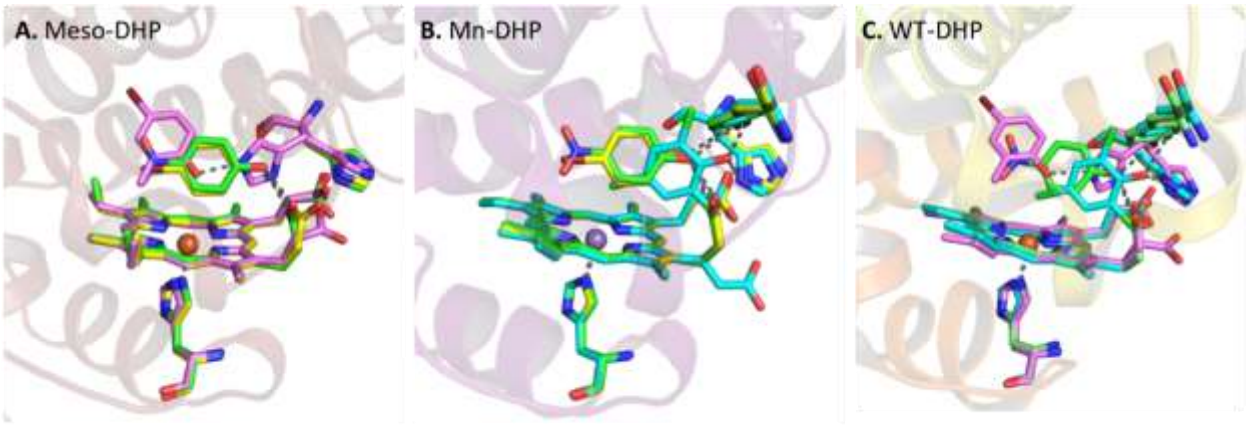

Figure S3.17. Substrate overlay with Meso-, Mn-, and WT-DHP to compare substrate binding positions.

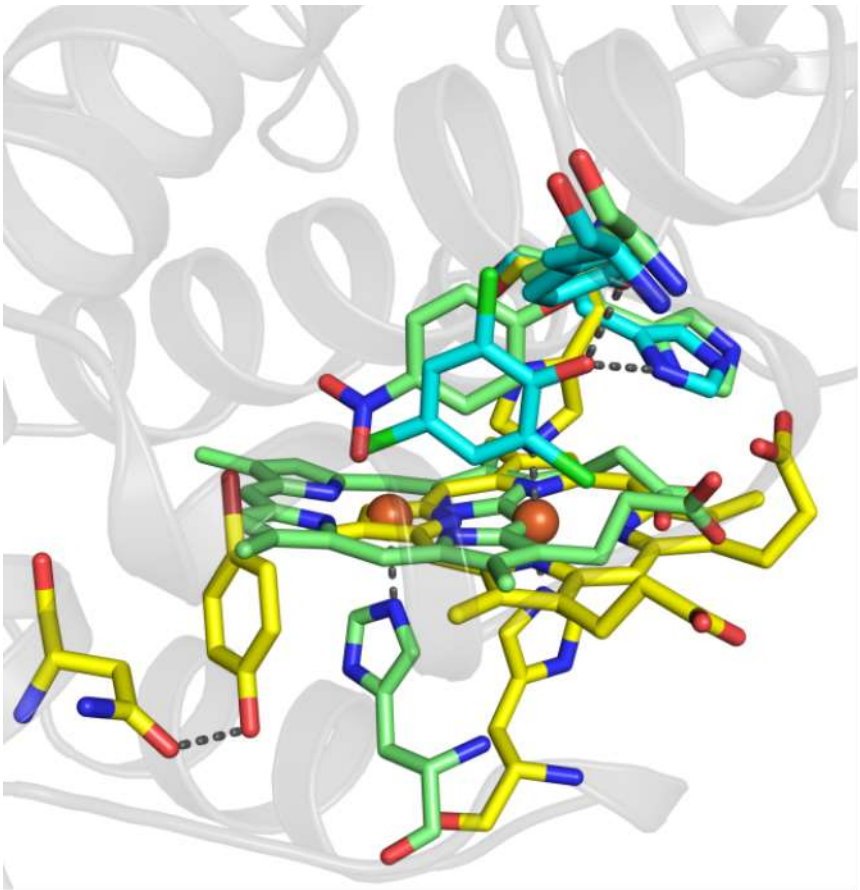

Figure S3.18. Overlay of Deu-DHP bound with 4-BP (yellow), TCP (teal), and 4-NP (green).

Chapter 4

New Reactivies of Dehaloperoxidase: C-H Activation Chemistry

Ashlyn H. McGuire, Osami Shoji and Reza A. Ghiladi

Department of Chemistry, North Carolina State University, Raleigh, North Carolina, 27695

ABSTRACT: The multifunctional Dehaloperoxidase (DHP) was utilized in C-H activation chemistry. As a hemoenzyme capable of oxidization by H_2O_2 to an Fe(IV)=O, the oxygen is subsequently incorporated into small molecule substrates. Epoxidation chemistry was analyzed with styrene and *trans*-β-methylstyrene a slight enantioselectivity to (R)-styreneoxide (70%). The hydroxylation of ethylbenzene and indane were also analyzed leading to an equivalent ratio of (R) and (S) products. Thioanisole oxidation resulted in the (R)-enantiomer (75:25). The last new activity, the cyclopropanation of styrene through a carbene species, lead to four diastereomers with the trans isomer in excess. These new substrates demonstrate the increasing functionality of the multifunctional DHP, a globin with peroxidase and P450 reactivities.

INTRODUCTION

Unfunctionalized hydrocarbons are some of the most inert chemical groups, though laboratories and nature have designed mechanisms that can overcome this barrier.[1] Some synthetic avenues include the Jacobsen[2] and Sharpless[3] epoxidations, or transition metal directed sp^3 C-H activations.[4–6] In biotechnology and nature, metal containing enzymes, such as peroxygenases, are capable of direct O-atom incorporation into inactivated C-H positions. The benefits of enzymes in comparison to synthetic molecules include, i.) greener chemistry, as aqueous solutions are used instead of harsh organic solvents, ii) reactions occur at neutral pH's, and iii) enzymes work at less extreme temperatures.[7] Some proteins, such as myoglobin, have been structurally modified to be capable of C-H activation by site-directed mutagenesis or cofactor exchange. By modifying myoglobin's cofactor to be iron porphycene the turnover number of the cyclopropanation of styrene was increased by 28-times the native enzyme.[8] Biocatalysis provides a new direction in C-H activation as new peroxygenases are being discovered. Dehaloperoxidase (DHP), recently determined to possess peroxygenase activity,[9] is a viable candidate to explore C-H activation chemistry.

Initially discovered as the hemoglobin of *Amphitrite ornata*,[10,11] DHP has demonstrated heme-mediated direct O-atom incorporation onto small molecules such as indoles, nitrophenols, cresols and pyrroles.[9,12–14] These compounds are structurally similar to less 'activated' substrates such as styrene, ethyl benzene, indane, etc. It is a promising biological technique to demonstrate that the globin, DHP, can act as a biocatalyst to hydroxylate unactivated C-H bonds without the use of tradition chemicals or methods.

EXPERIMENMAL PROCEDURES

Materials. Ferric samples of WT DHP B were expressed and purified as previously reported.[15] The WT enzyme concentration was determined spectrophotometrically using an ε_{Soret} of 116400 M^{-1} cm^{-1}. Solutions of H_2O_2 (in 100 mM KP_i, pH 7) and *m*CPBA (in MeOH) were prepared fresh daily and kept on ice until they were needed. Stock solutions of substrates were prepared in MeOH and stored in the dark at −80 °C until they were needed. Porphyrins were purchased from Frontier Scientific. Acetonitrile (MeCN) was high-performance liquid chromatography (HPLC) grade, and all other reagent grade chemicals were purchased from VWR, Sigma-Aldrich, or Fisher Scientific and used without further purification.

Nonnative Cofactor DHP Preparation. Following a modified Teale-Butanone extraction method,[16,17] DHP B dissolved in 100 mM KP_i was adjusted to pH 2.3 - 2.5 by dropwise additions of 0.1 M HCl and immediately mixed with an equal volume of ice-cold 2-butanone. The mixture was vigorously shaken for 30 s and allowed to stand at 0 ℃ for 1 min until the deeply colored upper layer of butanone phase (heme-containing) separated from the colorless lower layer of aqueous phase (apoenzyme). The butanone phase was siphoned off. The remaining aqueous phase was treated twice more with 2-butanone and dialyzed against 10 mM KP_i in quadruplicate to remove the dissolved butanone. The dialyzed solution was centrifuged to remove insoluble material and stored at 4 ℃. The apoenzyme in 10 mM KPi (pH 7.0) was mixed with excess of the desired porphyrin (2-4 mg) in 400 μL 0.1 M NaOH and allowed to stand at 0 ℃ for 30-60 min. The mixture was then passed through a carboxymethyl cellulose column equilibrated with 10 mM KPi (pH 7.0). The complex was absorbed on the column, whereas the unbound porphyrin passed through the column. The column was washed with of 100 mM KPi (pH 7.0). The absorbed

complex was slowly eluted with 40 mM KPi (pH 7.0) and stored in 40% (v/v) glycerol at -80 ℃. Molar absorptivities of the enzyme with substituted cofactors were determined via ICP-OES.

Epoxidation of styrene compounds. The epoxidation of styrene (and other substrates) was carried out in 100 mM KPi at 25°C for 10 min in the presence of 10 μM DHP, 1 mM substrate (in MeOH), and 1 mM H_2O_2. The final volume of the reaction mixture was 1 mL containing 10% (v/v) MeOH. After 10 min reaction, dichloromethane was added to the reaction mixture to quench the reaction, and the products were extracted into the organic layer and concentrated by rotary evaporation. Phenylmethyl acetate was added to reaction mixture as an internal standard prior to evaporation.

Hydroxylation of ethylbenzene: GC-MS conditions: column temperature: 110°C (30 min); 20°C min^{-1}; 220°C (15 min), injection temperature: 250°C, interface temperature: 200°C, ion source temperature: 200°C, carrier gas: helium. The retention times of products and the internal standard were as follows: phenylmethyl acetate (11.7 min), (R)-1-phenylethanol (13.6 min), (S)-1-phenylethanol (14.6 min), 2-ethylphenol (24.7 min) and 4-ethylphenol (28.2 min).

Hydroxylation of Indane: Reaction was completed as above, but products were derivatized to silylated alcohols by BSTFA-TMCS (99:1) through a 30 min incubation period prior to rotary evaporation. GC-MS conditions: column temperature: 110°C (30 min); 20°C min^{-1}; 220°C (15 min), injection temperature: 250°C, interface temperature: 200°C, ion source temperature: 200°C, carrier gas: helium. Retention times: indane (4.7 min), phenylmethyl acetate (11.9 min), (R)-1-indanol-BSTFA derivative (18.7 min), (S)-1-indanol-BSTFA derivative (19.7 min), 4-indanol-BSTFA derivative (23.4 min), 1-indanone (28.7 min), and 5-indanol-BSTFA derivative (30.7 min). The peak of 1-indanone and 4-indanol-BSTFA derivative was assigned by GC-MS fragmentation.

Cyclopropanation of Styrene: Reaction was carried at anaerobically in 100 mM KP_i in the presence of 20 µM DHP, 10 mM dithionite, 10 mM styrene and 10 mM ethyl diazoacetate (400 µL total). The reaction was mixed for 18 h and then quenched with and equivalent volume of DCM. The compound 2-phenyl-2-propanol was added as an internal standard prior to quenching. GC-MS conditions: column temperature: 130°C (25 min); 50°C min^{-1}; 220°C (10 min), injection temperature: 250°C, interface temperature: 200°C, ion source temperature: 200°C, carrier gas: helium.

RESULTS AND DISCUSSION

New reactivity: Epoxidation

Previous research has demonstrated that DHP B is capable of reactivity with traditional peroxygenase substrates. In an attempt to expand the substrate scope further, other peroxygenase substrates can be examined. Styrene was selected due to its prevalence in the cytochrome P450 literature to enhance enzyme-catalyzed asymmetric epoxidation.[18–20] Chiral epoxides are important in small molecule and biologically active molecule synthesis.[21] Preliminary, *qualitative* data of DHP B-catalyzed stereoselective epoxidation of styrene was examined with both WT and Mn-DHP B, and employing either H_2O_2 or *meta*-chloroperoxybenzoic acid (*m*CPBA) as oxidants (Figure 3.3). The oxidant *m*CPBA (green chromatogram) has some ability of turning over the initial substrate with no stereoselectivity (54:46, *R*:*S*) with (*R*/*S*)-styrene oxide as the major product compared to 2-PAA (87:13). Product stereoselectivity is introduced when the reaction is DHP-catalyzed, with the greatest enantioselectivity obtained with the DHP B/H_2O_2 reaction (yellow chromatogram); an increase in 2-PAA product formation is also demonstrated (42:58, styrene oxide:2-PAA). The maximum amount of 2-PAA was observed in the Mn-DHP B/*m*CPBA reaction with the 2-PAA peak area percentage equaling 82 % of the total products.

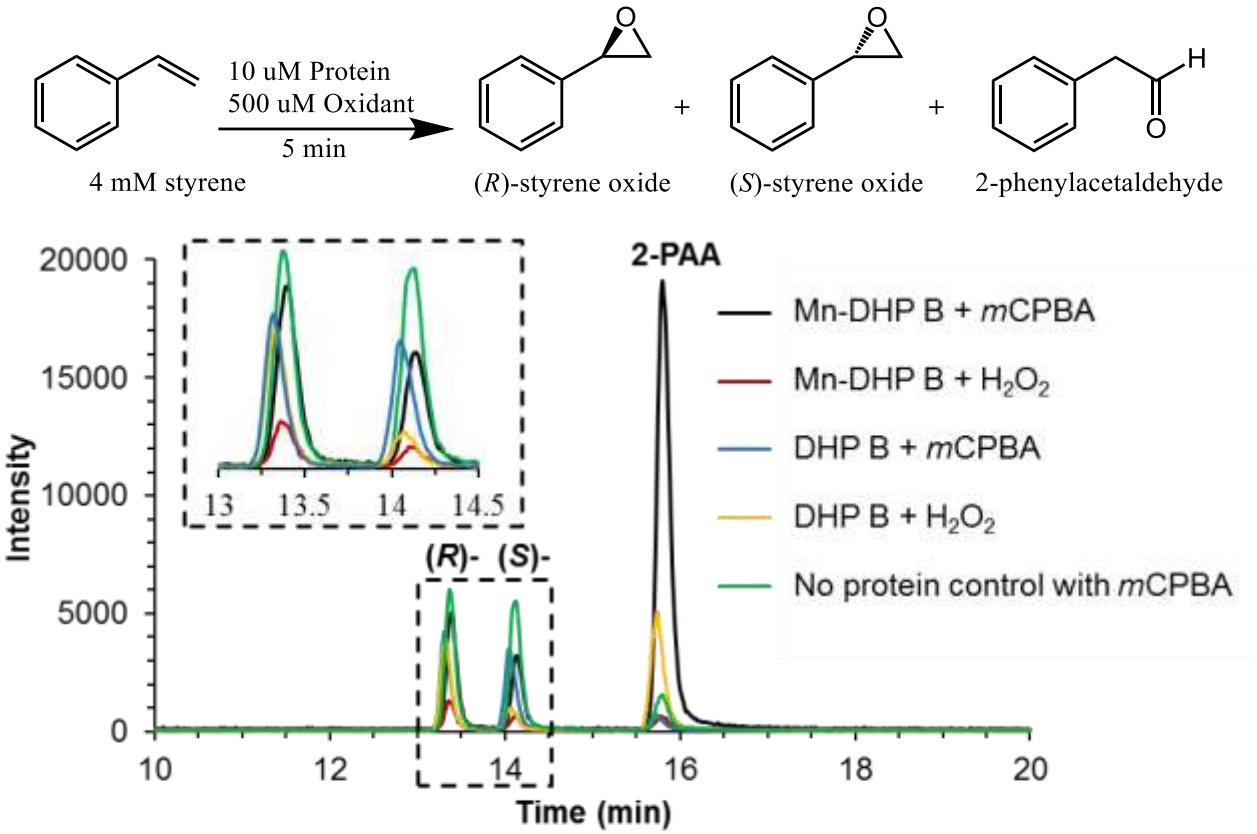

Peak Area Ratio	Mn-DHP B *m*CPBA	Mn-DHP B H_2O_2	DHP B *m*CPBA	DHP B H_2O_2	*m*CPBA
(*R*) : (*S*), %	63 : 37	70 : 30	54 : 46	84 : 16	54 : 46
(*R*/*S*) : 2-PAA, %	18 : 82	68 : 32	93 : 7	42 : 58	87 : 13

Figure 4.1. DHP B catalyzed epoxidation of styrene to (R/S)-styrene oxide and 2-phenylacetyaldehyde (2-PAA). GC-MS retention times for the products were: 13.4 min [(*R*)-styrene oxide], 14.2 min [(*S*)-styrene oxide], and 15.8 min [2-PAA].

Styrene reactivity can be compared between wild type DHP B (Figure 3.3; yellow chromatogram) with wild type myoglobin, which demonstrated only a slight enantioselectivity for (*R*)-styrene oxide (9 % ee),[22] compared to the native stereoselectivity of DHP B to produce the (*R*)- enantiomer at an increased abundance (84:16, *R*:*S*). The enantioselectivity of the reaction was compared under different pH conditions pH (Table 4.1).

Table 4.1. Enatioselectivity (R-) of expoxidation products of styrene and *trans*-β-methylstyrene

	Styrene		*t*βMS
	WT DHP	**Meso-DHP**	**WT DHP**
pH Effects			
pH 5	70.5 ± 0.9	71.5 ± 0.2	53.1 (±0.1)
pH 6	68.4 ± 0.9	71.6 ± 1.8	56.4 (±0.4)
pH 7	65.6 ± 2.8	74.6 ± 1.0	64.0 (±0.3)
pH 8	67.5 ± 0.6	71.8 ± 0.1	71.2 (±0.6)
pH 9	---	---	74.0 (±0.7)

The pH did not effect the enantioselectivity of styrene with the R-isomer as the dominant product, ~70 % for both WT and Meso-DHP. A difference was observed for *trans*-β-methylstyrene for WT DHP, at lower pH's the selectivity was about 50% and as the pH was increased to pH 9, the R-isomer was increased to 75%. Interestingly, cytochrome $P450_{SP\alpha}$ (CYP152B1) is unable to turnover styrene until single-point mutations were introduced: A245E (20 % ee, *S*), A245D (41 % ee, *S*), and A245H (0.5 % ee, *S*).[23,24] Taken together, these results support that DHP B and its non-native cofacter derivatives may prove to have increased reactivity in relation to other proteins with styrene turnover capability.

New Reactivity: Hydroxylation of sp^3 C-H bonds

Previous studies in the Ghiladi lab have demonstrated DHP B peroxygenase reactivity with various substituted indoles. The homology of these substrates' structures with indane supported that it may be promising new substrate.[9] Indane was determined to have reactivity with both DHP B and Mn-DHP B (Figure 3.4); although, the nonnative cofactor proved to provide better stereoselectivity (28:72, *R*:*S*). It was also interesting to note that the absence of oxidant controls also resulted in a small amount of product, but with no stereoselectivity. The hydroxylation has been previously investigated using cytochrome P450BM3; the WT enzyme was determined to

prefer the *S*- enantiomer (16 % ee) without the presence of a decoy molecule, but the % ee could be adjusted to either enantiomer with the use of different decoy molecules.[25]

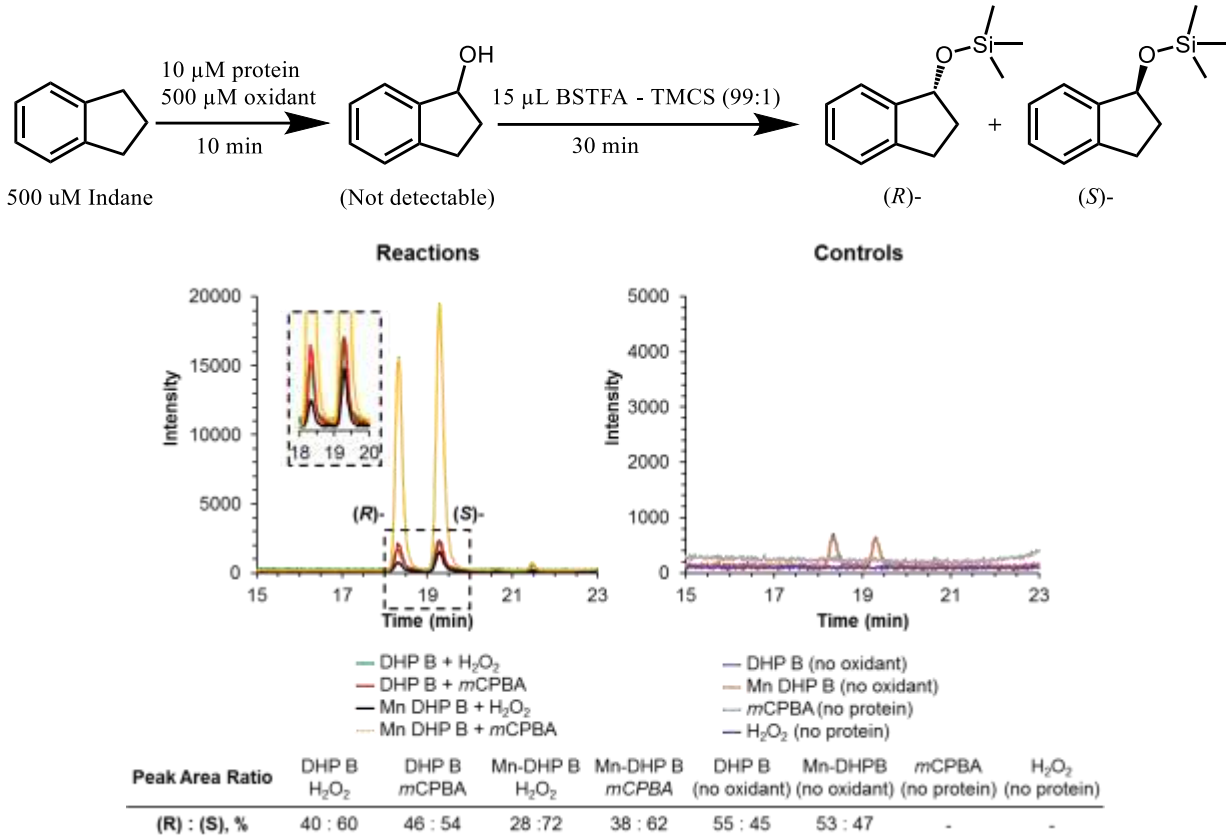

Peak Area Ratio	DHP B H_2O_2	DHP B *m*CPBA	Mn-DHP B H_2O_2	Mn-DHP B *m*CPBA	DHP B (no oxidant)	Mn-DHPB (no oxidant)	*m*CPBA (no protein)	H_2O_2 (no protein)
(R) : (S), %	40 : 60	46 : 54	28 :72	38 : 62	55 : 45	53 : 47	-	-

Figure 4.2. DHP B catalyzed hydroxylation of indane to (*R*/*S*)-1-indanol. GC-MS retention times for the products were: 18.4 min [(*R*)-1-indanol] and 19.4 min [(*S*)-1-indanol].

Ethylbenzene was the second substrate established to undergo sp^3 C-H hydroxylation in the presence of Mn-DHP B and *m*CPBA (WT DHP B was not tested but will be in future experiments). The reaction was not stereoselective and the product (*R*)-1-phenylethanol was only slighty perferred (Figure 3.5). The reaction was determined to be enzyme catalyzed due to the lack of reactivity when only in the presence of *m*CPBA. These results show that the DHP B catalyzed reaction of ethylbenzene is the least enantioselective reaction of the new substrates tested. When compared to WT P450BM3, the reactions were recorded to be (*R*)- favored and the percent ee reanged from 39-85 % depending on the decoy molecule used.[25] Reactivity studies with myoglobin determined that manganese-substituted myglobin increased the rate of hydroxylation compared to

WT myoglobin.[26] Future experiments will determine if the same trend is true for WT DHP B and Mn-DHP.

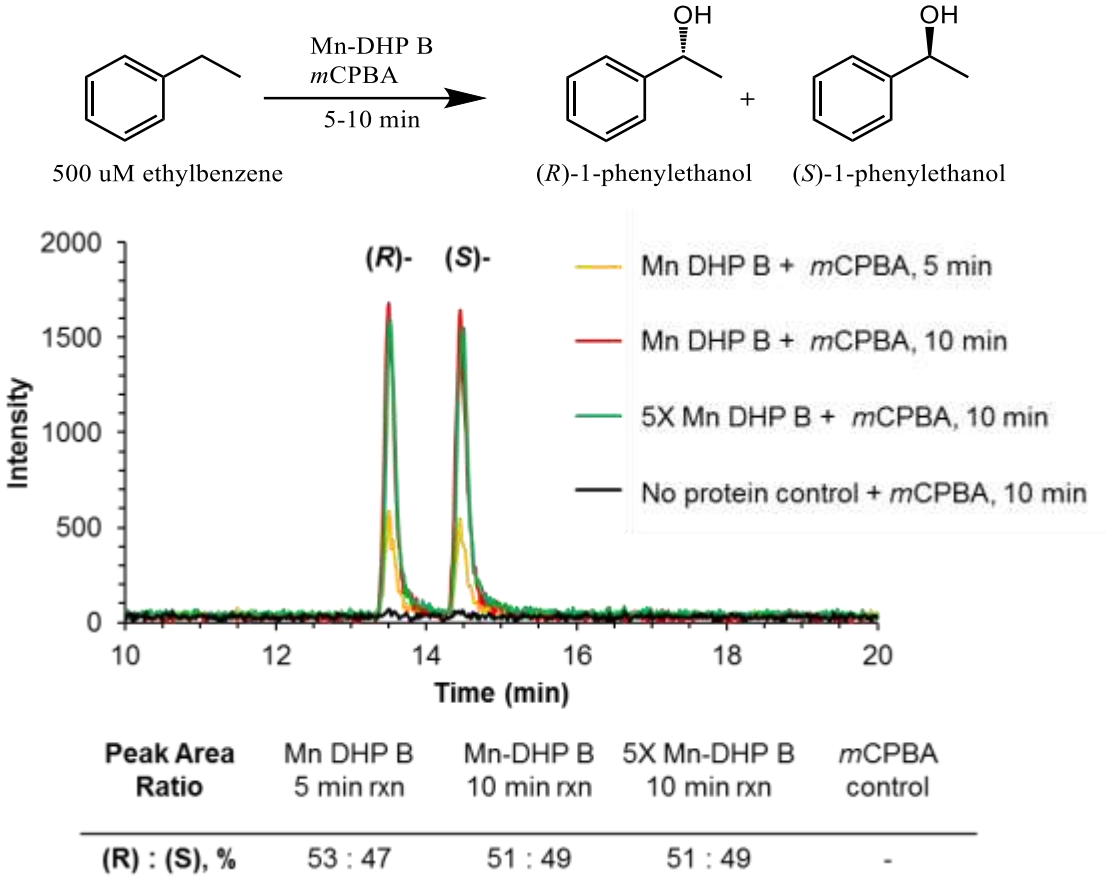

Peak Area Ratio	Mn DHP B 5 min rxn	Mn-DHP B 10 min rxn	5X Mn-DHP B 10 min rxn	*m*CPBA control
(R) : (S), %	53 : 47	51 : 49	51 : 49	-

Figure 4.3. DHP B catalyzed hydroxylation of ethylbenzene to (*R*/*S*)-1-phenylethanol. GC-MS retention times for the products were: 13.5 min [(*R*)-1-phenylethanol] and 14.6 min [(*S*)-1-phenylethanol].

New Reactivity: Sulfoxidation

The thioanisole substrate class is another commonly studied peroxygenase substrate, but until recently it had not been investigated as a potential substrate for DHP. In a reaction with DHP B (both wild type and Mn PPIX) and H_2O_2, it was determined that thioanisole turnover could be catalyzed by DHP B (Figure 3.6). In this case, WT DHP B resulted in strong stereoselectivity towards the (*R*)- enantiomer (86:14, *R*:*S*: green) with a slightly decreased stereoselectivity when Mn-DHP B was utilized (74:26, *R*:*S*: black), albeit with a drastically decreased product

concentration (products were concentrated by 1000-fold in order to be visualized by GC-MS). This may be due to the reduced reactivity of Mn-DHP B with H_2O_2, rather than *m*CPBA which is reactive with the substrate and therefore could not be utilized as the oxidant. The non-oxidant and non-enzymatic controls did not result in substrate turnover supporting that the reaction is co-catalyzed by DHP B and H_2O_2.

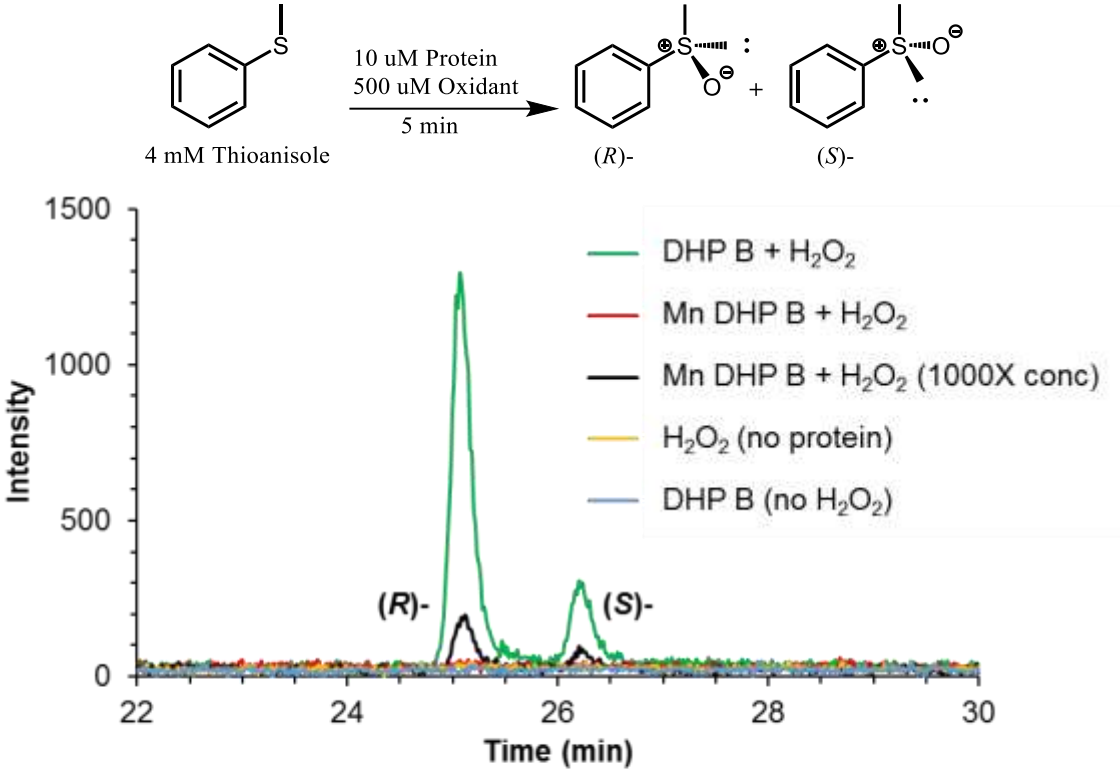

Peak Area Ratio	DHP B H_2O_2	Mn-DHP B H_2O_2	Mn-DHP B H_2O_2 (1000X)	H_2O_2	DHP B (no H_2O_2)
(R) : (S), %	86 : 14	-	74 : 26	-	-

Figure 4.4. DHP B catalyzed sulfoxidation of thioanisole to (R/S)-methyl phenyl sulfoxide. GC-MS retention times for the products were: 25.2 min [(*R*)-] and 26.25 min [(*S*)-].

As mentioned previously, thioanisole is commonly used to determine the stereoselectivity of cytochrome P450s. In the case of $P450_{BS\beta}$, *R*- stereoselectivity was preferred with % ee values ranging from 4-29 % depending on the decoy molecule introduced.[27,28] When compared to another

P450, the presented results have a similar stereo-distribution with $P450_{cam}$ (72:28, *R*:*S*).[29] Horseradish peroxidase has also been found to have reactivity and stereoselectivity (70 % ee, *S*-) with greater than 90 % of the incorporated oxygen deriving from hydrogen peroxide.[30] The presented preliminary results appear to have similar stereoselectivity (% ee) with HRP, but towards the opposite enantiomer. Enantioselectivity of the thioanisole products has also been examined in myoglobin, the ee (%) of wild type was determined to be 25 % (*R*)[22,31] but could be increased with the insertion of a nonnative Mn-salen to 50 % (*S*).[32]

New Reactivity: Cyclopropanation of Styrene with Ethyl Diazoacetate

The reaction of styrene and ethyl diazoacetate (EDA) mediated by DHP was analyzed by GC-MS (Figure 5 and 6, Table 2).

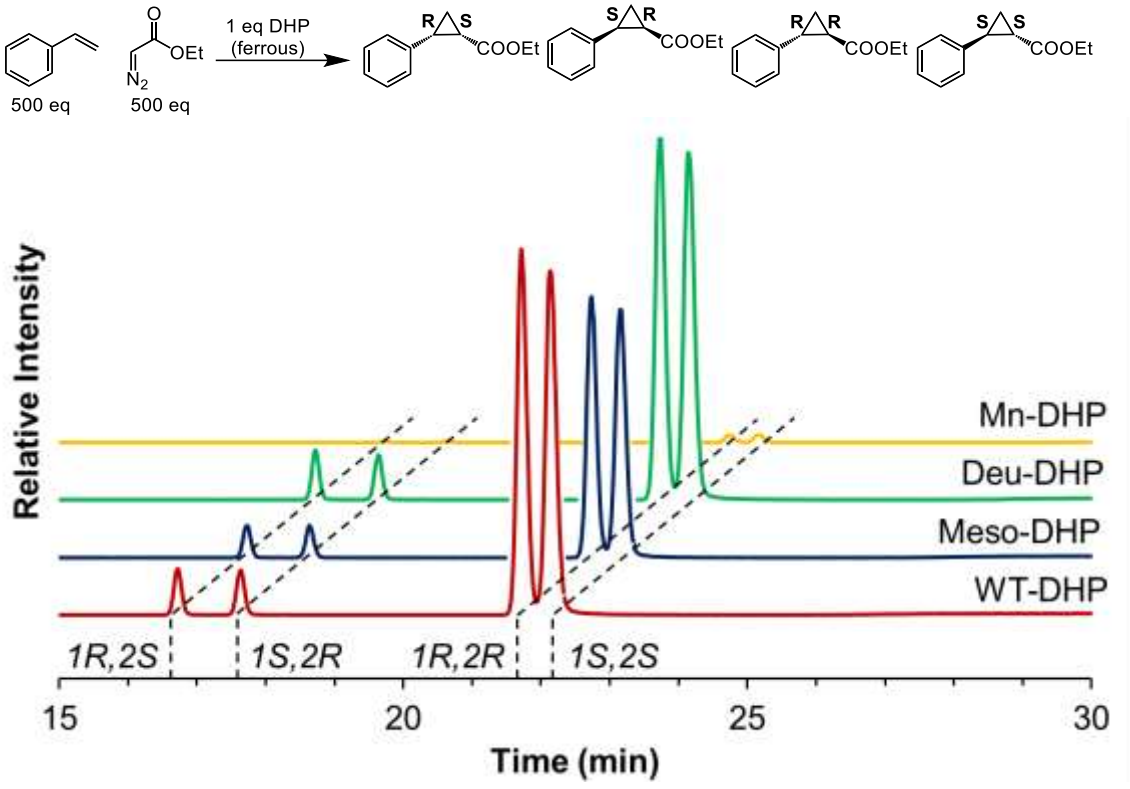

Figure 4.5. Cyclopropanation of styrene with WT-, Meso-, Deu-, and Mn-DHP

Table 4.2. Enantioselectivity of DHP-mediated cyclopropanation of styrene and EDA

	% Product Yield			
	Cis-		*Trans-*	
	1R,2S	**1S,2R**	**1R,2R**	**1S,2S**
Mn-DHP	6.6	6.9	42.4	44.0
Deu-DHP	4.7	4.5	44.8	46.1
Meso-DHP	4.5	4.5	45.3	45.7
WT-DHP	4.5	4.5	44.9	46.2

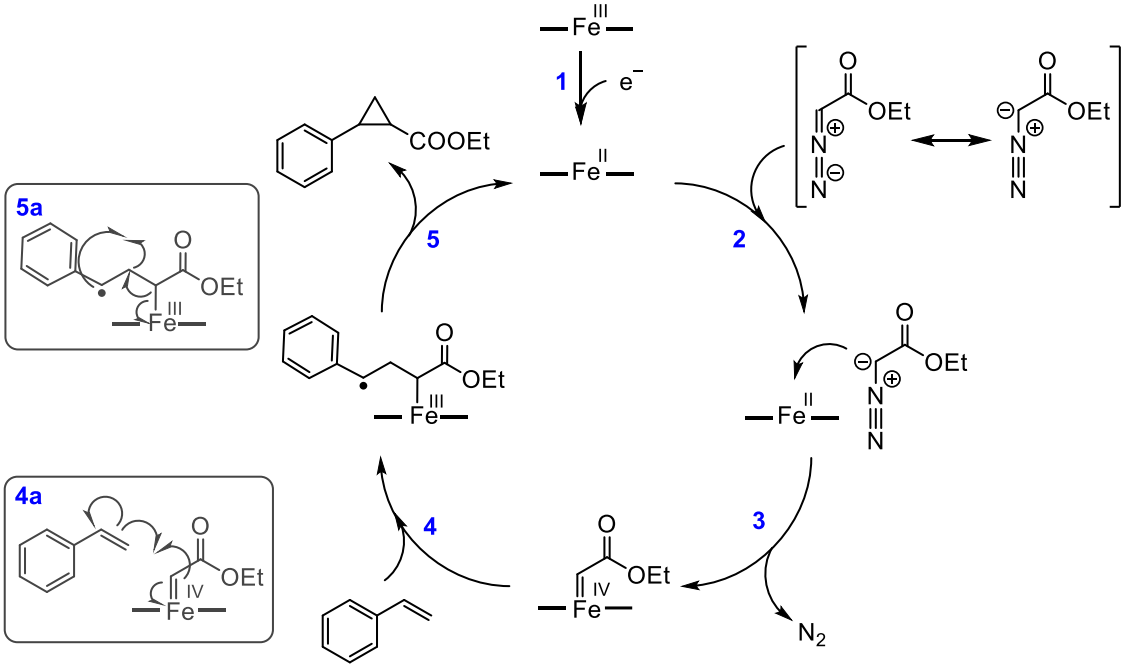

Figure 4.6. Mechanism of the heme-mediated cyclopropanation of styrene and EDA

The products of the reaction included both *cis* (1R,2S and 1S,2R) and *trans* (1R,2R and 1S,2S) with the trans products representing 90% of the mixture. This is equivalent to other peroxygenases, most notably, $P450_{BM3}$, which was 63% selective towards the trans enantiomers. Further mutations demonstrated that the T268A mutant increased the selectivity to 99%.[33] Myoglobin has also been

shown to conduct this reaction but incorporation of a new cofactor to iron porphycene increased the rate substantially.[34]

CONCLUSION

DHP is capable of $sp^2$and sp^3 C-H activation catalyzed by H_2O_2. Both the native enzyme and the cofactor variants demonstrate these new activities. Interestingly, the reactions analyzed all leaned towards the R-isomer. The cyclopropanation of styrene is the promising new activity, as carbene insertion These reactions slightly enantioselective, but as previous literature suggests, it is expected that with the use of amino acid point mutation, the % ee can be improved. The ability of DHP of act as a biocatalyst is an exciting advancement to compete with traditional chemical methods in attempt to make chemistry greener.

REFERENCES

1. Piontek, K. *et al.* Structural Basis of Substrate Conversion in a New Aromatic Peroxygenase CYTOCHROME P450 FUNCTIONALITY WITH BENEFITS *. (2013). doi:10.1074/jbc.M113.514521
2. Jacobsen, E. N., Zhang, W., Muci, A. R., Ecker, J. R. & Deng, L. Highly enantioselective epoxidation catalysts derived from 1,2-diaminocyclohexane. *J. Am. Chem. Soc.* **113**, 7063–7064 (1991).
3. Finn, M. G. & Sharpless, K. B. Mechanism of asymmetric epoxidation. 2. Catalyst structure. *J. Am. Chem. Soc.* **113**, 113–126 (1991).
4. Li, H., Li, B. J. & Shi, Z. J. Challenge and progress: Palladium-catalyzed sp3 C-H activation. *Catalysis Science and Technology* **1**, 191–206 (2011).
5. Chu, J. C. K. & Rovis, T. Complementary Strategies for Directed C(sp 3)−H Functionalization: A Comparison of Transition-Metal-Catalyzed Activation, Hydrogen Atom Transfer, and Carbene/Nitrene Transfer. *Angewandte Chemie - International Edition* **57**, 62–101 (2018).
6. Giri, R., Shi, B. F., Engle, K. M., Maugel, N. & Yu, J. Q. Transition metal-catalyzed C-H activation reactions: Diastereoselectivity and enantioselectivity. *Chemical Society Reviews* **38**, 3242–3272 (2009).
7. Koeller, K. M. & Wong, C.-H. Enzymes for Chemical Synthesis. *Nature* **409**, 232–240 (2001).
8. Oohora, K. *et al.* Catalytic Cyclopropanation by Myoglobin Reconstituted with Iron Porphycene: Acceleration of Catalysis due to Rapid Formation of the Carbene Species. *J. Am. Chem. Soc* **139**, 17265–17268 (2017).
9. Barrios, D. A. *et al.* Peroxygenase and oxidase activities of dehaloperoxidase-hemoglobin from Amphitrite ornata. *J. Am. Chem. Soc.* **136**, 7914–7925 (2014).
10. Chen, Y. P., Woodin, S. A., Lincoln, D. E. & Lovell, C. R. An unusual dehalogenating peroxidase from the marine terebellid polychaete Amphitrite ornata. *J. Biol. Chem.* **271**, 4609–4612 (1996).
11. Roach, M. P. *et al.* Notomastus lobatus chloroperoxidase and amphitrite ornata dehaloperoxidase both contain histidine as their proximal heme iron ligand. *Biochemistry* **36**, 2197–2202 (1997).
12. McCombs, N. L., D'Antonio, J., Barrios, D. A., Carey, L. M. & Ghiladi, R. A. Nonmicrobial nitrophenol degradation via peroxygenase activity of dehaloperoxidase-hemoglobin from amphitrite ornata. *Biochemistry* **55**, 2465–2478 (2016).
13. Malewschik, T., de Serrano, V., McGuire, A. H. & Ghiladi, R. A. The multifunctional globin dehaloperoxidase strikes again: Simultaneous peroxidase and peroxygenase mechanisms in the oxidation of EPA pollutants. *Arch. Biochem. Biophys.* **673**, 108079 (2019).
14. McCombs, N., Smirnova, T. & Ghiladi, R. Oxidation of Pyrrole by Dehaloperoxidase-Hemoglobin: Chemoenzymatic Synthesis of Pyrrolin-2-Ones. *Catal. Sci. Technol.* (2017). doi:10.1039/C7CY00781G
15. D'Antonio, J. *et al.* Spectroscopic and mechanistic investigations of dehaloperoxidase B from amphitrite ornata. *Biochemistry* **49**, 6600–6616 (2010).
16. Teale, F. W. J. Cleavage of the haem-protein link by acid methylethylketone. *BBA - Gen. Subj.* **35**, 543 (1959).

17. Yonetani, T. Studies on cytochrome c peroxidase. X. Crystalline apo-and reconstituted holoenzymes. *J. Biol. Chem.* **242**, 5008–13 (1967).
18. Zhang, C. *et al.* Engineering P450 Peroxygenase to Catalyze Highly Enantioselective Epoxidation of cis -β-Methylstyrenes. *Chem. - A Eur. J.* **22**, 10969–10975 (2016).
19. Kluge, M., Ullrich, R., Scheibner, K. & Hofrichter, M. Green Chemistry Stereoselective benzylic hydroxylation of alkylbenzenes and epoxidation of styrene derivatives catalyzed by the peroxygenase of Agrocybe aegerita. *Green Chem* **14**, 440–446 (2012).
20. Shoji, O. & Watanabe, Y. Peroxygenase reactions catalyzed by cytochromes P450. *J. Biol. Chem.* **19**, 529–539 (2014).
21. Choi, W. J. & Choi, C. Y. Production of chiral epoxides: Epoxide hydrolase-catalyzed enantioselective hydrolysis. *Biotechnol. Bioprocess Eng.* **10**, 167–179 (2005).
22. Ozaki, S.-I., Matsui, T. & Watanabe, Y. Conversion of Myoglobin into a Peroxygenase: A Catalytic Intermediate of Sulfoxidation and Epoxidation by the F43H/H64L Mutant. *J. Am. Chem. Soc* **119**, 6666–6667 (1997).
23. Shoji, O. *et al.* A substrate-binding-state mimic of H2O2-dependent cytochrome P450 produced by one-point mutagenesis and peroxygenation of non-native substrates. *Sci. Technol* **6**, 5806–5811 (2016).
24. Fujishiro, T. *et al.* Crystal Structure of H2O2-dependent Cytochrome P450SPalpha with Its Bound Fatty Acid Substrate Insight into the Regioselective Hydroxylation of Fatty Acids at the Alpha position. *J. Biol. Chem.* **286**, 29941–29950 (2011).
25. Suzuki, K. *et al.* Control of stereoselectivity of benzylic hydroxylation catalysed by wild-type cytochrome P450BM3 using decoy molecules. *Catal. Sci. Technol* **7**, 3332–3338 (2017).
26. Stone, K. L. & Ahmed, S. M. Advances in Engineered Hemoproteins that Promote Biocatalysis. *Inorganics* **4**, (2016).
27. Fujishiro, T., Shoji, O. & Watanabe, Y. Non-covalent modification of the active site of cytochrome P450 for inverting the stereoselectivity of monooxygenation. *Tetrahedron Lett.* **52**, 395–397 (2011).
28. Polic, V. & Auclair, K. Controlling substrate specificity and product regio- and stereo-selectivities of P450 enzymes without mutagenesis. *Bioorg. Med. Chem.* **22**, 5547–5554 (2014).
29. Fruetel, J., Chang, Y.-T., Collins, J., Loew, G. & Ortiz De Montellano, P. R. Thioanisole Sulfoxidation by Cytochrome P450cam (CYP101): Experimental and Calculated Absolute Stereochemistries. *J. Am. Chem. SOC* **116**, 11643–11648 (1994).
30. Harris, R. Z., Newmyer, S. L. & Ortiz De Montellano, P. R. Horseradish Peroxidase-catalyzed Two-electron Oxidations: Oxidation of Iodide, Thioanisoles, and Phenols at Distinct Sites. *J. Biol. Chem.* **268**, 1637–1645 (1993).
31. Ozaki, S., Matsui, T. & Watanabe, Y. Conversion of Myoglobin into a Highly Stereo-specific Peroxygenase by the L29H/H64L Mutation. *J. Am. Chem. Soc* **118**, 9784–9785 (1996).
32. Carey, J. R. *et al.* A Site-Selective Dual Anchoring Strategy for Artificial Metalloprotein Design. *J. Am. Chem. Soc.* **126**, 10812–10813 (2004).
33. Coelho, P. S., Brustad, E. M., Kannan, A. & Arnold, F. H. Olefin Cyclopropanation via Carbene Transfer Catalyzed by Engineered Cytochrome P450 Enzymes. *Science (80-.).* **339**, 307–310 (2013).
34. Wei, Y., Tinoco, A., Steck, V., Fasan, R. & Zhang, Y. Cyclopropanations via Heme

Carbenes: Basic Mechanism and Effects of Carbene Substituent, Protein Axial Ligand, and Porphyrin Substitution. *J. Am. Chem. Soc.* **140**, 1649–1662 (2018).